A MULTI-NICHE CULTURE METHOD FOR MIMICKING HUMAN BONE MARROW

A Dissertation
Presented to
The Academic Faculty

by

Michael R. Nelson

In Partial Fulfillment
of the Requirements for the Degree
Doctor of Philosophy in Biomedical Engineering in the
Wallace H. Coulter Department of Biomedical Engineering

Georgia Institute of Technology and Emory University
August 2019

A MULTI-NICHE CULTURE METHOD FOR MIMICKING HUMAN BONE MARROW

Approved by:

Krishnendu Roy, PhD, Advisor
Department of Biomedical Engineering
Georgia Institute of Technology

Brandon Dixon, PhD
Department of Mechanical Engineering
Georgia Institute of Technology

Manu Platt, PhD
Department of Biomedical Engineering
Georgia Institute of Technology

Frances Eun-Hyung Lee, MD
Department of Medicine
Emory University

Johnna Temenoff, PhD
Department of Biomedical Engineering
Georgia Institute of Technology

Date Approved: May 16, 2019

If science teaches us anything, it teaches us to accept our failures, as well as our successes, with quiet dignity and grace.

- Gene Wilder, *Young Frankenstein*

ACKNOWLEDGEMENTS

First, I would like to thank my advisor, Krishnendu Roy, who has always supported my growth as a researcher and my career aspirations outside of the lab. The numerous current and former members of the Roy Lab have helped in many ways. I would especially like to thank Joscelyn and Delta who contributed directly to this work and spent many hours helping with experiments. I am also grateful to have shared my time in graduate school with Kirsten, Joscelyn, and Jiaying, who have always been eager to help troubleshoot and have been a joy to work with. I have been fortunate to have worked with and learned from talented high school and undergraduate students, Anagha, David, Emily, Omari, and Gita, who contributed to this work at various points in time. I would also like to thank the BME, EBB, Petit Institute, and Marcus Center staff, especially Carol Mills, Andrea Soyland, Carolyn Yeago, and Aaron Lifland.

I am grateful for my friends and family that have made my life in graduate school and Atlanta better. To my parents, Bob and Kim, thank you for always prioritizing my education and providing me with the best opportunities in life. I am thankful for my sister and brother-in-law, Sarah and Dan, who are a model of what you can achieve in life with hard work and kindness. I would like to thank my second parents, Mike and Michelle, for their relentless support of family. Thank you to my friends in Atlanta, including Andrew, Casey, Chad, Jim, Kevin, Muaz, and Rob, for providing ample distractions from my work when needed. Most importantly, none of this would have been possible without my wife, Kristin, who I moved to Atlanta to be with six years ago. Thank you for your love and understanding, and for always reminding me what is most important in life.

TABLE OF CONTENTS

LIST OF TABLES

LIST OF FIGURES

LIST OF SYMBOLS AND ABBREVIATIONS

Ang-1	Angiopoietin-1
BM	Bone marrow
CAR cell	CXCL12 abundant reticular cell
CAR T cell	Chimeric antigen receptor T cell
CFU	Colony forming unit
EC	Endothelial cell
ECM	Extracellular matrix
ELISA	Enzyme-linked immunosorbent assay
EtDA	Ethylene diamine
FN	Fibronectin
GAG	Glycosaminoglycan
G-CSF	Granulocyte colony stimulating factor
GM-CSF	Granulocyte macrophage stimulating factor
HA	Hyaluronic acid
HPC	Hematopoietic progenitor cell
HSC	Hematopoietic stem cell
HSPC	Hematopoietic stem and progenitor cell
HUVEC	Human umbilical vein endothelial cell
ICC	Inverted colloidal crystal
IL	Interleukin
IR	Ionizing radiation
LDH	Lactate dehydrogenase

LN	Laminin
LSK	$Lin^{-}Sca1^{+}cKit^{+}$
LT-HSC	Long term hematopoietic stem cell
MFI	Mean fluorescence intensity
MK	Megakaryocyte
MSC	Mesenchymal stem/stromal cell (or medicinal signaling cell)
OB	Osteoblast
OPN	Osteopontin
PA	Poly(acrylamide)
PAAc	Poly(acrylic acid)
PDMS	Poly(dimethyl siloxane)
PEGDA	Poly(ethylene glycol) diacrylate
PES	Poly(ether sulfone)
PET	Poly(ethylene terephthalate)
S1P	Sphingosine-1-phosphate
SCF	Stem cell factor
SDF-1	Stromal derived factor-1 (or CXCL12)
ST-HSC	Short term hematopoietic stem cell
TCPB	Tantalum coated porous biomaterials
TCPS	Tissue culture polystyrene
TPO	Thrombopoietin
TUNEL	Terminal deoxynucleotidyl transferase-mediated dUTP-biotin nick-end labelling
VEGF	Vascular endothelial growth factor
VLA	Very late antigen

SUMMARY

Bone marrow is a complex, heterogeneous, primary immune tissue that is composed of distinct microenvironments. The stromal cells that make up these microenvironments regulate normal hematopoietic function and are instrumental in the tissue's response during illness or therapeutic intervention. These stromal cells create the two primary niches in bone marrow: the endosteal and perivascular niches. While there are a sizeable number of examples of *in vitro* culture methods that recreate aspects of the bone marrow microenvironment using biomaterials, co-cultures, or ectopic implants, there are relatively few examples that recreate both the endosteal and perivascular niches in a single, defined culture. It is critical for both *in vitro* modeling of disease and furthering our understanding of the normal physiological processes of the bone marrow that we can recapitulate these basic structures of bone marrow together in a single platform.

The overall goal of this dissertation was to create a multi-niche bone marrow mimic to study the role of the endosteal and perivascular niches in hematopoietic stem cell biology. In Aim 1, we designed, fabricated, and developed a microfluidic device, human bone marrow-on-a-chip (hBM-on-a-chip) that recreates the endosteal surface with adjacent microvasculature. In Aim 2, we assessed the utility of the hBM-on-a-chip as a platform for studying hematopoietic stem cell mobilization and the effects of radiation on the bone marrow microenvironment. The work presented in this dissertation provides tools for the *in vitro* study of human bone marrow, the hematopoietic system, and therapeutics that aim to alter its physiologic state.

CHAPTER 1. INTRODUCTION*

1.1 Overview

Hematopoietic stem cells (HSCs) are responsible for continuously populating the body's blood and immune cells through the process of hematopoiesis. During early developmental stages, HSCs reside in the fetal liver and eventually move to the spleen and finally to the bone marrow (BM), where HSCs exist and hematopoiesis is ongoing in healthy adults [2]. Within the BM, specific signals from the local microenvironment (1) direct HSCs to maintain a multipotent population, (2) signal HSCs to differentiate into hematopoietic progenitor cells (HPCs), and (3) support differentiation into lineage restricted hematopoietic cells (B cells, T cells, natural killer cells, dendritic cells, neutrophils, macrophages, eosinophils, basophils, mast cells, megakaryocytes (MKs), and erythrocytes) to maintain homeostasis of blood and immune cells within the body. Replicating the intricacies of the HSC 'niche' *in vitro* is a complex task, but efforts toward this goal further our understanding of HSC physiology and can create useful preclinical models for understanding therapeutic effects in physiologically relevant culture systems.

The concept of an HSC 'niche' was first conceived by Schofield in 1978 [3] and our understanding of it has continued to evolve since. At first, the niche was largely believed to be endosteal, supported by cells on or near the inner lining of the bone [4-6]. More recently there have been several studies that have identified the HSC niche to be

*Adapted from [1] Nelson, M. R. & Roy, K. Bone-marrow mimicking biomaterial niches for studying hematopoietic stem and progenitor cells. *J Mater Chem B* **4**, 3490-3503, doi:10.1039/c5tb02644j (2016). Reproduced by permission of the Royal Society of Chemistry.

perivascular, adjacent to the sinusoids and vasculature that permeate BM [7,8]. Regardless, it is evident that both the endosteal and perivascular niches play an important role in the maintenance of the hematopoietic system throughout adulthood.

There have been many efforts to replicate or mimic some or all the components of the hematopoietic niche in order to study hematopoietic stem and progenitor cells (HSPCs) or affect HSPCs toward a desired outcome using an *in vitro* culture. The first reports of HSC culture and differentiation *in vitro*, the Dexter culture [9], used a two-dimensional layer of BM stromal cells in the presence hydrocortisone and serum. Dexter cultures were able to sustain hematopoiesis, but without the addition of cytokines differentiation was lineage restricted [10]. Many cytokines have been used for the expansion of HSCs, including stem cell factor (SCF), thrombopoietin (TPO), Flt3 ligand, and interleukins (IL)-6 and -11 [11]. Additionally, a number of stromal cell lines have been developed for co-culture because they express high levels of cytokines that are specific to HSC expansion or that support differentiation of specific hematopoietic lineages [11]. Over the last twenty years, *in vitro* HSC cultures have moved beyond 2D co-cultures with cytokine stimulation and researchers have begun to use more complex biomaterial based systems that imitate a greater number of variables that are present within the HSC niche [12-18]. However, there are no examples of fully human, *in vitro*, BM cultures that contain both the endosteal and perivascular niches.

There are many potential applications for a human, *in vitro* BM culture model. In addition to the expansion and differentiation of HSCs for specific therapeutic needs, the culture system could serve as a platform to study both basic HSC biology and the effects of clinical intervention on HSCs and the BM microenvironment.

Clinically, HSCs have been used to treat a range of blood related pathologies for over fifty years in BM transplantation [19]. Transplantation typically falls within two categories based on the source of the transplanted cellular material: allogeneic (donor tissue originating from someone other than the patient) or autologous (transplanted cells generated from healthy patient tissue). While the quantity of healthy allogeneic donor cells is typically enough, there are several problems associated with allogeneic transplantation, mainly the matching of donor and patient tissue to avoid rejection of implanted cells or development of graft-versus-host disease. Although autologous transplantation is preferred because it eliminates problems with compatibility of transplanted tissue, there are limited numbers of HSCs that can be harvested from a patient for transplantation and *ex vivo* expansion is necessary to achieve adequate numbers of cells for an effective dose. Transplantation of HSCs first requires collection of HSCs from the donor (the patient themselves in the case of autologous transplantation) and the preparation of the recipient tissue. To collect HSCs, typically the cells are mobilized from the BM compartment into peripheral blood so that they can be collected by leukapheresis. Second, any malignancy in the patient must be ablated, either by radiotherapy or chemotherapy, prior to transplantation, which will also deplete any remaining HSPCs. Then, previously harvested cells can be administered to reconstitute a healthy hematopoietic system. Preclinical approaches to studying HSC mobilization and engraftment are currently limited to animal models.

Because BM is responsible for ongoing hematopoiesis during adulthood, it is protected from natural sources of radiation by the bone it is encased within [20]. There are circumstances, both clinical and accidental, where people are exposed to high doses of

radiation and this can lead to failure of the hematopoietic system. Our understanding of radiation exposure is limited to animal models and patients from widespread exposures (e.g. Fukushima, Chernobyl). A defined *in vitro* model could allow us to further our understanding of the effects of radiation on the BM and the role that the microenvironment plays in alleviating or aggravating the resulting damage to the hematopoietic system.

As with other *simple in* vitro models and more complex organ-on-chip technologies, there are potential applications for preclinical drug screening, especially in the context of anti-cancer therapeutics. Multiple myeloma (MM), leukemia, and other hematologic malignancies originate or reside within the BM compartment, and screening therapeutics (especially those that do not act directly on cancerous cells) in a BM specific microenvironment could increase the efficacy of preclinical testing. Testing of cellular therapies (like chimeric antigen receptor T cells) in complex environments is critical, because the tumor associated tissue can dramatically impact the activity of the therapeutic cells. Similarly, tissue specific culture models are important for preclinical testing of clinical interventions that specifically target the BM or BM resident cells.

In addition to multipotent HSCs for the reconstitution of the hematopoietic system, there is also a clinical need for differentiated hematopoietic cells. There is a high and growing demand for blood [21] and platelets [22] for transfusion and due to stagnate donor pools and increasing costs, *ex vivo* expansion of therapeutic cells may be an alternative. Efficient *ex vivo* generation and expansion of therapeutic cells is necessary to realize the full clinical potential of HSCs and this requires *in vitro* culture systems that can replicate the complexities of the microenvironment within the BM and other hematopoietic niches.

1.2 Hypothesis

The overall hypothesis of this dissertation was that using a poly(dimethyl) sulfoxide (PDMS) microfluidic platform, the endosteal and perivascular niches of BM could be recapitulated in a physiologically relevant manner. The overall objective was to develop this platform and to assess the relevance in two preclinical applications.

1.3 Specific aims

1.3.1 Aim 1: Design, fabrication, and characterization of human bone marrow-on-a-chip (hBM-on-a-chip) to mimic the human bone marrow microenvironment.

In the first aim, multiple iterations of design and characterization were performed to develop a microfluidic, organ-on-a-chip model of human BM that recapitulated basic characteristics of the endosteal and perivascular BM microenvironments. This was accomplished through two, interconnected sub-aims (Figure 1):

A. Design a PDMS microfluidic platform, hBM-on-a-chip, and optimize the fabrication process.
B. Characterize the bone marrow microenvironments and HSPC behavior in hBM-on-a-chip.

1.3.2 Aim 2: Use hBM-on-a-chip as a model system to study effects of therapeutics and disease on bone marrow.

In the second aim, the device designed and characterized in Aim 1 was evaluated for its ability to model BM physiology in two clinically relevant situations of BM perturbation: the mobilization of HSPCs from the BM niche and the irradiation of BM.

This was accomplished through two, distinct sub-aims (Figure 1):

A. Study mobilization of HSPCs from hBM-on-a-chip and therapeutic effects on the bone marrow microenvironment.
B. Investigate the effects of radiation on the bone marrow microenvironment and HSPC fate.

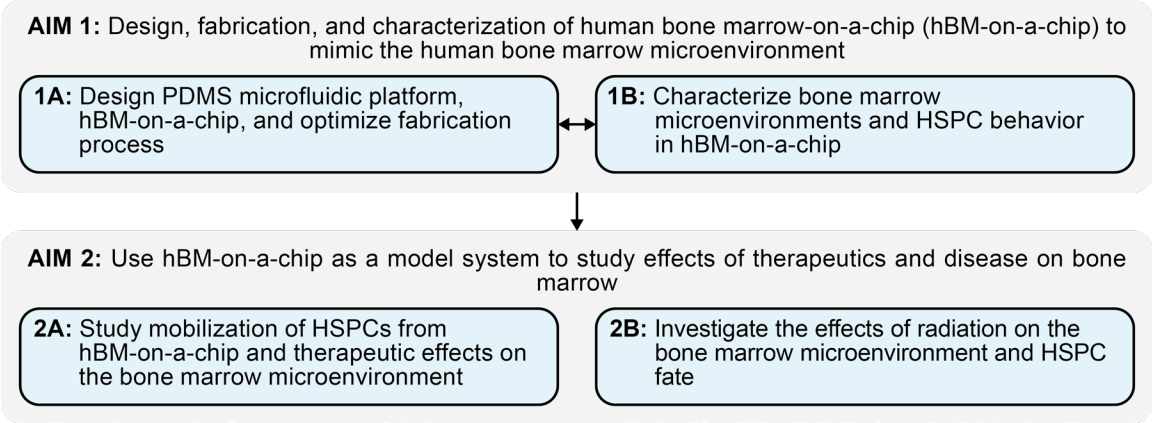

Figure 1. Relationship between aims.

1.4 Outline

In CHAPTER 2, we provide background information that details the BM microenvironment and previous work that has been done to recreate part of or all the HSC niche *in vitro*. In CHAPTER 3 the design and fabrication methods (Aim 1A) of hBM-on-a-chip is presented and in CHAPTER 4 the characterization of hBM-on-a-chip (Aim 1B) is shown. CHAPTER 5 (Aim 2A) and CHAPTER 6 (Aim 2B) demonstrate the application of hBM-on-a-chip in HSC mobilization and BM radiation studies, respectively. Finally, in CHAPTER 7 conclusions from this work and potential future directions are discussed.

CHAPTER 2. BACKGROUND AND SIGNIFICANCE*

2.1 Hematopoietic stem and progenitor cell niche in BM

BM is a densely populated, highly vascularized, and non-uniform environment (Figure 2). Although HSCs have been the most studied of adult stem cells, there still exists some uncertainty of the exact location and environment of the HSC niche within BM. Most studies to date of the HSC niche have used *in vivo* models. However, due to the relative scarcity of HSCs in BM (<0.005% of BM cells) [23] it is challenging to study niche characteristics in animal models. Similarly, studies of HPCs and differentiation are difficult, although not impossible, to track longitudinally *in vivo*. In 2009, Lo Celso *et al*. reported a technique for *in vivo* imaging of single hematopoietic cells from specific stem and progenitor populations using confocal and two-photon microscopy [24]. More recently, several studies have used whole marrow imaging techniques to identify, with more specificity, the niche characteristics of HSCs [25]. *In vivo* and *in vitro* approaches to studying the hematopoietic niche are complementary; while *in vivo* models have much greater physiological complexity, *in vitro* models are much easier to manipulate, control, and observe in real time. To design biomaterials and cultures for HSPC expansion and differentiation, the native microenvironment must be understood so that specific properties can be emulated to elicit natural behavior *in vitro*.

*Adapted from [1] Nelson, M. R. & Roy, K. Bone-marrow mimicking biomaterial niches for studying hematopoietic stem and progenitor cells. *J Mater Chem B* **4**, 3490-3503, doi:10.1039/c5tb02644j (2016). Reproduced by permission of The Royal Society of Chemistry.

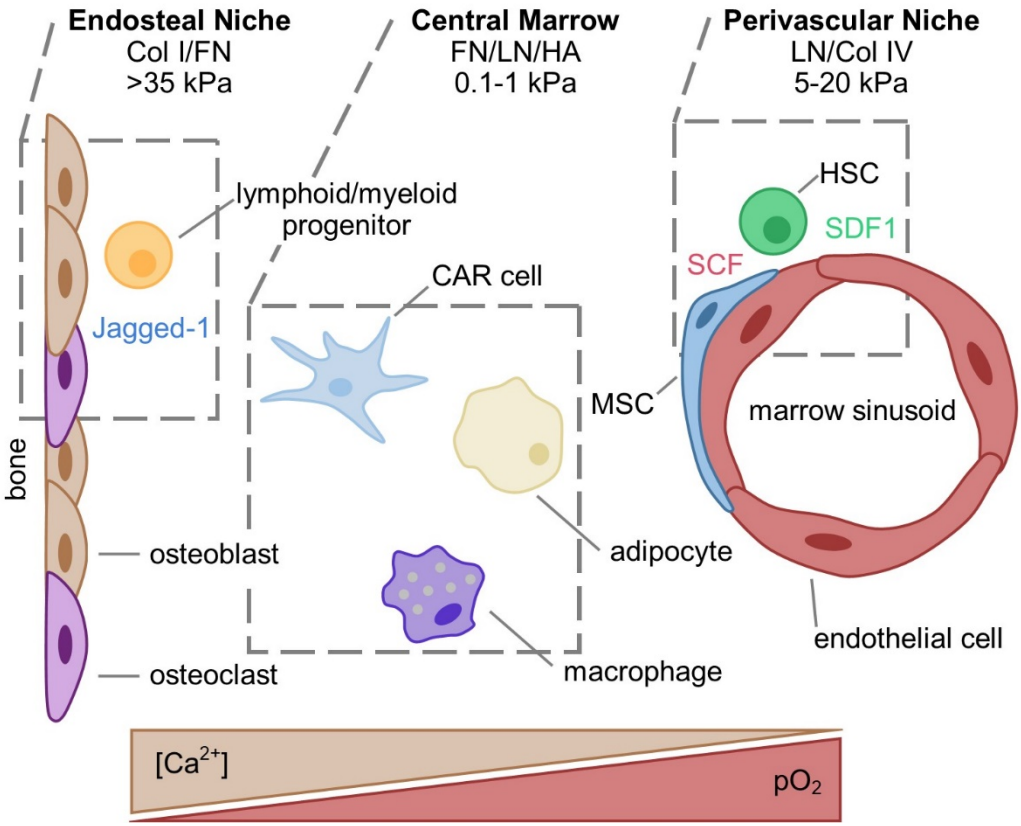

Figure 2. Cellular, biochemical, and physical characteristics of human bone marrow microenvironments [1]. BM can be divided into three distinct microenvironments: the endosteal niche, the central marrow, and the perivascular niche. Each of these microenvironments has different cellular constituents, ECM characteristics, biochemical signals, and physical properties that direct hematopoietic cell behavior. HSCs and hematopoietic progenitor cells occupy different niches within the BM and are instructed to maintain multipotency through senescence, to proliferate, or to differentiate by the signals in the occupied niche. Chemical gradients of Ca^{2+} and pO_2 are established across the BM and are important to homing and proliferation of hematopoietic cells.

2.1.1 Hematopoietic stem and progenitor cells (HSPCs) in BM

HSCs (human: $Lin^-CD34^+CD38^-CD90^+$; mouse: $Lin^-Sca1^+cKit^+$ (LSK) $CD34^-$) are multipotent, adult stem cells that can differentiate into all cell types in the hematopoietic lineage (Figure 3). The ability of HSCs to self-renew and reconstitute the hematopoietic system upon engraftment can either be categorized as long-term (LT-HSC) or short-term (ST-HSC), depending on the duration for which the HSC can self-renew and reconstitute

the hematopoietic system. HSCs differentiate into multipotent progenitors (human: $Lin^-CD34^+CD38^-CD90^-$; mouse: $Lin^-Sca1^+cKit^+CD34^+$) that can differentiate into all hematopoietic lineages but are incapable of self-renewal. Multipotent progenitors further differentiate into common myeloid progenitors (CMP) and common lymphoid progenitors (CLP) that are oligopotent and can differentiate into lineage restricted progenitors [26]. Lineage restricted progenitors can terminally differentiate into mature effector cells, although in many cases this process occurs outside of the BM in peripheral tissues. Collectively, HSCs, multipotent progenitors, oligopotent, and lineage restricted progenitors are referred to as HSPCs.

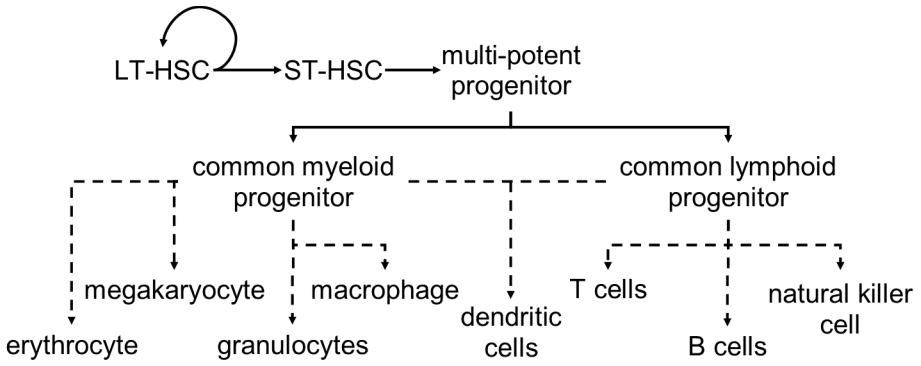

Figure 3. The differentiation of hematopoietic cells from HSCs [1]. LT-HSCs are capable of self-renewal and differentiation toward ST-HSCs and multi-potent progenitor cells. Multi-potent progenitor cells differentiate into common oligopotent progenitor cells for the myeloid and lymphoid lineages. Common myeloid and lymphoid progenitors differentiate into lineage restricted progenitor cells that can develop into mature effector cells, although the final steps of maturation often occur outside of the BM. Dotted lines indicate a series of lineage restricted progenitor cells.

2.1.2 Multiple niches for HSPCs within BM

One challenge in understanding the HSC niche within BM is that it is unlikely that a single niche exists. Rather, recent findings have pointed towards multiple, distinct niches

existing within the BM that support different functions. There are three regions within the bone marrow that we can consider: (1) the endosteal niche, BM is contained within long bones and has a large surface area of contact with the inner, endosteal surface; (2) the perivascular niche, BM is highly vascularized with microvasculature and larger sinusoids; and (3) the central marrow, the densely populated, heterogeneous, cellular regions that exist between the sinusoids and the endosteal surface. Early research of the BM niche suggested that the endosteal surface and osteoblasts formed the HSC niche [6,27] and that calcium signaling was critical to engraftment of LT-HSCs [28]. However, recently the field has shifted and the current paradigm is that LT-HSCs reside in a perivascular niche [8] and are supported by perivascular stroma and endothelial cells. In addition, it is now thought that hematopoietic progenitors occupy distinct niches in the endosteal and central marrow spaces [7]. This change in paradigm highlights the relative uncertainty that remains in our current understanding of BM microenvironments [29-31]. Despite the new understanding of HSC niche location, the model of the BM niche is still incomplete and furthermore these microenvironments do not exist in isolation. For example, the vasculature in BM exists throughout the entire organ, meaning there are both perivascular niches that are distant from and adjacent to the endosteal surface. In certain niches, cells can inhabit two of these environments simultaneously. *In vitro*, biomaterial-based culture systems can provide a means to explore how the different properties of these microenvironments direct hematopoietic fate and function in isolation and in the context of one another.

2.1.3 Many cell types interact with HSPCs in the BM niche

In addition to the numerous hematopoietic cells that occupy BM, many stromal cells exist within BM and have various roles in influencing the maintenance, proliferation,

and differentiation of HSCs. The endosteal niche is occupied by osteoblasts [32], which line the endosteal surface depositing extracellular matrix (ECM), and osteoclasts [32], macrophage derived cells responsible for bone resorption. HSCs in the perivascular niche interact with several cells, including endothelial cells, CXCL12 abundant reticular (CAR) cells, mesenchymal stromal cells (MSCs), and neurons. Sinusoidal endothelial cells [29,32] provide a barrier for entry to and exit from circulation and express cytokines that signal to HSCs [8]. CAR cells secrete the chemokine CXCL12 (or stromal derived factor-1 (SDF-1)) that maintains hematopoietic cells in BM through binding of the CXCR4 surface receptor [33,34]. $Nestin^{+}$ MSCs in mice were found to be spatially associated with HSCs near the vasculature, creating a dual, adult stem cell niche [35]. Recently, HSC behavior has been shown to also be influenced by neural signaling: nonmyelinating Schwann cells have been observed to influence HSC dormancy [36] and sympathetic nervous system signaling can control mobilization of HSCs [37]. The central marrow contains a number of hematopoietic cells, including macrophages, adipocytes, CAR cells, and fibroblasts [32]. The interactions between hematopoietic cells and the resident stromal cells within the central marrow are less understood.

2.1.4 Extracellular matrix (ECM) in BM is spatially varying

The ECM in BM varies greatly between the different niches; collagen (COL) types I and IV [38,39], fibronectin (FN) [38,39], laminin (LN) [38-41], hyaluronic acid (HA) [38,42,43], heparin [38], osteopontin (OPN) [44-46], and several other ECM proteins [47] are present in BM. However, the ECM is not continuous throughout the different microenvironments. ECM in the stem cell niche is important for regulating cellular behavior. HSCs are typically considered non-adherent cells; however, they do have several

surface receptors that are capable of binding to ECM proteins and glycosaminoglycans (GAGs). ECM proteins and GAGs can also influence HSCs indirectly by providing unique environments for stromal cells and by immobilizing cytokines and chemokines. In the endosteal niche, osteoblasts create a distinctive ECM environment that is typical to bone matrix. Endosteal ECM contains collagens I and IV, OPN and FN [39,44]. The perivascular niche contains ECM that is typical to the basement membrane of endothelial cells, including collagen IV, LN, and FN [39,40]. The central marrow contains less ECM than the endosteal and perivascular niche, however FN, LN, HA, and heparin exist within the central marrow at low concentrations [38,39,43].

2.1.5 Biochemical signals in BM

To achieve maintenance, proliferation, and HSCs all within a relatively small environment, BM stromal cells signal through a milieu of soluble, membrane-bound, and ECM bound cytokines and chemokines. We will only briefly discuss a couple of these signals; a number of reviews have explored this topic in greater detail [31,47,48]. CXCL12, secreted by CAR, endothelial and other stromal cells, is a chemoattractant that is bound by cells that express CXCR4 on their surface. The CXCL12-CXCR4 chemokine axis is the primary mechanism by which HSPCs are recruited and maintained within BM. A key component of maintaining HSCs, SCF is expressed by endothelial cells and MSCs and is both secreted and presented to HSCs in a membrane bound form [31,47]. SCF promotes survival and proliferation and activates HSC integrins VLA-4 and VLA-5 and promotes adhesion of HSCs to stromal cells. Other membrane bound signaling proteins include the Notch ligands, Jagged-1 and Jagged-2, which promotes differentiation and proliferation, and is presented on the surface of osteoblasts [49].

Soluble molecules within the BM have also been found to effect HSC behavior [2]. There exists a Ca^{2+} gradient (higher concentration of Ca^{2+} at the endosteal surface) because of calcium deposition that occurs during bone matrix formation. HSCs can bind Ca^{2+} through a calcium-sensing receptor and it effects the ability of HSCs to engraft to the BM niche [28]. The concentration of oxygen has been implicated in maintaining HSC populations by limiting HSC metabolism in a hypoxic environment on the endosteal surface [49]. However, a recent study by Spencer *et al* showed that the endosteal surface is actually less hypoxic than perisinusoidal regions, although the oxygen tension in the bone marrow overall was found to be relatively low [50].

2.1.6 Physical characteristics of BM

Most of hematopoiesis and HSC maintenance occurs in the trabecular region of long bones. Trabecular, or cancellous, bone is characterized by a highly porous, lattice network of bone that is filled with marrow. The topography of the bone surface may be important for creating specific cellular behaviors. The mechanical properties of adult stem cell niches have been examined closely since Engler *et al.* demonstrated that the fate of MSCs is dependent on the stiffness of the surface on which they are grown [51]. The mechanical properties of the three BM niches are quite different and there is a range of material stiffness within BM [52]. The endosteal surface is stiff (>35 kPa) [53], the marrow sinusoids are structured but more compliant (2-10 kPa) [54,55], and the central marrow is very soft (~0.3 kPa) [56].

2.2 Considerations for engineering the BM Niche

There are several variables that need to be considered when designing a biomimetic niche: the type of material (synthetic, natural), the physical properties of the material (stiffness), the topography of the material, the surface chemicals structure, and immobilization of specific ECM or cytokines [57-63]. Here we will discuss recent work that has shown how HSCs respond to these different variables *in vitro*.

2.2.1 Physical properties

2.2.1.1 Substrate stiffness

In 2010, Holst *et al* demonstrated that HSC behavior is dependent on substrate elasticity. HSPCs cultured *ex vivo* on tropoelastin, a highly elastic biomaterial, coated plates were able to expand two- to three- fold times more than HSPCs cultured on tissue culture polystyrene (TCPS) [64]. In addition, in 2009, Adamo *et al* showed that mouse embryonic hematopoiesis is enhanced by fluid shear stress [65]. These two findings, when taken together, suggest that hematopoietic cells are capable of sensing and responding to an environment's physical characteristics.

Since this first evidence of substrate elasticity effect on HSC function, a range of different material stiffness have been tested and HSCs have been found to be responsive to a range of material stiffness that corresponds to the range of mechanical properties found within BM. Several biomaterial culture systems have been used to modulate the physical characteristics of the culture surface while maintaining biochemical function. Murine HSCs cultured on collagen functionalized poly(acrylamide) (PA) substrates were responsive to a range of substrate stiffness from ~0.1 kPa to ~200 kPa. HSPCs cultured on

a soft surface (0.0442 kPa) had greater viability than cells cultured on stiffer surfaces [66]. Similarly, $CD34^+$ HSPCs cultured on FN functionalized, polyvinyl alcohol-co-itaconic acid-coated dishes with elasticity ranging from 12.2 kPa to 30.4 kPa were shown to expand 1.4 times more than $CD34^+$ HSPCs cultured on TCPS [67]. These two experiments indicate that proliferation and viability of HSCs are associated with softer culture surfaces. In contrast, migration of hematopoietic cells appears to be enhanced on stiffer substrates. $CD34^+$ HSPCs cultured on polyethylene glycol diacrylate (PEGDA) hydrogels with surface stiffness corresponding to a higher range of stiffness (20 kPa to 38 kPa) migrated faster on the stiffer (38 kPa) surface, demonstrating that matrix elasticity within the endosteal niche may provide a signal for mobilization [68]. Interestingly, it appears hematopoietic cells are sensitive to small differences in substrate stiffness – even within the range found in the central marrow. A range of stiffness found within the central marrow was tested using collagen matrices with elasticity of 0.05 kPa, 0.2 kPa, and 0.8 kPa; murine LSK cells showed increased proliferation on the 50 Pa substrate and increased clonogenic maintenance on the 800 Pa substrate [69]. The physical properties of a substrate should be considered when designing a hematopoietic culture system. Whether to choose a relatively soft or stiff material depends entirely upon the desired outcome.

2.2.1.2 Spatial Constraint

The effects of spatial constraints on HSCs culture have been tested to determine whether the pore size or surface topography of a material could affect the behavior of HSCs. Microcavities formed by PDMS have been used to isolate HSPCs in spatially constrained cultures. FN was immobilized on amino-silanized PDMS microcavities ranging from 15 μm to 80 μm in diameter. HSCs in smaller microcavities proliferated less

and thus maintained higher levels of multipotent marker expression than those in larger microcavities [70]. The mechanism through which microcavity size impacts cell behavior is unclear. One suggestion is that secreted soluble factors are concentrated in a smaller cavity, changing the biochemical environment of a cell. Another hypothesis is that the cells can physically sense or are impeded by the small size of the cavity during proliferation in culture. The state of differentiation can also affect a cells behavior in a microcavity. Repopulation experiments with lethally irradiated mice established that ST-HSCs were maintained better in single-cell sized microcavities, while LT-HSCs were maintained in small and large microcavities [71]. Spatial constraint may prove to be a powerful tool for maintaining potency of hematopoietic cells *ex vivo*.

2.2.2 Functionalization

2.2.2.1 Surface chemistry

The characteristics of the chemical groups on the surface of a biomaterial can directly interact with a cell through membrane proteins and they can also affect the binding and localization of soluble factors in media and secreted by cultured cells to the material surface. To test the effect of different chemical groups on HSC expansion, Chua *et al* cultured $CD34^+$ HSPCs on a carboxylated, aminated, or hydroxylated poly(ether sulfone) (PES) nanofiber mesh. After 10 days of culture, human $CD34^+$ HSCs cultured on hydroxylated or carboxylated PES nanofiber mesh showed little proliferation, while cells cultured on the aminated surface demonstrated expansion equal to TCPS with better maintenance of colony forming units (CFUs) [72]. The length of the aminated conjugate was also tested by inserting ethylene, butylene, or hexylene spacers. $CD34^+$ HSCs showed greater expansion on ethylene and butylene spacers, while hexylene spacers enhanced

preservation of $CD34^+$ phenotype [73]. The effect of surface amine density was tested by creating PES nanofiber mesh with varying amine density. $CD34^+$ cells had greater expansion on PES nanofiber mesh with higher amine densities [74]. The reason for specific enhancement in HSC culture on aminated surfaces may be due to surface absorption of SCF, which has an isoelectric point of 5.76 and is negatively charged at neutral pH. Overall, these studies suggest that HSPCs are highly sensitive to small changes in the chemistry of the local microenvironment.

2.2.2.2 ECM and cytokine surface immobilization for HSC maintenance and expansion

Significant effort has gone into functionalizing biomaterial surfaces with proteins, GAGs, and cytokines because it has potential to replicate specific signals within the BM environment in a controlled and defined manner. There are a few examples of studies that have tested a panel of functionalized surfaces or have compared the effects of immobilized ECM or cytokines versus presentation in a soluble form. In 2007, Franke *et al* cultured $CD133^+$ HPCs on a number of surface immobilized ECM components (FN, heparin, heparin sulfate, HA, tropocollagen I, co-fibrils of collagen I with heparin and collagen I with HA) [75]. High cell-matrix interactions were observed with FN, heparin, heparin sulfate, and the collagen I co-fibrils; insignificant adhesion and spreading was observed in tropocollagen I and HA cultures. In 2011, Celebi *et al* cultured $CD34^+$ HSCs on TCPS coated with collagens I and IV, LN, FN, a mix of all four ECM proteins, and a mix of collagens IV, LN, and FN to replicate the basement membrane [76]. $CD34^+$ HSCs exhibited relatively similar viability on all the single coated ECM surfaces, although it was observed that FN and LN favored differentiation to erythroid and MK progenitors, respectively. Interestingly, the ECM mix without collagen I showed decreased ability to support

expansion than the complete mixture of ECM proteins.

While studying panels of ECM coated surfaces has helped further our understanding of the role of ECM within BM microenvironments, FN has been the most used and remains the best ECM component for HSC expansion *in vitro* [77-80]. In 1998, Dao *et al* showed that FN coated TCPS was able to support $CD34^+$ HSCs over 72 hours *ex vivo* and sustain LT-HSC populations better than a stromal layer [78]. Similarly, Bhatia *et al* in 2002 compared $CD34^+$ HSC culture with stromal support and on three different integrin binding FN fragments over 7 days and found that culture on FN fragments improved preservation of progenitor potential [79]. Jiang *et al* further explored the effect of different integrin binding FN domains by culturing $CD34^+$ HSCs on two integrin binding FN domains, the CS-1 binding motif (EILDVPST) and RGD motif (GRGDSPC) [77]. Total cell expansion was not increased on CS-1 and RGD functionalized surfaces, however the expansion of $CD34^+$ HSCs was significantly increased in cultures with the two fibronectin fragments, with CS-1 coated surfaces producing the greatest $CD34^+$ HSC fold expansion. Based on these findings, it is believed that HSPCs can bind FN through VLA-4 and VLA-5 integrin, which bind CS-1 and RGD, respectively, and this can impact expansion and maintenance of the cells in *in vitro* cultures.

For presentation of ECM and cytokines, covalent conjugation on the culture surface has many advantages over presentation in a soluble form. From a cost perspective, covalent immobilization generally requires less material to affect cells than soluble presentation or surface absorption because local concentrations at the culture surface are elevated. For ECM components, covalent conjugation of FN and collagen I on PET mesh resulted in 100-fold and 73-fold expansion, respectively, of $CD34^+$ cells after 10 days; however,

soluble FN resulted in a 10-fold expansion and surface absorbed FN induced only 2-fold expansion [77]. Immobilization of cytokines has shown mixed ability to effect HSPCs with similar efficacy as their soluble forms. When RGD and SCF or CXCL12 mixtures were covalently attached to a PEGDA hydrogel, 32D myeloid progenitors expanded equally in the presence of covalently immobilized or soluble SCF. However, migration of 32D cells was significantly increased in the presence of soluble CXCL12 when compared to the surface conjugated form [81]. Functional ECM motifs are typically bound within large networks of ECM proteins and GAGs in the extracellular space and accordingly the covalent conjugation of these components to culture surfaces results in increased biological activity because it likely recreates a more biologically relevant environment. However, cytokines and chemokines can be soluble, membrane bound, or bound to ECM and consequently the context of presentation of these proteins is important to the capacity to elicit a biological response. While SCF can be soluble, it is also presented in a surface-bound form within BM microenvironments and this could explain why surface conjugated SCF is able to produce a strong biological response.

2.2.2.3 ECM components have unique effects on hematopoiesis

The ability of ECM components to support *in vitro* generation of hematopoietic progenitors from HSCs under differentiation conditions has been tested by a number of groups [82-87]. For erythropoiesis (the development of red blood cells), LN has been shown to support $CD34^+$ HSC differentiation toward erythrocytes while FN inhibited the process in an MSC co-culture [82]. For the differentiation of MKs, collagen and LN provide poor surfaces for attachment of megakaryocytic-erythroid progenitors, however FN allows for attachment [83], increases expansion and maturation [84], and promotes

proplatelet formation [85,86]. The difference in ECM ability to support different differentiation pathways underscores the concept of multiple BM niches; separate hematopoietic processes may occur under different microenvironment conditions and biomaterial cultures must be tailored to specific processes and outcomes.

2.3 Examples of biomaterials for in vitro BM niche engineering

Several fabrication techniques have been used to create 3D environments with differing qualities for HSPC culture. Culture platforms have varied from porous scaffolds (scaffolds with pores large enough for cell penetration that represent truly 3D culture), nanofiber scaffolds (fibrous scaffolds with small pore sizes that form a 3D surface, but cells do not penetrate the scaffold), and hydrogels (a polymeric network that encapsulates the cells).

2.3.1 Porous scaffolds

Various materials have been used to create porous scaffolds that mimic the architecture of trabecular bone. With large pore sizes, these scaffolds allow for cellular penetration so that the cells are cultured in a truly 3D environment. In 1992, Wang *et al* reported that collagen microspheres, 500-600 μm in diameter and with 20-40 μm pores, in a perfusion bioreactor supported hematopoiesis for up to 4 months with a continuous output of hematopoietic cells [10]. Tantalum coated porous biomaterials (TCPB), ~300 μm pore size, have been reported to support hematopoiesis in a number of culture conditions [88-91]. $CD34^+$ HSCs have been cultured on TCPB (with and without a coating of FN) in the absence of exogenous cytokines and have shown to have greater expansion than standard BM stromal co-culture [88-91]. TCPB does not have an active biochemical interaction with

cultured hematopoietic cells; the reason for improvement in culture outcomes is attributed to the 3D nature of the culture alone. Numerous porous scaffolds have been used for HSC expansion; these culture systems have generally depended on improved culture conditions of 3D environment compared to 2D culture systems to generate improved expansion and maintenance of HSCs, rather than specific functionalization or replication of niche components. To further replicate the BM niche, stromal co-culture has been employed to directly fulfill stromal signals from the niche. Designing biomaterial-based culture systems for HSC/stroma co-culture requires the surface of the material to have functionality that permits cell adhesion and growth for the stromal layer.

2.3.1.1 Synthetic materials used for porous scaffolds

Except for TCPB, most porous scaffolds have been used to facilitate co-culture of hematopoietic cells with various stromal cells. Nylon [92], borosilicate glass [93], PCL [94], PLGA [94,95], PA inverted colloidal crystal (ICC) [96-98], and PET [99] are some examples of synthetic materials that have been used to support co-culture. These materials have varying pore sizes and surface chemistries that affect the 3D architecture of the culture and the adhesion (and therefore phenotype) of the supporting stromal cells. Differences associated with different surface chemistries of the materials are negligible, as most of the scaffolds are coated or functionalized with an ECM protein or to promote adhesion of the stromal cells. Interestingly, in 2003 Sasaki *et al* assessed the phenotypic differences between murine ST2 stromal cells cultured on a 2D surface and on a polyester nonwoven fabric disk. The authors found no difference in secreted factors (SCF, TPO), but found a significant increase in ECM deposition in the 3D culture [100]. This is the clear advantage of using a 3D porous scaffold in a co-culture system.

2.3.1.2 Natural materials used for porous scaffolds

Natural materials used to create porous scaffolds are typically those that are found in bone. Hydroxyapatite [101], collagen [94], and 'bio-derived bone' [102] HSC/stroma co-culture and have various efficacies that all show improvement over 2D co-culture systems. Hydroxyapatite and 'bio-derived bone' cancellous bone porous scaffolds are the most complete models of the ECM and biochemical environment found in the endosteal niche. Both materials contain calcium and are the only materials discussed here that can establish a gradient of Ca^{2+} within a culture. Although natural biomaterial porous scaffolds have desirable biochemical properties, they are not as easy to manipulate as synthetic materials with regards to modulating physical characteristics (elasticity, pore size) and functionalization.

Recently, decellularized bone has been used as a scaffold for a vascularized BM mimic using a microfluidic perfusion system [103]. ECs and MSCs were co-cultured in the bone matrix and when cultured under physiologically relevant interstitial flow conditions formed tubule structures in the porous space between the decellularized trabecular bone. This is one of the few examples of BM vascular niche engineering in the context of bone, although the bone matrix itself did not contain OBs.

2.3.2 Nanofiber scaffolds

Nanofiber scaffolds have been fabricated using various materials, typically by using electrospinning to deposit the material in a uniform, fibrous mesh. There is limited evidence of cell penetration to within electrospun scaffolds because of small pore sizes within the mesh networks. Culture on nanofiber scaffolds is therefore not a truly 3D environment, although the 'pseudo' 3D environment that is created has been widely shown

to improve upon standard 2D cultures. Several synthetic polymers, including PCL [104], PES [72-74], PET [77], PLGA [94,105], polyester [100,106-108], and PU [109] have been reported to support HSC expansion with or without stromal co-culture. Because synthetic nanofiber scaffolds can be fabricated from a range of materials, with different physical characteristics (fiber size, fiber stiffness), that can be chemically modified to change the biological activity of the scaffold, nanofiber scaffolds are an incredibly useful platform for testing and developing unique engineering BM niches. The incorporation of natural materials into nanofibers for hematopoietic cell culture has been less widely reported [110]. Because nanofiber scaffolds are not truly 3D, they have limited ability to mimic the macro structures of trabecular bone (which may or may not be important to recreating the BM niche). The 'pseudo' 3D structure can also be a positive; because cells do not enter the scaffold, retrieval of cells for analysis or harvest is much easier. Recently, Batnyam *et al* demonstrated that PU nanofiber scaffolds seeded with human BM MSCs and CB $CD34^+$ cells could be layered to create a 3D structure. HSPCs cultured in the layered nanofiber structure had similar expansion to a single layer of PU nanofiber culture, however the 3D layered structure had significantly higher colony forming potential [109].

2.3.3 Hydrogels

An alternative to solid scaffold architecture, hydrogels are mechanically softer and can be constructed from natural materials that are found in the BM; hydrogels offer a useful platform for study of the BM niche, especially the central marrow. Alginate [111], collagen [69], FN [94], gelatin methacrylate [112], and HA [113] have been used to create hydrogels for the encapsulation of HSCs or differentiation of hematopoietic cells. The biological activity of cultured cells is dependent on the hydrogel material and the mechanical

properties of the hydrogels. The hydrogel material is important because they are bioactive and can recreate signals like the ECM microenvironments in BM, without obligatory stromal support. However, stromal co-culture provides many signals that improve cell phenotype *in vitro*. Chitteti *et al* demonstrated that co-culture of calvarial osteoblasts with LSK cells significantly increased expansion and maintenance potency ($Lin^{-}SCA1^{+}$) when compared to LSK cells cultured alone in collagen hydrogels across a range of hydrogel stiffnesses [69]. Most hydrogel systems that have been reported have been constructed using a uniform, single structural component, despite that BM ECM is complex and consists of multiple proteins and GAGs in each microenvironment. Hydrogels have been layered using photopatterning to create composite RGD functionalized PEGDA hydrogels that contained different stromal cells in order to model the bone marrow microenvironment [114]. Mahadik *et al* recently showed that a microfluidic device can be used to generate a gradient hydrogel, with spatially varying concentrations of cells, ECM components, or ECM bound cytokines [115]. These complex approaches to hydrogel construction, that create hydrogels composed of multiple ECM components in a spatially organized manner may be useful for more accurately replicating BM microenvironments *in vitro*.

2.4 Effect of hydrogel stiffness on encapsulated MSCs*

Prior to starting the main body of work in this dissertation, a study was performed that examined the effect of hyaluronic acid hydrogel stiffness on the phenotype of MSCs.

*Adapted from Nelson, M. R., Mejías, J. C., & Roy, K. Low stiffness hyaluronic acid-poly(ethylene glycol) hydrogels increase expression of hematopoietic niche specific factors by human mesenchymal stem cells. *In preparation*.

2.4.1 Introduction

Mesenchymal stromal cells (MSCs) are found in the bone marrow where they are a part of the stromal microenvironment. Not only are MSCs capable of differentiation into other stromal cells, including osteoblasts and adipocytes [116], MSCs actively support the hematopoietic niche and secrete a number of cytokines that direct the fate of hematopoietic stem cells (HSCs) and hematopoietic progenitor cells (HPCs) [8,117]. MSCs express cytokines related to HSC maintenance, including stem cell factor (SCF) (both in soluble and membrane bound forms), and CXCL12 [118,119]. As well, MSCs express cytokines associated with hematopoietic differentiation, including IL-6, which is a key signaling cytokine during B lymphopoiesis [118]. MSCs have been widely used as supporting cells for recapitulating and controlling hematopoiesis in *in vitro* co-culture; both in 2D co-culture systems and in 3D co-cultures on both solid scaffolds and in hydrogels [11,16,18]. Understanding how MSC phenotype changes with the properties of these culture platforms is essential for designing *in vitro* biomaterial based culture platforms that recreate the bone marrow microenvironment.

The extracellular matrix (ECM) in the bone marrow is spatially organized and is a key component in the regulation of hematopoietic function. Fibronectin, collagen, laminin, and hyaluronic acid (HA) have all been identified as important components of bone marrow ECM [39]. HA is an anionic, non-sulfated glycosaminoglycan that in tandem with CXCL12 signaling, plays an important role in the engraftment of HSCs to BM, through binding of surface expressed CD44 [120]. MSC phenotype as a function of interaction with protein components of ECM (fibronectin, collagen) has been characterized in *in vitro* cultures [121-123], comparatively less work has been done exploring how HA-CD44

interactions effect MSC phenotype. HA has been used extensively to create hydrogels for the encapsulation of MSCs for the purpose of differentiation [124,125]. MSCs can migrate on HA surfaces through CD44 binding of the glycosaminoglycan [126], however migration and proliferation are greatly increased through the introduction of RGD peptides [127].

It is well known that the phenotype of MSCs is dependent on the mechanical environment [51]. In the bone marrow, there are distinct microenvironments that have different mechanical properties. The endosteal surface is stiff (~ 35 kPa) [53], the marrow sinusoids are relatively compliant (5-20 kPa) [54], and the central marrow space is much softer ranging from 0.1 to 1 kPa [56]. There are several studies showing that over a large range of surface stiffness, MSCs exhibit different differentiation and secretory properties [51,128]. Less is known about how MSCs respond to changes in the mechanical environment on the scale that is observed within bone marrow. Recent work has shown that osteoblasts cultured on 800 Pa collagen surfaces had improved ability to support proliferation and maintenance of $Lin^{-}Sca\text{-}1^{+}c\text{-}Kit^{+}$ (LSK) cell than those cultured on a 50 Pa surface [69]. However, there is little work examining how MSC phenotype, with regards to establishing the HSCs niche, responds to environments within this mechanical range.

Here, we show that MSCs encapsulated in HA hydrogels respond to differences in mechanical properties that correspond to the range that has been measured for the central marrow. This work has implications for designing biomaterial systems for studying the role of MSCs in the bone marrow microenvironment and for creating culture systems for the support of hematopoiesis.

2.4.2 Methods

2.4.2.1 Cell culture

Human MSCs (RoosterBio) were initially expanded in hMSC High Performance Media Kit (RoosterBio). After initial expansion, MSCS were verified by flow cytometry to be $CD34^-$, $CD45^-$, $CD73^+$, $CD90^+$, and $CD105^+$. For subsequent passages, MSCs were cultured in αMEM (Sigma Aldrich) supplemented with 10% FBS (Hyclone) and 1% Penicillin-Streptomycin (Hyclone). MSCs were cultured at 37 °C and 5% CO_2. For all experiments, MSCs were used at passage 3.

2.4.2.2 HA-PEGDA hydrogel encapsulation

For encapsulation in HA-PEGDA hydrogels, passage 3 MSCs were resuspended in 10 mg/mL HA-thiol (Glycosil, ESI BIO) at a density of $1x10^6$ cells/mL. The HA-thiol cell suspension was mixed 4:1 with 1%, 2%, or 4% (w/v) 3400 Da PEG-DA (Extralink, ESI BIO) to make hydrogels with final concentrations of 0.8% w/v HA and 0.2%, 0.4%, or 0.8% PEGDA. 50 µL of unpolymerized hydrogel cell suspension were transferred to modified 1 mL syringes [129] and hydrogels polymerized over ~30 minutes at room temperature. After polymerization, hydrogels were transferred to a 48-well plate and were cultured at 37 ºC, 5% CO_2 with 1 mL αMEM (Sigma Aldrich) supplemented with 10% FBS (Hyclone) and 1% Penicillin-Streptomycin (Hyclone). Media was exchanged on days 1, 4, 7, and 10.

2.4.2.3 Rheometry

Hydrogel storage and loss moduli was measured by dynamic oscillatory strain and frequency sweeps using an MCR 302 Rheometer (Anton Paar) with a 9 mm diameter 2° cone and plate geometry. Hydrogels were synthesized, allowed to swell in PBS overnight,

and then loaded between the cone and plate. One gel per group was used to determine the linear viscoelastic range of the hydrogel using a strain amplitude sweep with angular frequency of 10 rad/s; strain from the linear portion was then used for the oscillatory frequency sweeps. Frequency sweeps were run with constant strain with ω = 0.1-100 rad/s.

2.4.2.4 MSC viability

Hydrogels were washed with PBS and stained with calcein AM and ethidium homodimer III (EthD-III) (Biotium). Stained hydrogels were imaged on a spinning disk confocal microscope (Perkin Elmer). The number of live and dead cells were counted using ImageJ software [130,131] and the percentage of live cells was calculated by dividing number of calcein AM positive cells by the total (calcein AM and EthD-III) positive cells.

2.4.2.5 Immunohistochemistry

Hydrogels were collected after 10 days culture. Hydrogels were washed with PBS and fixed with 4% paraformaldehyde (ThermoFisher) for 30 minutes. Hydrogels were washed again with PBS and suspended in OCT overnight at 4 ºC before being snap frozen in OCT and stored at -80 ºC.[132] The hydrogels were cut into 20 µm sections using a cryostat (Leica). Sections were blocked (1% goat serum, 0.05% Tween-20 in PBS), stained with rabbit anti-SCF (ab64677, Abcam) overnight at 4 ºC, washed with blocking buffer, and then stained with goat anti-rabbit-AF647 (ThermoFisher). Sections were mounted using Prolong Gold with 4',6-diamidino-2-phenylindole (DAPI) (Life Technologies). Stained hydrogel sections were imaged using a spinning disk confocal microscope (Perkin Elmer). Images were analyzed using Volocity software and representative images were processed using ImageJ software [130,131].

2.4.2.6 ELISA

Supernatants were collected at 1, 4, 7, and 10 days; and stored at -80 ºC until analysis. Standard enzyme-linked immunosorbent assays (ELISA) were performed according to the manufacturer's protocol to detect CXCL12α (SDF-1α), SCF, and IL-6 (Peprotech). Uncultured media samples were used to correct for background in absorbance; absorbance values lesser or equal to background correction are reported as zero values.

2.4.2.7 Statistical analysis

All data in the text are presented as mean ± SEM. Sample numbers are indicated in figure captions. Data were analyzed using GraphPad Prism software. Between group comparisons were performed using two-way analysis of variance (ANOVA) followed by Tukey's post hoc test.

2.4.3 Results

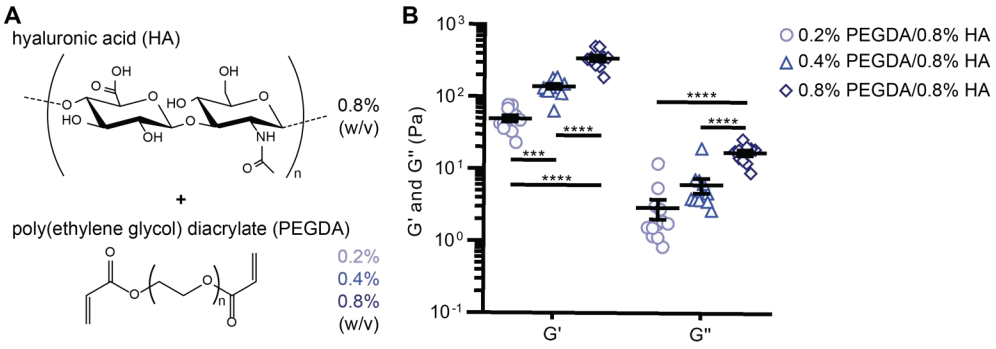

Figure 4. Varying the mechanical properties of HA-PEGDA hydrogels. (A) Hydrogels were made with 0.8% (w/v) hyaluronic acid (HA) and 0.2%, 0.4%, or 0.8% (w/v) poly(ethylene glycol) diacrylate (PEGDA). (B) Storage (G') and loss (G'') moduli of the three HA-PEGDA hydrogel compositions measured by dynamic oscillatory rheological testing. Data are shown as mean ± SEM (n = 13, 11, 10 hydrogels for 0.2%, 0.4%, 0.8% PEGDA, respectively). Data analyzed using one-way ANOVA with Tukey's multiple comparisons test. ***p < 0.001. ****p < 0.0001.

Human MSCs (hMSCs) were encapsulated in HA-PEGDA hydrogels and cultured for a period of 10 days (Figure 5). Viability of the MSCs in the three HA-PEGDA hydrogel compositions was measured to be >90% after 1 day, indicating that there was not significant loss in viability during the hydrogel encapsulation process (Figure 5B). Viability of MSCs declined to between 74% and 78% by day 4. However, viability of the cells was relatively stable up to day 10, when viability was measured to be between 65% and 78% for the three PEGDA concentrations. At day 10, MSCs encapsulated in 0.4% PEGDA w/v hydrogels were measured to have slightly lower viability (65.4% live cells) than the 0.2% w/v and 0.8% w/v hydrogels (78.1% and 77.6%, respectively) (Figure 5A). However, there did not appear to be any trend in increased or decreased viability of MSCs associated with the mechanical properties or concentration of PEGDA of the hydrogels.

To explore the effects of the mechanical properties of the HA-PEGDA hydrogels on functional MSC phenotype, we measured MSC expression of both surface-presented and soluble cytokines after culture in the three different HA-PEGDA hydrogels. After 10 days of culture, MSCs encapsulated in HA-PEGDA hydrogels were fixed and embedded for cryosectioning. Staining of hydrogel sections for SCF showed higher levels of expression in 0.2% PEGDA w/v hydrogels when compared to 0.4% w/v and 0.8% w/v PEGDA hydrogels (Figure 6A and 6Bi). While the average MFI of cells encapsulated in 0.2% PEGDA hydrogels was significantly higher than 0.4% w/v ($p < 0.05$) and 0.8% w/v ($p < 0.01$), when individual cells are analyzed it reveals a large amount of heterogeneity in the encapsulated MSC population (Figure 6Bii). While many cells exhibit similarly low levels of SCF expression in all three hydrogels, there are increasing numbers of MSCs with high expression levels of SCF at lower PEGDA concentrations.

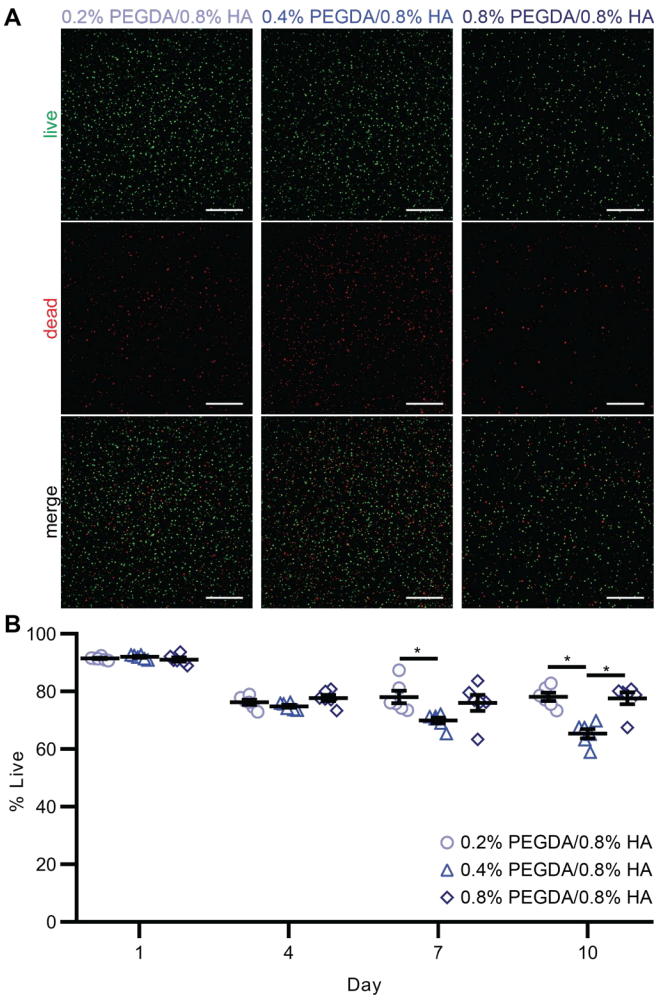

Figure 5. Viability of MSCs encapsulated in HA-PEGDA hydrogels. MSCs encapsulated in HA-PEG hydrogels were stained with calcein AM (live) and EthD-III (dead) to quantify the number of viable MSCs in the hydrogels at 1, 4, 7 and 10 days. Data are shown as mean ± SEM (n = 6 hydrogels). Data are analyzed using two-way ANOVA with Tukey's multiple comparisons test. *$p < 0.05$.

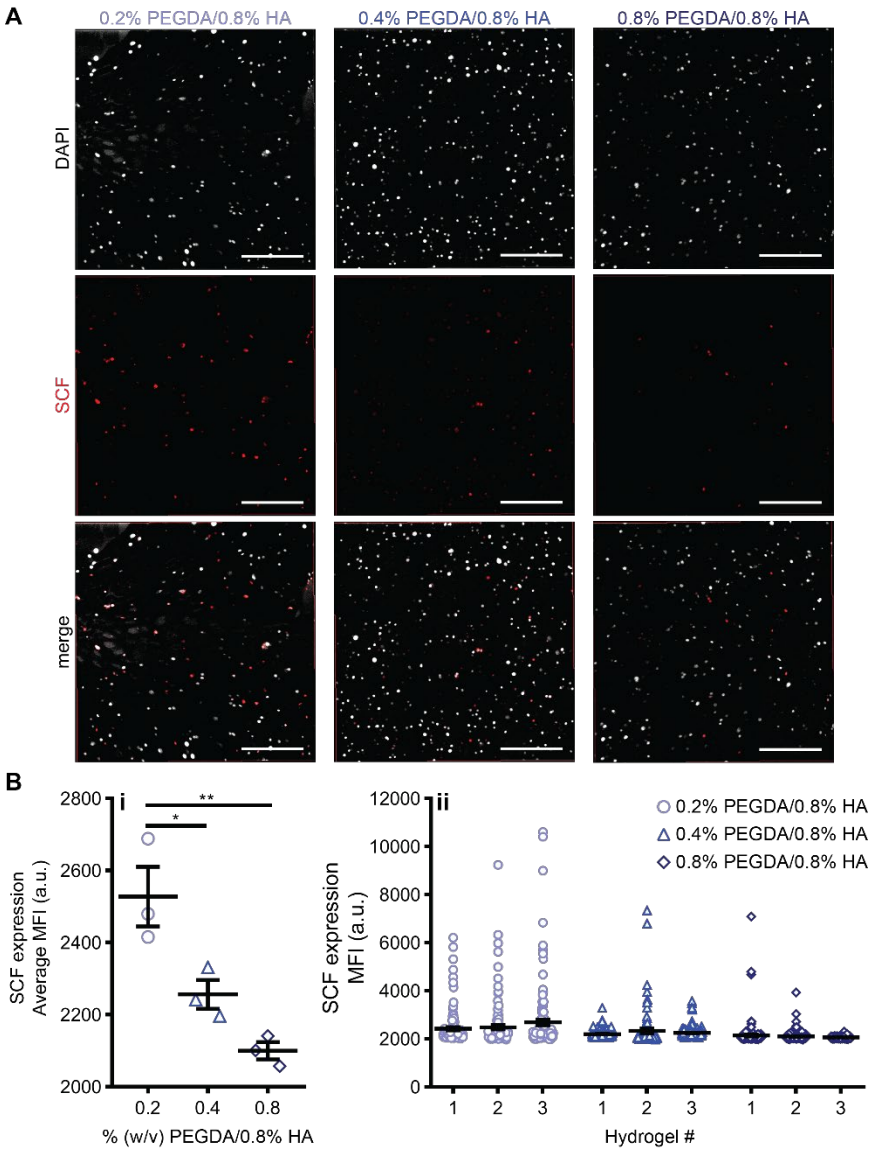

Figure 6. MSCs surface expression of SCF when encapsulated in HA-PEGDA hydrogels. (A) Representative fluorescence microscopy of SCF (red) and DAPI (white) of MSCs encapsulated in HA-PEGDA hydrogels. (B) Quantification of average MFI of SCF staining. Data are shown as mean ± SEM (n = 3 hydrogels). Data are analyzed using one-way ANOVA with Tukey's multiple comparisons test. *p < 0.05. **p < 0.01. (C) Quantification of SCF staining MFI of individual cells shown in (B). Data are shown as mean ± SEM (n =76-256 cells per hydrogel).

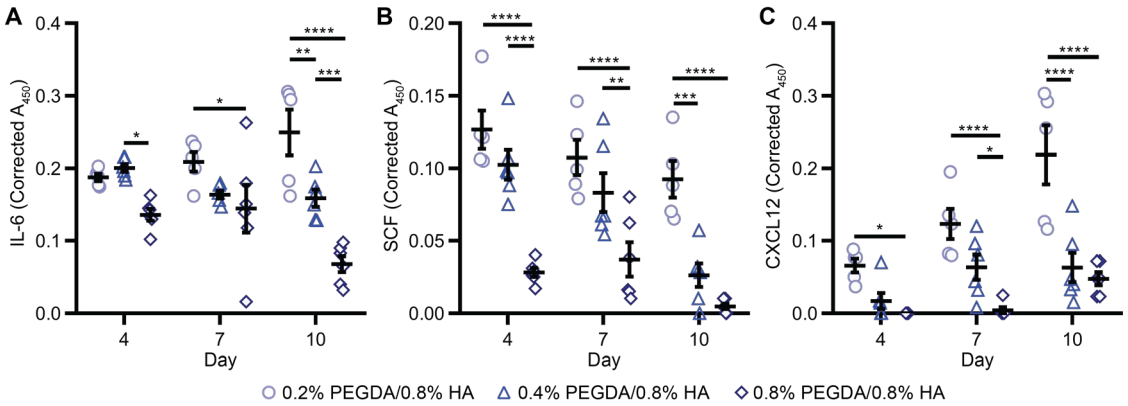

Figure 7. Secretion of cytokines by MSCs encapsulated in HA-PEGDA hydrogels.(A) IL-6, (B) SCF, and (C) CXCL12 detected by ELISA in hydrogel culture media on days 4, 7, and 10. Data are shown as mean ± SEM (n = 5 hydrogels). Data are analyzed using one-way ANOVA with Tukey's multiple comparisons test. *p < 0.05. **p < 0.01. ***p < 0.001. ****p < 0.0001.

Supernatants collected at days 4, 7 and 10 were analyzed by ELISA to determine relative secretion of cytokines relevant to signaling to hematopoietic cells. Overall, low levels of cytokines were detected in supernatant; all three cytokines measured were near the lower limit of the standard curve and therefore reliable concentrations cannot be reported. However, cytokines were detected above background (of uncultured media control) and the background corrected absorbance (450 nm) as measured by ELISA is reported. MSCs encapsulated in lower percentage PEGDA hydrogels secreted higher concentrations of IL-6 (Figure 7A), SCF (Figure 7B), and CXCL12 (Figure 7C) than MSCs secreted in higher percentage PEGDA hydrogels. Additionally, IL-6 and CXCL12 secretion increased in 0.2% PEGDA/0.8% HA hydrogels from day 4 to day 10, conversely SCF secretion decreased over the same time period.

2.4.4 Discussion

The bone marrow microenvironment has non-uniform mechanical properties and accurately modeling the biomechanical niche is important for *in vitro* modeling of the

microenvironment [53,54,56]. While the effect of surface mechanics has been studied across a wide range of surface stiffnesses, relatively less work has been done testing the effect of surface stiffness on the narrow range that is found in the bone marrow microenvironment. Here we have demonstrated that MSC cytokine expression is variable within a narrow, physiologically relevant mechanical range.

The phenotype of MSCs has been shown to be dependent on signals through binding of ECM and the mechanical properties of the local microenvironment [51,128]. The focus of much of the previous work in the field has been on how these factors contribute to the differentiation potential of MSCs; however, we believe that they can also contribute to a MSCs ability to act as a stromal cell in the hematopoietic microenvironment. To our knowledge, there are no studies evaluating MSC cytokine expression within this range of mechanical properties.

Using HA-PEGDA hydrogels, we were able to create hydrogels with elastic mechanical properties from ~50 Pa to ~350 Pa by varying cross-linker density and without changing the concentration of HA. These hydrogels fit within the previously reported range of the elastic modulus for the central marrow region of bone marrow (0.1-1 kPa) [56]. Even within a relatively narrow range of elastic moduli, we found that MSCs had increased expression of hematopoietic niche specific factors in ~50 Pa hydrogels relative to stiffer, ~350 Pa hydrogels. SCF, a surface bound and soluble cytokine responsible for maintaining HSC potency [5,48,133], was expressed more in both forms by MSCs encapsulated in the lower modulus hydrogels. We also measured the secretion of two soluble factors, CXCL12 (or stromal derived factor 1 (SDF1)), a chemokine responsible for maintaining the hematopoietic cells in the bone marrow [34,117], and IL-6, a cytokine responsible for both

the formation of osteoclasts and B cells in bone marrow [134,135]. These findings are complementary to recently reported work that showed osteoblasts supported increased LSK expansion when encapsulated in mechanically stiffer collagen gels within a similar range [69]. This suggests that MSCs and their stromal progeny have differing responses to mechanical stimuli and could serve similar functions in different niches within the bone marrow.

It is worth noting that MSCs do not interact with single ECM components in isolation. It is well reported that the density of RGD binding sites within a material can impact the proliferation and migration behavior of MSCs [127]. In order to fully understand the influence of ECM and mechanical stimuli on stromal cell behavior, more complex hydrogels and scaffolds must be used that recreate a the milieu of ECM in the bone marrow microenvironment [136].

2.4.5 Conclusions

In this work, we evaluated the effect of PEGDA crosslinker concentration and mechanical stiffness on MSC cytokine secretion when cultured in HA-PEGDA hydrogels. By varying the PEGDA concentration, we created HA-PEGDA hydrogels with a range of mechanical properties similar to the central marrow region of bone marrow. MSCs encapsulated in low PEGDA percentage (and low modulus) hydrogels, expressed more surface bound SCF and secreted more soluble IL-6, SCF, and CXCL12. These results suggest that MSCs are responsive to small differences in mechanical properties and that mechanical properties of *in vitro* hematopoietic niche or bone marrow cultures may be fine-tuned to illicit desired phenotypes of stromal cells.

2.5 In vitro differentiation of HSPCs

Differentiation of mature hematopoietic cells from HSPCs has traditionally required large amounts of cytokine supplementation or very specific stromal cell support and the yet these cultures have typically had relatively low yield. Biomaterial approaches for differentiation may allow for 3D cultures with greater culture surface area for cell growth that could reduce the cost of cytokine addition, the functionalization of materials to increase the efficiency of signaling to cultured cells, and the creation of physical environments that are essential to the desired phenotype. Early *ex vivo* differentiation work used porous scaffold to test for improved efficacy over traditional 2D cultures. Using a relatively simple packed-bed reactor of macroporous collagen microspheres, low concentrations of erythropoietin were able to sustain erythropoiesis in BM cultures over several weeks [137]. Long-term erythropoiesis has been achieved using a 3D hollow fiber reactor with minimal input of exogenous cytokines [138]. This approach created a heterogeneous and diverse BM-like microenvironment of stromal and hematopoietic cells that supported physiologically relevant cell densities and ongoing production of erythrocytes. Differentiation of adaptive immune system cells (T and B cells) has been achieved in porous scaffold co-culture systems with differentiation specific cytokine addition. Using a PA ICC scaffold, co-culture of BM stroma and $CD34^+$ HSCs produced mature B-lymphocytes after 14 days [96]. In a TCPB co-culture with murine thymic stroma, Poznansky *et al* were able to generate 70% $CD3^+$ T cells from $CD34^+$ progenitors and improve yield over a monolayer co-culture by 3-fold [139]. Stromal contact is not necessary for lymphocyte differentiation and the signals can be replaced by functionalized material surfaces. Previous research by our group has shown that immobilization of Notch

ligands on magnetic microbeads or TCPS can replace direct stromal contact for the *in vitro* differentiation of LSK [140] or $CD34^+$ HSCs [141] to T lymphocytes.

Many materials-based systems have been designed for the differentiation of MKs for platelet production. 3D woven polyester fabric, PA ICC scaffold [97], aminated PES nanofiber [142], and pullulan/dextran hydrogel [143] cultures have all been used for $CD34^+$ HSC differentiation to MKs and supported the production of platelets over days and weeks of culture. One of the more complete spatial models of BM has been designed for the culture of MKs for sustained production of platelets. In 2011, the Balduini lab reported the development of a culture system composed of a collagen I gel that surrounds a silk micro-tube (marrow sinusoids) perfused with media [144]. Porous silk micro-tubes were prepared by dipping stainless steel wire into silk fibroin solutions containing poly(ethylene oxide) and then coated with various ECM proteins. In 2015, they further reported creating endothelialized silk micro-tubes in a similar manner [145]. This culture device allows for culture of MKs in a perivascular niche that closely mimics the *in vivo* biology. While there are a handful of other perivascular niche, fluidic models [146,147], the Balduini lab's MK perivascular niche model is one of the only known reported culture system to recreate the BM perivascular niche *in vitro*. Platforms like these could be created to model other hematopoietic cell niches in the BM or to create more complete BM cultures.

2.6 In vivo niche engineering

Another strategy for BM niche engineering has been the creation of ectopic BM in live animal models. By implanting scaffolds or hydrogels that are pre-seeded with stromal cells or that contain growth factors or cytokines for the recruitment of stroma, implants can

recruit hematopoietic cells from circulation and become vascularized to create an additional BM niche within the animal. In 2002, Krupnick *et al* showed that ectopic BM can be formed with as little as implanting BM cells and bone fragments suspended in a collagen type I gel [148]. Collagen scaffolds, heparinized to bind SDF1, implanted into mice are able to recruit a number of HPCs and stromal cells to create a microenvironment that can support differentiation of a limited number of hematopoietic cell types [149]. The use of collagen to create ectopic BM was further developed by the Ingber group in 2014; they showed that an implanted a collagen gel (loaded with demineralized bone powder, bone morphogenic protein 2 and 4) inside of a PDMS mold could form an ectopic marrow that could be removed an cultured *ex vivo* in a microfluidic device for up to 7 days [150]. Other scaffolds (including PA ICC [98] and PCL [104]) have also been used for the foundation of ectopic BM formation. This is a promising technique for the generation of an intricate BM niche that may be extremely useful for furthering the study of the BM niche. Although humanized ectopic BM implants have been produced [104] and further research may prove otherwise, this approach to BM engineering may be limited due to zoogenic complications and costs associated with animal intermediates.

2.7 Summary

A viable engineered bone marrow model would be beneficial for advancing knowledge of the BM niche and could potentially be used for several clinical applications, although we are years away from any significant, direct clinical translation. The largest target for biomaterial-based BM niche clinical applications is the *ex vivo* expansion of HSCs for transplant. However, recently reported methods of *ex vivo* expansion of HSCs in

clinical trials use simple 2D MSC co-culture or soluble factors only [151]. Several innovations in the applications of materials chemistry toward HSC culture have furthered our understanding of HSC dependence on several variables in *in vitro* culture; although, our understanding of the BM niche is not complete, and we are still not able to fully replicate BM. Further studies of HSPC interaction and behavior when cultured on materials that mimic complex ECM microenvironments and stromal cell membrane presented factors are needed. Various tools are now available to researchers to answer these questions with much richer metrics than total culture expansion or formation of CFUs. The development of microcavity cultures will be useful for studying HSPC interaction with complex ECM environments [152] and could also be employed for studying stromal cell interactions while tracking single-cell fates [153], and thus supplying richer methods of evaluation. Microcavities can be a practical for screening single aspects of *in vitro* HSPC culture for optimizing several culture parameters. Microfluidics will also be an important instrument for studying specific BM niche conditions because controlled gradients of cytokines, ECM, or stromal co-culture cells can be established within these devices [115,154]. These methods need to be fully utilized for our understanding of the HSC niche to approach a complete model.

To create a culture system that replicates the entirety of the BM environment, including the various HSPC niches, a composite culture is likely to be required because of the discontinuous environment of BM. Over the last twenty years, most studies have focused on the mimicking the endosteal niche (partly due to the previous understanding of the location of the HSC niche). As our understanding of the niche changes, so must the *in vitro* culture systems that attempt to replicate *in vivo* behavior. The endotheliazed BM

niche for MKs [145] and the vascularized decellularized bone [103] are first steps in studying this niche and the role it plays with respect to maintaining and directing HSPCs. Studying the cross-talk between stromal and hematopoietic cells that exist within these distinct niches will also be important as we try to assemble a complete model of BM [114,155]. Not all applications require a complete replicate of the BM; applications requiring expansion or differentiation of specific cell types may only require a single niche mimic, however these culture systems would also benefit from a wider understanding of the interaction between HSPC niches and how hematopoiesis is regulated *in vivo*. For these models to be developed, materials are required that can be tuned to replicate specific chemical, biological, and physical attributes of the BM niche.

CHAPTER 3. AIM 1A: DESIGN AND FABRICATION

3.1 Introduction

Microfluidic systems have been developed over the last 20 years for a wide variety of laboratory applications [156-160]. While standard, 2D cell culture techniques are simple and reliable, they do not allow for the complex, 3D arrangement of cells and ECM that can be achieved using microfluidic platforms. Organ-on-a-chip platforms that replicate basic 3D physiologic structures have been developed for lungs [161], gut [162], kidney [163], eye [164], and many other organ or tissue systems. These organ platforms have even been integrated together to create "human-on-a-chip" systems, composed of up to 10 interconnected organ models [165]. The design of several organ-on-chips rely on microfabrication of environments that create controlled barriers between, or arrangement of specific cell types that replicate the basic structures of native tissues.

PDMS has been an instrumental material for the development of microfluidic platforms in the laboratory setting. As a material for platform development, PDMS when used in soft lithography has many advantages, (1) it allows for rapid prototyping of microfluidic designs, (2) it is relatively inexpensive, (3) it is gas permeable allowing for prolonged cell culture, and (4) it is optically transparent which permits in-process imaging of the cells. However, there are some disadvantages to using PDMS as a cell culture material. PDMS can absorb small hydrophobic molecules, which can be problematic in drug screening applications [166]. Additionally, untreated PDMS is hydrophobic and does not readily support the attachment of adherent cells to its surface unless it is treated to promote sustained adsorption of adhesion proteins to the surface. Despite these drawbacks,

they are outweighed by the advantageous of using PDMS and it is widely used for the early development of organ-on-a-chip platforms.

The first and most widely used design of organ-on-chips consists of two channels, one on top of the other, separated by a membrane [161]. Recently, there has been work focused on creating multiple, interconnected microenvironments within a single microfluidic device without the use of a porous membrane to separate the discrete microenvironments. Microfluidic devices with PDMS posts separating adjacent channels allow for the controlled loading and placement of distinct hydrogels that can be seeded with different cell types to create complex arrangements of cells and environments [167]. Variations of this design, with a central hydrogel channel and flanking media channels, have been used extensively for angiogenesis and vasculogenesis studies where endothelial cells are cultured within a hydrogel in a central channel and are stimulated by cytokines or stromal cells (typically fibroblasts) situated in flanking hydrogel channels [147,168-171]. Compared with the more widely used approach of isolating endothelial cells in an entirely separate channel with a permeable barrier connecting the environments, using PDMS posts to create a 3D, hydrogel environment creates microvasculature that better mimics the structures found in native tissues.

Using a previously published approach for the basic design of the microfluidic device, here we present the design and fabrication methods of an hBM-on-a-chip device that supports the culture of both the endosteal niche and the perivascular niche. In addition, we implemented multiple techniques that progressed the device fabrication from a prototype, small-scale process to a reproducible, medium-scale process that enables the integration of hBM-on-a-chip into a standard well-plate format.

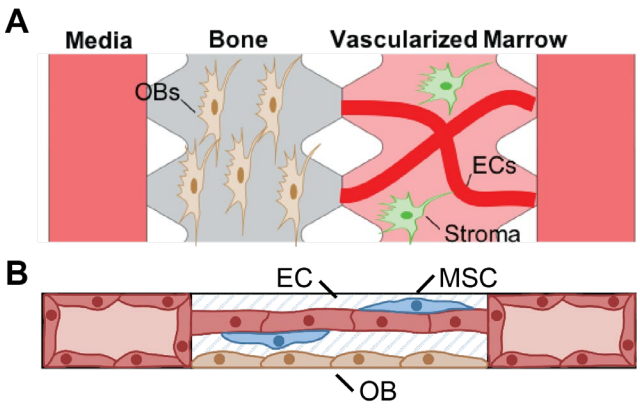

Figure 8. Early iterations of hBM-on-a-chip design. (A) Horizontal orientation of the endosteal and vascularized marrow niches in a 4-channel device resulted in inconsistencies in hydrogel interface formation and in incomplete formation of the endosteal niche. (B) A 3-channel device with vertically arranged endosteal and vascularized marrow niches eliminated the problems associated with the horizontal hBM-on-a-chip.

3.2 Results

3.2.1 Iterations of hBM-on-a-chip design

Our first design of hBM-on-a-chip consisted of horizontally adjacent channels that were to contain distinct bone and vascularized marrow microenvironments (Figure 8A). MSCs were first differentiated into osteoblasts for 10 days on TCPS and then loaded into the device in a collagen type I hydrogel. Subsequently, human umbilical vein endothelial cells (HUVECs) and MSCs were loaded within a fibrin hydrogel in the adjacent channel to form the "vascularized marrow" of the device. While this approach offered many advantages, including microenvironments separated in the x-y plane that could allow for clear delineation of the marrow microenvironments, there were several technical challenges that ultimately led to the redesign of the device. Among the technical challenges in implanting this design were: (1) delamination and ultimately collapse of the collagen type I hydrogel culture due to the contractile pull of the OBs; (2) difficulty achieving a

reliable interface between the two hydrogels (Figure 9A); and (3) incomplete formation of the endosteal niche because the hydrogels are loaded at the same time and there is no opportunity for prolonged culture of OBs (Figure 9B).

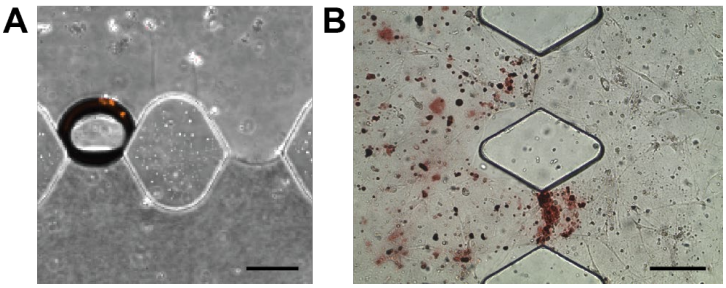

Figure 9. Limitations of horizontal arrangement of hBM-on-a-chip. (A) The interface between collagen (lower) and fibrin (upper) hydrogels was inconsistent and would frequently form air bubbles. (B) Alizarin red staining in endosteal niche (left) after 5 days of culture was minimal compared to marrow niche (right). Scale bar: 100 μm.

To overcome these limitations, a second generation of the hBM-on-a-chip was designed (Figure 8B). In the redesigned device, OBs were first seeded on the surface of the central channel and then HUVECs and MSCs were subsequently seeded on top of the "endosteal surface." This change in device designed addressed the technical challenges discussed above by: (1 & 2) OBs were no longer culture within a collagen type I hydrogel, but rather they were cultured on the PDMS surface, this eliminated hydrogel contraction and interface problems; and (3) eliminating the need for seeding the HUVECs and MSCs at the same time as the OBs allowed for prolonged culture of OBs and development of an endosteal niche. This redesign was successful, however a small alteration was made by adding outer hydrogel channels for the loading of stromal cells that supported vasculogenesis [170].

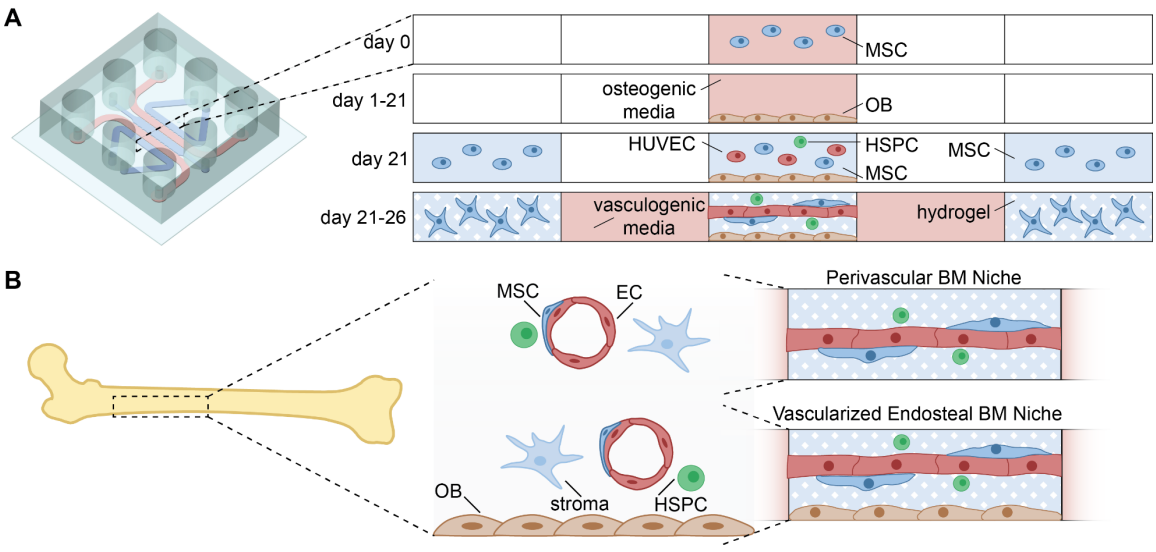

Figure 10. Approach for hBM-on-a-chip. (A) A 5-channel PDMS microfluidic device was fabricated using standard soft lithography techniques. MSCs are first differentiated for 21 days in the central channel of the device to form an endosteal layer, then HUVECs, MSCs, and HSPCs are loaded on top of the endosteal layer and vasculogenesis occurs over 5 days to form the hBM-on-a-chip. (B) The hBM-on-a-chip can recapitulate both the central perivascular BM niche (without OBs) and the vascularized endosteal BM niche (with OBs) that are found in the cavities of long bones.

3.2.2 Design of hBM-on-a-chip with simple, in-vitro design

A five-channel device was designed and fabricated with a height of 120-150 µm and consists of one central gel channel, two media channels, and two outer gel channels (Figure 10 and Figure 11). The process for culturing cells and creating the BM microenvironment involved first seeding MSCs in the central channel where the MSCs are differentiated over 21 days to form the endosteal niche. Second, HUVECs, MSCs and HSPCs were seeded on top of the endosteal layer and cultured for 5 days to allow for vascular formation prior to experimentation. The device was designed similarly to recently published methods [170,171], but with modifications that (1) promoted maintenance of the air-liquid interface between the central channel and adjacent media channels, and (2) allowed for loading of cells and hydrogel precursors into a previously wetted channel.

Essential to this approach is the ability to wet the central channel during the differentiation of MSCs while keeping the adjacent media channels dry throughout the process so that a second set of cells can be loaded within the central channel. To achieve this, the pores between the gel channels were narrowed (compared to similar, previously published devices) to 50 μm in width and the number of communication pores was limited to decrease the occurrence of media leaking from the central channel during osteogenesis (Figure 11C-E). Additionally, many previously published devices of similar design use a glass coverslip as a bottom surface of the device. However, glass is more hydrophilic than PDMS, and using glass as the bottom surface would not permit extended maintenance of the air-liquid interface between channels during extended culture. To overcome this, a PDMS surface (either a PDMS coated coverslip or a thin PDMS film) was used as the bottom surface of hBM-on-a-chip. With these modifications, the difference between advancing pressure and burst pressure is substantial, it was calculated to be 282 mmH_2O which allows for simple manual loading of fluid into the device without leakage into the adjacent media channels. However, the extended culture of the devices in a humid environment results in wetting of interior, dry surfaces of PDMS that leads to "failure" of the devices by leakage of the culture media into the adjacent media channels, which prevents subsequent isolated loading of cells in the central channel. This was mitigated by thorough cleaning of the devices with 70% EtOH and t drying overnight at 65 ºC and produced devices that "survived" the 21-day culture at a rate >90% (Figure 13).

To culture cells for a prolonged period and then load cells into the previously wetted channel, the central channel required both a media reservoir, to contain enough media during culture, and an accessible loading port (Figure 11B). This feature differentiates this

device from previously published methods, which do not require both prolonged culture prior to loading of a hydrogel and therefore can use only a single 1 mm loading port for the hydrogel channels. To include this design criteria into the PDMS device, it was necessary to adapt a multi-step approach to fabrication.

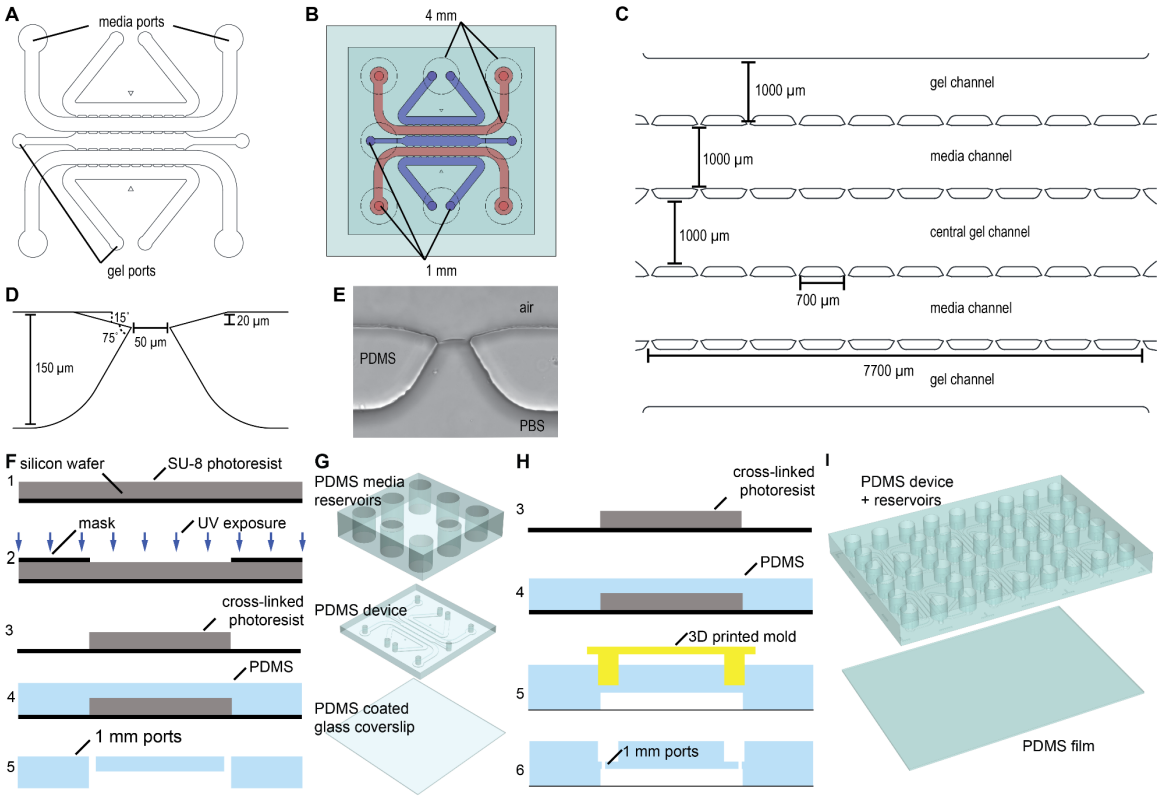

Figure 11. Design details and fabrication process of v1.0 and v1.1 hBM-on-a-chip. (A) The 5-channel PDMS microfluidic device was accessible through 1-mm gel loading ports (for central and outer channels) and media loading ports. (B) These 1-mm loading ports were accessible through 4-mm media reservoirs that permitted sustained culture in media using both the central channel (during osteogenesis) and the media channels (during vasculogenesis). (C) Each channel has a width of 1000 µm and the channels are connected via 11 communication pores that are formed by 10 posts. (D) The communication pores are 50 µm in width and are designed to enable consistent formation of air-liquid-interface. (E) Example of air-liquid interface formed at a communication pore. (F) For v1.0, PDMS features were fabricated using standard soft lithography techniques. (1) A silicon wafer was spun coat with SU-8 photoresist, (2) exposed to UV light through a patterned photomask and (3) then the uncrosslinked SU-8 was removed leaving the patterned, SU-8 master mold. Then, (4) PDMS was cast on the SU-8 master mold and loading ports were created in the PDMS device layer. (G) The PDMS device layer was bonded to a PDMS media reservoir layer and to a PDMS coated coverslip to create a finished device. (H) For v1.1, the initial steps of fabrication (1-4) were unchanged from version 1.0. (5) To form the media reservoirs, a 3D printed mold was placed on top of the PDMS device layer and additional PDMS was cast to form the media reservoirs, after which (6) loading ports were made. (I) The PDMS device/media reservoir layer was plasma bonded to a thin PDMS film and cut into individual devices.

Table 1. Version 1.0 device fabrication.

Step	Description	Time (per device)	Efficiency	Variability
Cast PDMS on SU-8 master mold	• Mix PDMS 10:1 • Pour and degas • Cure at 65 ºC	1	100%	Low
Cast PDMS reservoir layer	• Mix PDMS 10:1 • Pour and degas • Cure at 65 ºC • 20 devices per batch	0.5	100%	Low
Cut + punch ports in device layer	• Punch ports • Cut devices	0.5	100%	Low
Cut + punch holes in reservoir layer	• Cut devices • Punch holes	0.5	90%	Low
Plasma bond device layer to reservoir layer	• Plasma activate • Align and bond • 3 devices/batch	1	90%	Low
PDMS coat coverslips	• Coat coverslips • Cure at 65 ºC	0.5	80%	High
Plasma bond device to reservoir to coverslip	• Plasma activate • Align and bond • 3 devices/batch	1	90%	High
	TOTAL	**5 min**	**58%**	**High**

Table 2. Version 1.1 device fabrication.

Step	Description	Time (per device)	Efficiency	Variability
Cast PDMS on SU-8 master mold	• Mix PDMS 10:1 • Pour and degas • Cure at 65 ºC	1	100%	Low
Cast PDMS reservoir layer w/ 3D printed mold	• Mix PDMS 10:1 • Place 3D-printed mold • Pour PDMS • Cure at 65 ºC	1	90%	Medium
Punch holes in device layer	• Remove PDMS from 3-D printed mold • Punch holes • Cut devices	0.5	100%	Low
Cast PDMS film	• Coat petri dish • Cure at 65 ºC	0.5	100%	Low
Plasma bond PDMS device to PDMS film	• Plasma activate • Align and bond • 12 devices/batch	0.25	95%	Low
Cut individual devices		0.25	100%	Low
	TOTAL	**3.5 min**	**86%**	**Medium**

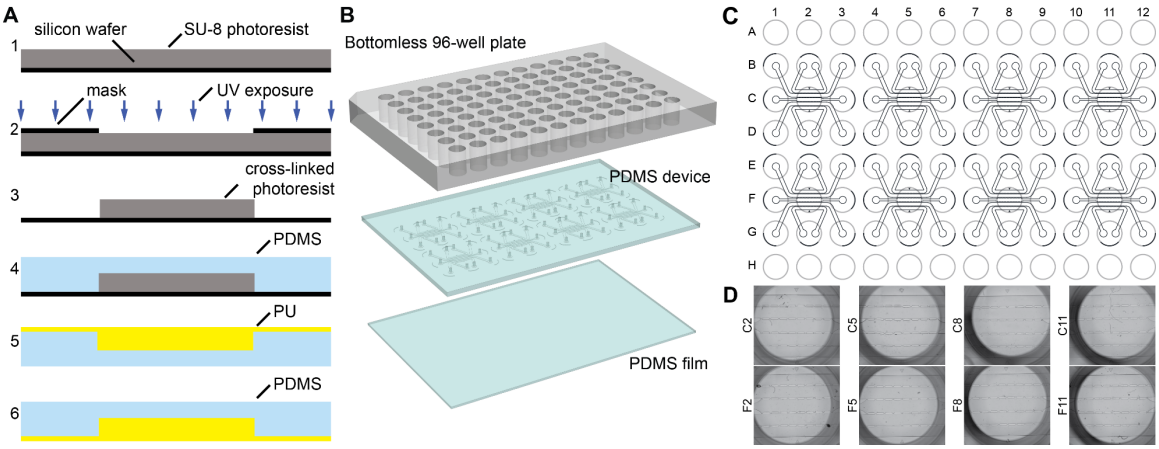

Figure 12. v2.0 device fabrication. (A) The initial steps of fabrication (1-4) were unchanged from v1.0. To assemble a 2x4 array of devices, a polyurethane master mold was cast from two 2x2 device arrays. (B) The device layer of PDMS was first bonded to a thin PDMS film, then using a chemical gluing technique, the device layer was bonded to a bottomless 96-well plate. (C) The resulting device created a 2x4 array of devices that utilizes the wells of the well plate as media reservoirs, loading ports, and imaging windows. (D) Alignment of the devices creates 8 uniform devices in a single, standard well plate format.

Table 3. Version 2.0 device fabrication.

Step	Description	Time (per device)	Efficiency	Variability
Cast PDMS on SU-8 master mold	• Mix PDMS 10:1 • Pour and degas • Cure at 65 ºC	1	100%	Low
Punch holes in PDMS device layer	• Punch holes • Cut devices	0.5	100%	Low
Cast PDMS film	• Coat petri dish • Cure at 65 °C	0.5	100%	Low
Plasma bond PDMS device to film	• Plasma activate • Align and bond • 8 devices/batch	0.38	100%	Low
Plasma bond PDMS device to 96-well plate	• Silane treat plate • Plasma activate • Align and bond 8 devices/batch	0.38	100%	Low
Plasma bond cover glass to device	• Plasma activate • Align and bond • 8 devices/batch	0.38	100%	Low
	TOTAL	**3.14 min**	**100%**	**Low**

3.2.3 High-throughput fabrication of hBM-on-a-Chip

During our initial studies, we approached this challenge by fabrication a 3-layer PDMS device (Figure 11F, G) consisting of (1) a PDMS coated glass coverslip, (2) a middle-feature layer, and (3) a reservoir layer. This fabrication method was appropriate and useful for initial studies because it allowed for fabrication of individual devices while failure rates were high, and its modular composition permitted parallel iteration of the component parts. However, as the design because finalized, this fabrication method proved to be inefficient, time intensive, and generated variable final products (Table 1). The individual coating of coverslips with PDMS produced non-uniform surfaces and the bonding of these coverslips to the device created devices that were not consistently oriented with respect to the coverslip, which impaired downstream imaging and analysis because each device was uniquely oriented.

To improve efficiency of fabrication, we developed a simplified method that combined the feature layer and the reservoir layer through a two-step PDMS casting protocol where a 3D printed mold was used to create media reservoirs (Figure 11H, I). This fabrication protocol substantially decreased device fabrication time and increased material efficiency (Table 2). Additionally, the PDMS coated glass coverslip was replaced with a thin PDMS film that creates a more uniform surface and decreased device variability.

To further improve on the design and standardization of hBM-on-a-chip, a microfluidic platform was developed to integrate the platform into a standard, well-plate format. Using previously published methods [172-174], the PDMS "device" layer was bonded directly to a commercially available, bottomless 96-well plate (Figure 12A, B). The resulting array of 8 devices uses the wells of the plate as media reservoirs and as a window

for imaging the central channel of the device (Figure 12C). This process creates an array of devices that are consistently oriented within known well locations, making the platform easily transferable to automated imaging, or potentially, media handling instrumentation. An unexpected benefit of moving to this fabrication method was the increased "survival" of devices during the 21-day differentiation of MSCs. Most likely because the PDMS portion of the construct is fixed to a rigid polystyrene frame, there are no longer small deformations due to handling of the devices during loading and culture, which results in a much lower frequency, less than 5%, of device "failure".

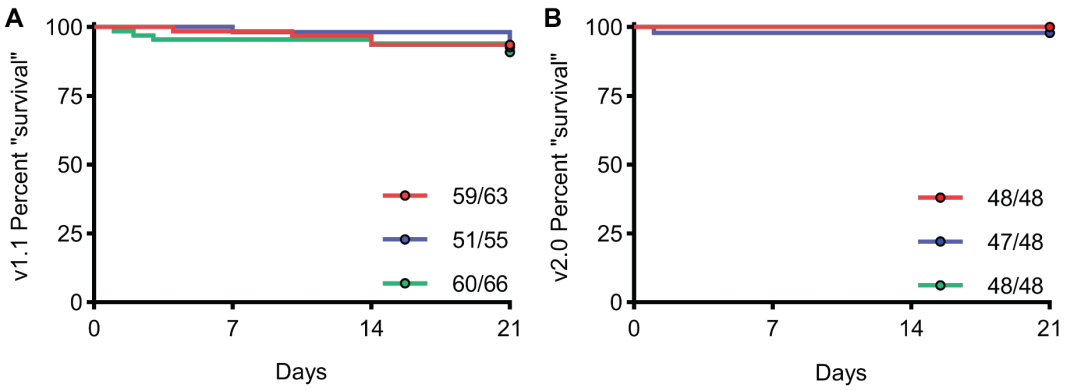

Figure 13. "Survival" of devices during 21-day differentiation. "Survival" of viable devices using (A) v1.1 and (B) v2.0 hBM-on-a-chip device. Devices "fail" when media leaks from the central channel into adjacent media channels, rendering it impossible to isolate the central channel when loading cells on top of the endosteal layer.

3.2.4 Enabling cell attachment to PDMS surface

A challenge that had to be overcome for this approach was the sustained adhesion of MSCs to the PDMS surface during differentiation to OBs. Untreated PDMS is hydrophobic and does not support the attachment of adherent cells [175]. To allow for cell attachment, the surface must be treated or coated with an ECM protein. We investigated

the coating of the PDMS surface with collagen type I and FN (Figure 14) and found that fibronectin allowed for moderate initial adhesion, while collagen type I marginally improved adhesion over PDMS alone. We then attempted a previously published approach for improving PDMS coating where the PDMS is first coated with polydopamine (0.01%) which improves the adsorption of collagen type I to the PDMS surface. Using this technique, we observed substantially improved adhesion of MSCs to the PDMS surface after 24 hours.

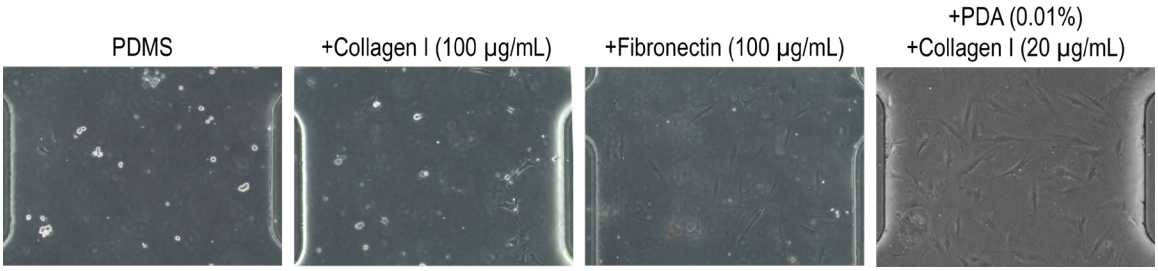

Figure 14. ECM coating to promote MSC adhesion to PDMS. Phase contrast images of MSCs 24 hours after seeding in PDMS hBM-on-a-chip devices that were uncoated or coated with collagen 1 (100 µg/mL), fibronectin (100 µg/mL), or PDA (0.01%) and collagen I (20 µg/mL).

3.3 Methods

3.3.1 Photomask design

Photomasks (CAD/Art Services) were designed using AutoCAD software (Autodesk). Photomasks were specified as right-read, darkfield, emulsion down. A detailed description of photomask design criteria can be found in Appendix B.

3.3.2 Soft lithography

An SU-8 master mold was fabricated using previously described soft lithography

techniques [176]. Briefly, SU-8 2150 (MicroChem) was spun to a thickness of ~120 μm on a silicon wafer (University Wafers) using a G3P8 Spin Coater (SCS). SU-8 was exposed with UV light through the photomask using an MJB4 mask aligner (Suss Microtec). Uncrosslinked SU-8 was removed with SU-8 developer (MicroChem) and silicon wafers were treated by vapor phase deposition of trichloro(1H,1H,2H,2H-perfluorooctyl silane (Sigma-Aldrich) to increase surface hydrophobicity. A detailed protocol can be found in Appendix B.

3.3.3 PDMS device fabrication

3.3.3.1 Version 1.0 device fabrication

PDMS (Dow Corning) was mixed 10:1 (elastomer base: curing agent) and cast on SU-8 master mold. PDMS was cured at 65 °C. The PDMS layer containing the features was then removed from the master mold and loading ports were made using a 1 mm biopsy punch (Integra Miltex). To form the media reservoir layer, PDMS was mixed 10:1 and cast in a 100 mm petri dish to a thickness of 5-6 mm. PDMS was cured at 65 °C. The thick disc of PDMS was then cut into single-device sized squares and media reservoirs were made using a 4 mm biopsy punch. The top surface of the device layer was then bonded to the media reservoir layer using a plasma cleaner (Harrick Plasma). To form the PDMS coated coverslips, PDMS was mixed 10:1 and 50 μL were applied to a clean glass coverslip, the coverslip was then sheared against a glass slide to evenly coat the surface and the PDMS was cured at 65 °C. The PDMS coated coverslip was then bonded to the bottom surface of the device layer using a plasma cleaner (Figure 11). Prior to use, devices were washed with 70% EtOH.

3.3.3.2 Version 1.1 device fabrication

PDMS was mixed 10:1 and cast on SU-8 master mold. PDMS was cured at 65 ºC. The PDMS layer containing the features was then removed from the master mold, a 3D printed reservoir mold was aligned on top and additional PMDS (10:1) was poured on top of the device to form media reservoirs. After curing at 65 ºC, loading ports were made using 1 mm biopsy punch. A thin film of PDMS was made by mixing PDMS 5:1, casting a thin layer (~300 μm) in a 150 mm petri dish and curing at 65 °C. Devices were bonded to the thin film of PDMS using a plasma cleaner, and individual devices were cut for use in cell culture (Figure 11). Prior to use, devices were washed with 70% EtOH.

3.3.3.3 Version 2.0 device fabrication

hBM-on-a-chip was integrated into a standard well-plate format using previously published methods (Figure 12) [172-174]. Because a standard 100 mm silicon wafer does not have enough area to pattern the entire 4x2 hBM-on-a-chip array (Figure 45), a polyurethane master mold was first fabricated from PDMS cast on a SU-8 master. PDMS was mixed 10:1 (elastomer base: curing agent) and cast on the SU-8 master mold () to create two copies of the 2x2 array. The two pieces were aligned, feature-side down, and made into a single block by casting in additional PDMS. A polyurethane master mold was then cast on the single PDMS piece containing the 4x2 array using a 2-part polyurethane liquid plastic (Smooth Cast 310, Smooth-On Inc.) [173]. To prevent adhesion of PDMS subsequently cast, the polyurethane master mold was treated by vapor phase deposition of trichloro(1H,1H,2H,2H-perfluorooctyl) silane (Sigma-Aldrich).

PDMS was mixed 10:1, cast on the polyurethane master mold, and cured at 65 °C. The PDMS layer containing the features was then removed from the master mold and

loading ports were made using a 1 mm biopsy punch. A thin film of PDMS was made by mixing PDMS 5:1, casting a thin layer (~600 µm) in a 150 mm petri dish and curing at 65 °C. The feature layer of PDMS was then bonded to the PDMS film using a plasma cleaner. The bonded PDMS devices were then attached to a bottomless 96-well plate (Greiner Bio-One) using a chemical gluing method [174]. Briefly, the 96-well plate was immersed in 2% (v/v) 3-mercaptopropyl trimethoxysilane (Sigma-Aldrich) in methanol for 1 minute, rinsed with deionized H_2O, and dried. The bonded PDMS devices were then plasma bonded to the 96-well plate using a plasma cleaner. To provide support to the bottom PDMS surface, glass coverslips (Fisher Scientific) were adhered to the PDMS film by plasma bonding. Prior to use, devices were washed with 70% EtOH and DI H_2O.

3.3.4 Burst pressure calculations

Burst pressure was calculated using an approached described by Wang *et al*. 2016, which is briefly described below [177]. The pressure difference at the air-liquid interface for advancing liquid within the gel channel can be represented by the Young-Laplace equation (Equation 1):

$$P_{liquid\ advance} - P_{air} = -2\gamma\left(\frac{cos\theta_A}{w_{channel}} + \frac{cos\theta_A}{h}\right) \quad (1)$$

Where $P_{liquid\ advance}$ is the liquid pressure inside the gel channel, γ is surface tension (γ = 0.072 N m^{-1}), θ_A is the critical contact angle where liquid will burst or advance (θ_A = 140º), w is the width of the channel, and h is the height of the channel. The advancing pressure for liquid within gel channel ($w_{channel}$ = 1000 µm, h = 150 µm) was found to be 845 Pa or 86 mmH_2O.

The burst pressure at the air-liquid interface at the pores is represented in Equation

2:

$$P_{liquid\ burst} - P_{air} = -2\gamma\left(\frac{cos\theta_A^*}{w_{pore}} + \frac{cos\theta_A}{h}\right) \quad (2)$$

Where θ_A^* is the contact angle of the liquid with the inner facing side wall of the channel dividers (however, θ_A^* is limited to 180º, the maximum contact angle for a liquid meniscus). The burst pressure at the communication pores (w_{pore} = 50 µm, h = 150 µm) is 3615 Pa or 369 mmH_2O.

The difference between $P_{liquid\ advance}$ and $P_{liquid\ burst}$ is 2770 Pa or 282 mmH_2O.

3.3.5 Surface coating of PDMS

To promote cell adhesion, the central gel channel was coated with 0.01% dopamine HCl (Sigma-Aldrich) in TE Buffer [pH 8.5] for 1 hour at room temperature, washed with PBS, coated with 100 µg/mL rat tail collagen I (Corning) in PBS for 1 hour at room temperature, washed with PBS, and then dried overnight at 65 ºC [178]. Devices were sterilized by UV exposure for at least 30 minutes prior to culture of cells.

3.4 Discussion

The approach and design of the hBM-on-a-chip went through several iterations in order to produce a simple and more reproducible device. The design that was initially proposed, a horizontal juxtaposition of the endosteal and perivascular microenvironments had several theoretical advantages: the two microenvironments were separated in the x-y plane, which would have allowed for simple niche classification during imaging; and the two niche hydrogels were loaded simultaneously, which would have permitted shorter culture times for the devices. However, these two theoretical advantages proved to be

logistical weaknesses of the design. Given the previous published work with horizontal arrangement of the hydrogels [167], this approach is feasible, but we found the method to be inconsistent. While changing the design to a single BM channel, where the endosteal niche is formed and then the vasculature seeded on top of it, increased the duration of culture, it was a simpler approach that resulted in more consistent hBM-on-a-chip culture.

The fabrication methods for hBM-on-a-chip were iterated to create an improved hBM-on-a-chip. Improving upon the fabrication process for PDMS based organ-on-chips not only decreases the fabrication time and increases the inter-device consistency, but we have created a more robust process that is standardized to make hBM-on-a-chip more easily reproduced by other researchers.

CHAPTER 4. AIM 1B: CULTURE AND CHARACTERIZATION

4.1 Introduction

As we have described, BM is complex, heterogeneous, with distinct microenvironments. We can simplify our concept of BM to three basic microenvironments: the endosteal niche, the central marrow, and the perivascular niche. Osteoblasts reside on the endosteal surface of bone creating a microenvironment that is composed of mineralized matrix, and contains hematopoietic cytokines like CXCL12, SCF, JAG1, and OPN. The vasculature of the BM permeates through the organ and varies in size. Large BM sinusoids (>35 μm) are located in the center of BM, and smaller vessels (15-35 μm) and microvasculature (5-15 μm) branch off from the sinusoids into surrounding BM tissue, towards and into the bone itself [25].

There are many previously published *in vitro* methods that recreate the individual components of the BM microenvironment. The differentiation of MSCs into OBs, osteogenesis, is a common *in vitro* technique for the generation of bone tissue [179]. Osteogenesis is dependent on small molecules (e.g. dexamethasone, β-glycerophosphate, ascorbic acid), biologic (e.g. bone morphogenic proteins), ECM (e.g. fibronectin, collagen), and other physical or chemical variables (e.g. surface stiffness, hypoxia) [51,180,181]. There are several examples of these methods being applied in microfluidic cultures [178,182].

As discussed in CHAPTER 3, there are also a number of published methods for creating self-assembled vascular networks in microfluidic devices [183] and this was a primary factor in the design of the hBM-on-a-chip. Vasculogenesis is dependent on

mechanical (shear stress, interstitial flow), biochemical (e.g. VEGF, Ang-1), and biological factors (EC tissue source, co-culture with mural cells) [184] that can influence the rate and quality of networks formed *in vitro*.

Using hBM-on-a-chip devices that were developed and fabricated in CHAPTER 3, in this chapter we sought to develop methods for culture and characterization of the resulting BM microenvironments. First, we developed methods for the formation of the endosteal niche. Next, we optimized conditions for vasculogenesis and the creation of the perivascular niche. Finally, we investigated the inclusion of HSPCs in hBM-on-a-chip with and without stromal cells present.

4.2 Results

4.2.1 Osteogenesis in hBM-on-a-chip

The first process in the hBM-on-a-chip culture is the formation of the endosteal niche. Our original approach was to pre-differentiate MSCs into OBs over a 14-day period, then to load the OBs into the central channel of the device and culture for 10 days to form the endosteal niche within the microfluidic device. The strategy was originally chosen because it limited the culture time where an air-liquid interface was required to be maintained between the central channel and adjacent media channels. This was an especially attractive approach during early device development when we had not optimized the design of the device to accommodate extended, isolated culture in the central channel. We observed moderate deposition of mineralized matrix through Alizarin red (Figure 15A) and von Kossa (Figure 15B) staining; however, 10 days of culture was not enough to get consistent staining of the PDMS surface. There were two options for improving the results

using this approach: (1) to increase the differentiation time prior to device loading or (2) to increase the culture time within the device. Increasing the differentiation time prior to loading was practically difficult, as MSCs underwent osteogenesis they deposited a significant amount of ECM and become increasingly more difficult to harvest from a TCPS surface. Increasing the culture time within the device became more practical as the design of the device was optimized for this purpose, however, to simplify the cell sources for ongoing experiments we chose to complete a full 21-day differentiation of MSCs within the central channel to form the endosteal niche.

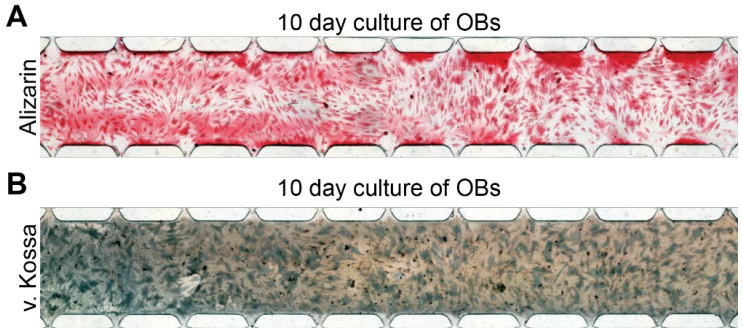

Figure 15. 10-day osteogenesis of pre-differentiated OBs to form the endosteal niche. (A) Alizarin red and (B) von Kossa staining of MSCs first pre-differentiated for 14 days on TCPS then differentiated an additional 10 days in hBM-on-a-chip.

MSCs were seeded at a high density ($5x10^5$ cells/mL) within the central channel of the device and differentiated with osteogenic media over a period of 21 days. Mineralization of matrix was observed by Alizarin red (Figure 16A,B) and von Kossa (Figure 16C,D) staining. Mineralization increased over the 21-day differentiation. At 21 days, 71 ± 18% of the area of the device stained positive for Alizarin red and the normalized mean intensity of the stained device was 0.64 ± 0.07. Similarly, at 21 days 91 ± 3% of the area of the device stained positive for von Kossa and the normalized mean intensity was

0.60 ± 0.06. In addition to mineralized matrix, the expression of specific cytokines and ECM components is of interest when creating a surrogate endosteal niche. After 21 days differentiation, the differentiated MSCs expressed cytokines (SCF, CXCL12, and JAG1) and ECM (FN, OPN) characteristics of the endosteal niche (Figure 16E-I).

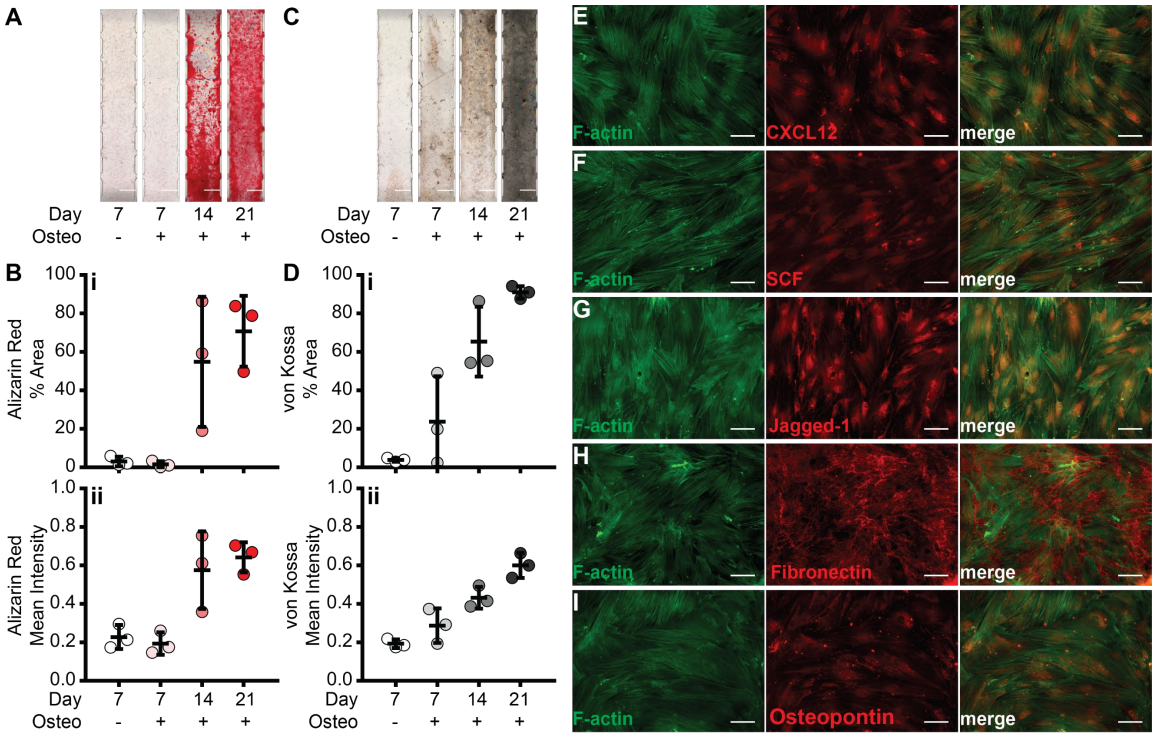

Figure 16. 21-day osteogenesis of MSCs to form the endosteal niche. MSCs were differentiated for 21 days within the central channel of the hBM-on-a-chip after which mineralization was measured. Representative images of (A) alizarin red and (C) von Kossa staining. Scale bars: 500 µm. Quantification of (B) alizarin red and (D) von Kossa staining by (i) percent area and (ii) mean intensity. Data are plotted as mean ± SD (n = 3 devices). Immunofluorescence staining of endosteal cytokines (E) CXCL12, (F) SCF, and (G) jagged-1. Immunofluorescence staining of endosteal ECM (H) fibronectin, and (I) osteopontin, was observed using immunofluorescence staining. Scale bars: 100 µm.

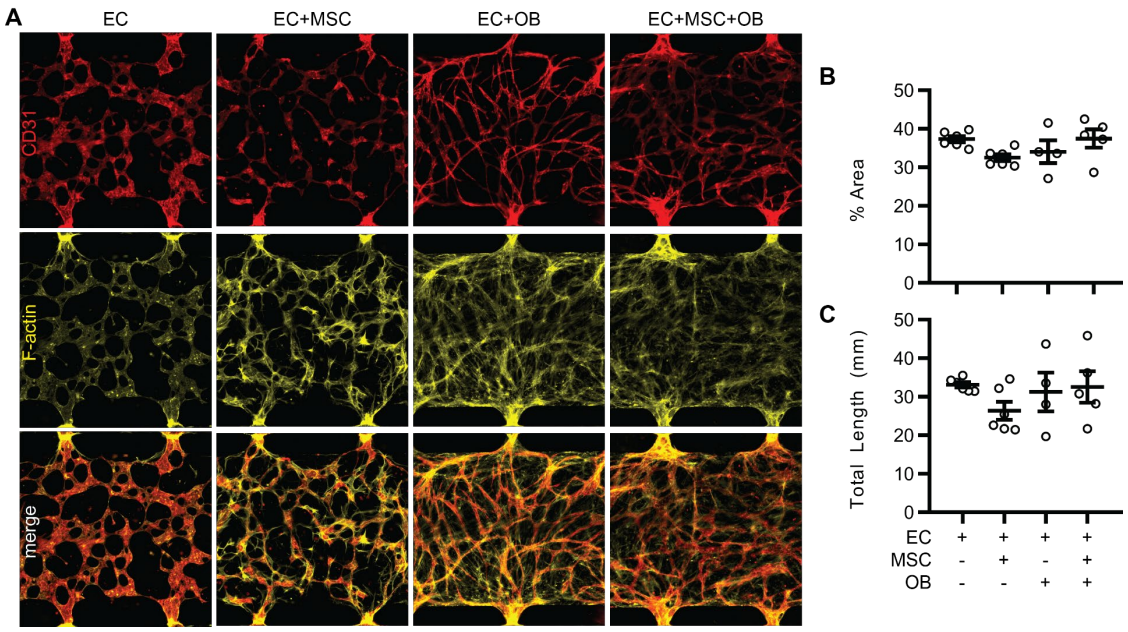

Figure 17. Effect of stromal cells on vasculogenesis in fibrin hydrogel without cytokine stimulation. (A) Immunofluorescence staining of CD31 (red) and F-actin (yellow) after 5 days vasculogenesis in hBM-on-a-chip with or without MSCs and OBs using a fibrin (5 mg/mL) hydrogel without any additional cytokine stimulation. Quantification of the (B) percent area and (C) total length of vascular networks. Data are plotted as mean ± SEM (n = 4-6 devices). Data were analyzed using a one-way ANOVA with Tukey's post hoc test. No significance found at $p < 0.05$.

4.2.2 Vasculogenesis in hBM-on-a-chip

Once the endosteal niche was formed, HUVECs and MSCs were suspended in a fibrin (5 mg/mL) hydrogel and loaded on top of the endosteal surface. Using a 5-channel device, as described in CHAPTER 3, MSCs were simultaneously loaded into the outermost channels in order to produce pro-vasculogenic cytokines and induce vascular formation. To determine the effect of stromal cells on vasculogenesis, we made devices with and without MSCs and OBs and measured the resulting vascular formation (Figure 17). F-actin staining of all cells (endothelial cells were differentiated by CD31 expression) showed perivascular stromal cells in MSC containing conditions and an endosteal layer in OB containing groups (Figure 17A). Qualitatively, the resulting vascular networks appeared

different. EC-only vasculature appeared larger and less homogeneous, while MSCs and OBs appeared to produce more consistent vasculature and decrease the vessel diameter. However, analysis of the vascular networks did not find any significant differences between groups for either the percent area or total lengths of the networks (Figure 17B, C).

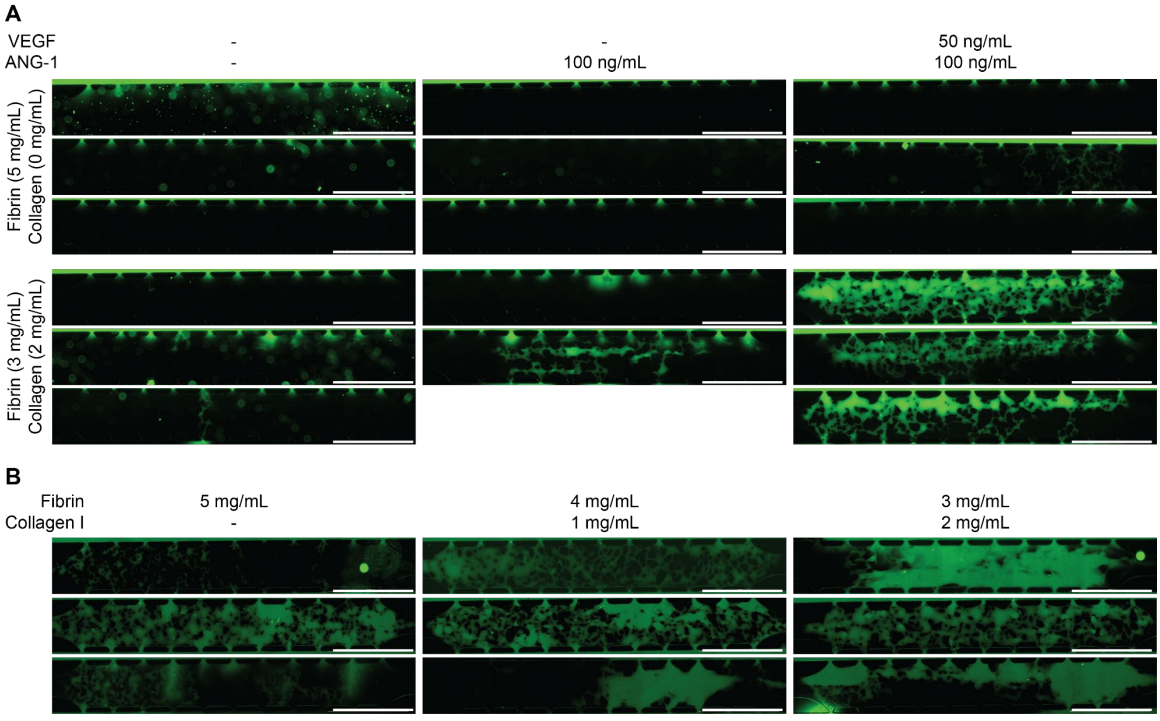

Figure 18. Optimization of hydrogel composition and cytokine supplementation for vasculogenesis. (A) Perfusion of vascular networks with 70 kDa dextran-FITC in hBM-on-a-chip (EC+MSC) using fibrin only (5 mg/mL) or fibrin-collagen co-gel (3 mg/mL, 2 mg/mL), with and without VEGF (50 ng/mL) and Ang-1 (100 ng/mL) supplementation. (B) Perfusion of vascular networks with 70 kDa dextran FITC in hBM-on-a-chip (without OB) with VEGF (50 ng/mL) and Ang-1 (100 ng/mL) supplementation, using fibrin only (5 mg/mL) or fibrin-collagen co-gels at 4:1 or 3:2 ratios Scale bar: 1000 µm.

While MSCs in the flanking channels were successfully promoting vasculogenesis, we observed that these vascular networks were not consistently forming open lumens at the channel pores and as a result were not consistently perfusable. To address this, we investigated how hydrogel composition and added cytokine supplementation might

improve the perfusability of the vascular networks (Figure 18). Using devices with MSCs and HUVECs only, we tested both fibrin (5 mg/mL) and fibrin-collagen I co-gels (3 mg/mL and 2 mg/mL) with and without added VEGF or Ang-1 (Figure 18A). Devices with the fibrin-collagen I co-gel supplemented with VEGF (50 ng/mL) and Ang-1 (100 ng/mL) produced vascular networks that were perfusable by 70 kDa dextran. To further optimize the hydrogel composition, we next tested three different hydrogel compositions with added cytokine supplementation: fibrin (5 mg/mL) only, fibrin-collagen I (4 mg/mL fibrin, 1 mg/mL collagen) and fibrin-collagen (3 mg/mL fibrin, 2 mg/mL collagen) (Figure 18B). The fibrin-collagen co-gel (4 mg/mL fibrin, 1 mg/mL collagen) produced more consistent, perfusable vascular networks than the co-gel with larger proportion of collagen I.

Using the fibrin-collagen I co-gel with supplemental cytokines (VEGF and Ang-1), hBM-on-a-chip microfluidic devices were created with and without MSCs and the differentiated endosteal layer (OBs) to measure the effect of stromal cells on vasculogenesis and cytokine secretion (Figure 19A). We observed no significant difference in the vasculature area containing MSCs (41.4 ± 4.4%), OBs (44.1 ± 2.9%), or both cell types (44.3 ± 3.1%) when compared between groups or to devices containing ECs only (43.39 ± 3.3%) (Figure 19B). Similarly, no significant difference in the total length of the vasculature networks was observed between devices containing MSCs (83.0 ± 13.0 mm), OBs (92.9 ± 12.2 mm), both MSCs and OBs (92.1 ± 10.8 mm), or neither (83.3 ± 6.2 mm) (Figure 19C). Although there was no significant difference, it is worth noting that the devices containing OBs exhibited vasculature that covered marginally less area and had a slightly increased total length of the network, which indicated a smaller average diameter of the newly formed vasculature compared to devices without OBs.

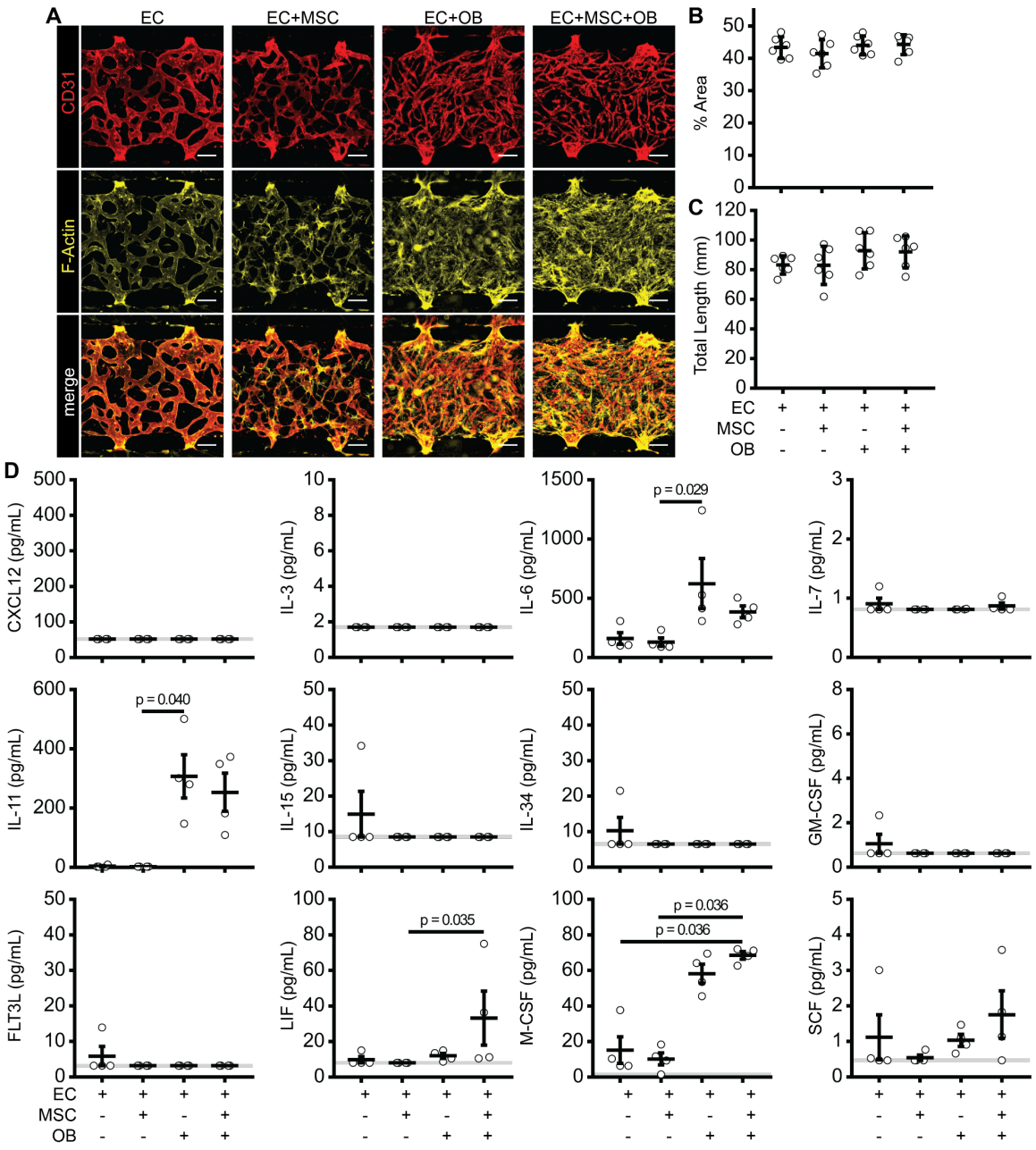

Figure 19. Effect of stromal cells on vasculogenesis in fibrin-collagen I co-gel with VEGF and Ang-1 supplementation. hBM-on-a-chip with or without MSCs and OBs created using a fibrin (4 mg/mL) and collagen I (1 mg/mL) co-gel with VEGF (50 ng/mL, days 1-5) and Ang-1 (100 ng/mL, days 3-5) supplementation. (A) Immunofluorescence staining of CD31 (red) and F-actin (orange). Scale bars: 100 µm. Quantification of the (B) percent area and (C) total length of vascular networks. Data are plotted as mean ± SD (n = 4-6 devices). Data were analyzed using a one-way ANOVA with Tukey's post hoc test. No significance found at $p < 0.05$. (D) Hematopoietic cytokine secretion measured in device supernatant collected on day 5. Data are plotted as mean ± SEM (n = 4 devices). Data were analyzed using Kruskal-Wallis w/ Dunn's post hoc test. Significance between groups ($p < 0.05$) is indicated in the figure.

4.2.3 Expression of cytokines and ECM in hBM-on-a-chip

We observed differences in cytokine expression as a function of stromal cell inclusion using multiplex cytokine detection to analyze the supernatant collected from the devices on day 5 of vasculogenesis (Figure 19D). OB containing devices, in general, secreted higher amounts of cytokines. IL-6, a cytokine involved in B cell differentiation, was highly expressed in EC+OB (624 ± 212 pg/mL) and EC+MSC+OB (386 ± 49 pg/mL) samples, less was expressed in EC (162 ± 49 pg/mL) and EC+MSC (132 ± 34 pg/mL). IL-11, which is responsible for signaling during megakaryocyte maturation, was measured in substantial concentrations in EC+OB (308 ± 73 pg/mL) and EC+MSC+OB (254 ± 64 pg/mL) devices, while trace concentrations were detected in EC (4.1 ± 1.8 pg/mL) devices and not at all in EC+MSC samples. Similarly, M-CSF, which induces macrophage differentiation of HSCs, was elevated in EC+OB (58.3 ± 5.3 pg/mL) and EC+MSC+OB (68.6 ± 2.1 pg/mL) devices, while little was detected in EC (15.2 ± 7.6 pg/mL) and EC+MSC (10.3 ± 3.5 pg/mL) devices.

Relatively small concentrations of IL-7 (promoter of lymphopoiesis), IL-34 (monocytes and macrophages), GM-CSF (granulocytes and macrophages), FLT-3L (dendritic cells), and SCF (HSC maintenance) were measured and there was no significant difference across groups. For both CXCL12 (hematopoietic chemoattractant) and IL-3 (myeloid progenitors), no measurable analytes were detected. A limitation of microfluidic cell culture is the small volume of media that is accessible to the cells and the small number of cells in each culture, which can result in low (and in this case below detection) concentrations of analytes. To circumvent this issue and obtain more concentrated samples, we were also able to recover the central hydrogel and assay the cell containing portion of

the device directly by cutting through the bottom PDMS film and retrieving the central hydrogel. However, this approach resulted in no increase in the recovery of soluble cytokines (Figure 20).

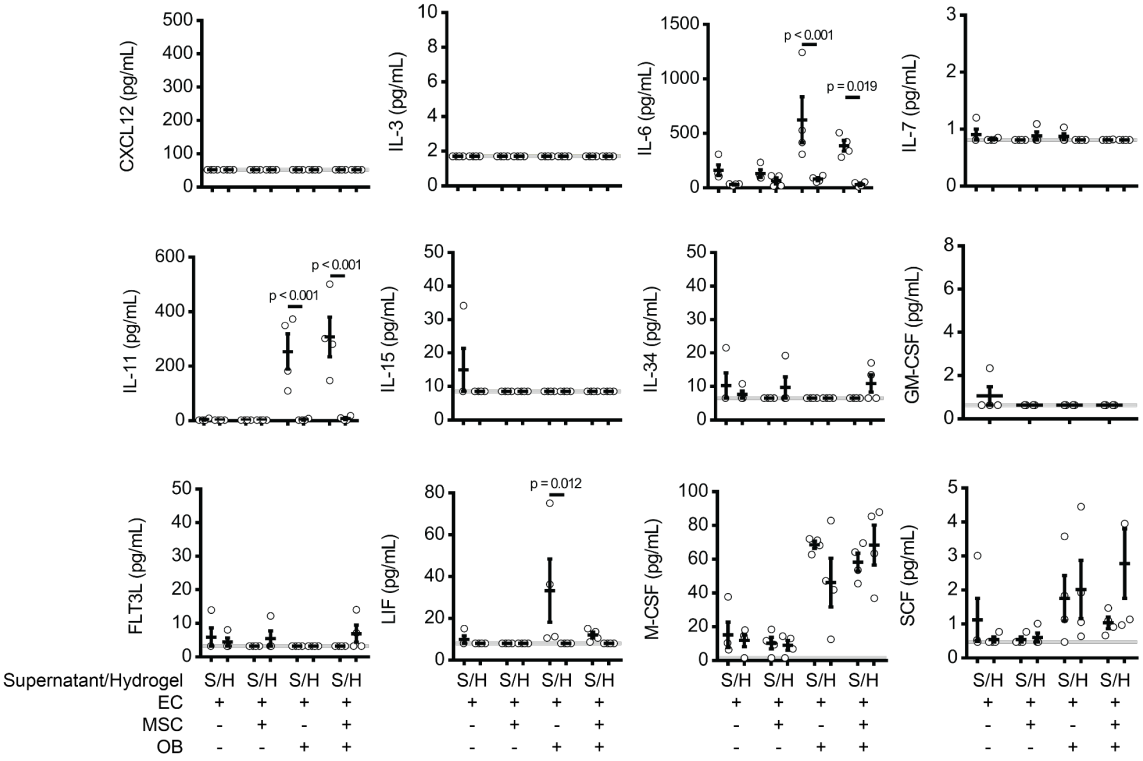

Figure 20. Comparison of cytokine recovery from supernatant and hydrogel. hBM-on-a-chip with or without MSCs and OBs created using a fibrin (4 mg/mL) and collagen I (1 mg/mL) co-gel with VEGF (50 ng/mL, days 1-5) and Ang-1 (100 ng/mL, days 3-5) supplementation. Hematopoietic cytokine secretion measured in device supernatant and in central hydrogel after 5 days of vasculogenesis Data are plotted as mean ± SEM (n = 4 devices). Data were analyzed using Kruskal-Wallis w/ Dunn's post hoc test. Significance between groups ($p < 0.05$) is indicated in the figure. Supernatant data is the same data shown in Figure 19.

After 5 days of vasculogenesis, hBM-on-a-chip containing the endosteal layer and subsequently seeded MSCs and HUVECs were fixed and stained to characterize the presence and localization of cytokines and ECM relevant to the BM niche by microscopy

(Figure 21). CXCL12 and SCF were both found to be expressed by perivascular and endothelial cells. Fibronectin was observed to be present in the "central marrow" space outside of the newly formed vasculature. This arrangement of cytokine expression is consistent with the distribution that has been seen *in vivo*.

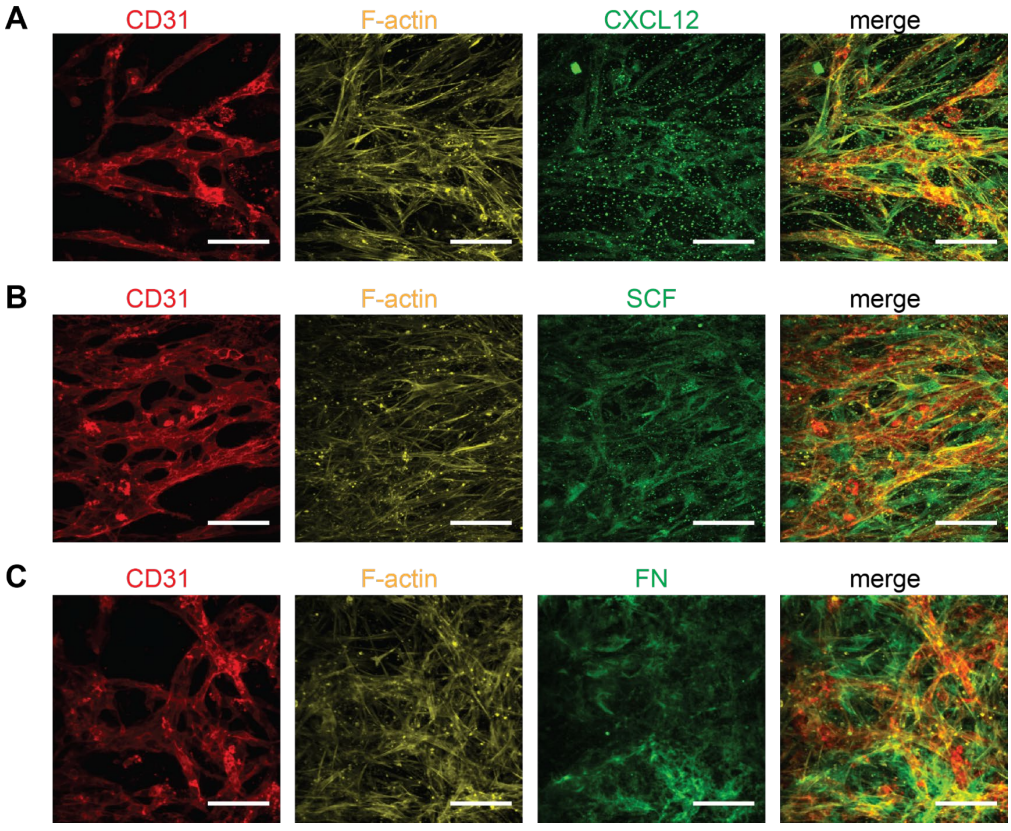

Figure 21. ECM and cytokine expression in hBM-on-a-chip. hBM-on-a-chip (EC+MSC+OB) with a fibrin (4 mg/mL) and collagen I (1 mg/mL) co-gel with VEGF (50 ng/mL, days 1-5) and Ang-1 (100 ng/mL, days 3-5) supplementation. Immunofluorescence staining of (A) CXCL12, (B), SCF, (C) FN after 5 days vasculogenesis. Scale bar: 100 µm.

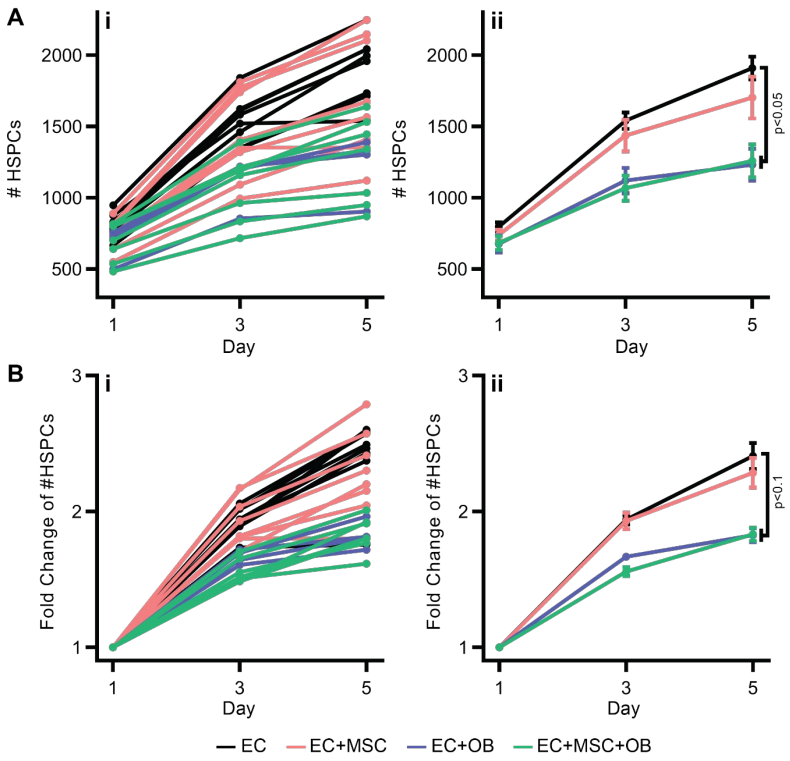

Figure 22. Expansion of HSPCs in hBM-on-a-chip.(A) Number of HSPCs ((i) individual devices and (ii) summary data) in hBM-on-a-chip with ECs only (black), with MSCs (red), OBs (blue), and both (green) on days 1, 3, and 5. (B) Fold change number of HSPCs ((i) individual devices and (ii) summary data) on days 1, 3, and 5. Data are shown as mean ± SEM. (n = 4 devices EC+OB, n = 7 devices EC+MSC +OB, n = 8 devices EC and EC+MSC). Data were analyzed using Kruskal-Wallis w/ Dunn's multiple comparisons test. (A) EC vs EC+OB p = 0.0210; EC vs EC+MSC+OB p = 0.0166. (B) EC vs EC+OB p = 0.0813; EC vs EC+MSC+OB p = 0.0162.

4.2.4 Culture of CD34+ HSPCs in hBM-on-a-chip

We next sought to investigate the inclusion of BM HSPCs in the hBM-on-a-chip and how MSCs and OBs affected their fate in our BM model. BM CD34+ cells were briefly expanded *in vitro* out of cryo-storage and then loaded into the central channel with HUVECs and MSCs. We measured the expansion of the HSPCs via microscopy over the 5 days of culture during vasculogenesis (Figure 22). On day 1, the number of HSPCs in hBM-on-a-chip was not significantly different in MSC and/or OB containing devices

(Figure 22A). By day 3 and continuing to day 5, devices without OBs had significantly more HSPCs than devices with the endosteal layer. HSPCs culture with ECs and MSCs expanded 2.41- and 2.28-fold, respectively, over 5 days, whereas both groups with HSPCs cultured in the presence of the pre-formed endosteal layer only expanded 1.83-fold (Figure 22B).

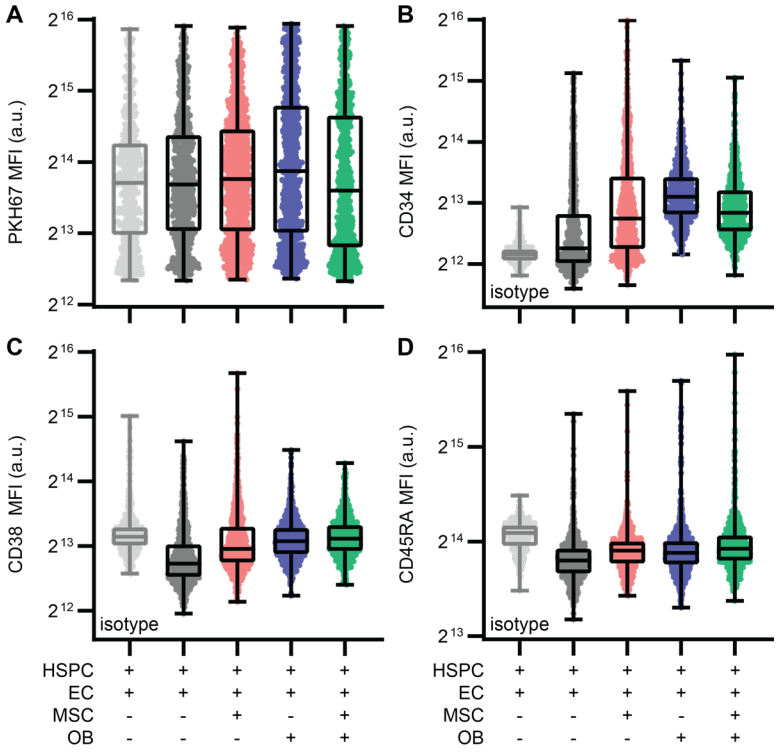

Figure 23. HSPC differentiation in hBM-on-a-chip. Quantification of immunofluorescence of HSPCs cultured for 5 days in hBM-on-a-chip with ECs only (black), with MSCs (red), OBs (blue), and both (green). MFI of (A) PK467 (cell tracker), (B) CD34, (C) CD38, and (D) CD45RA. Data are shown with median, quartiles, min and max (n = 452 cells for isotype from 1 device, n = 800 cells for EC, n = 907 cells EC+MSC, n = 945 cells EC+OB, n = 799 cells EC+MSC+OB pooled from 3 devices).

HSPCs will rapidly differentiate when cultured *in vitro*. We attempted to measure the effect of MSCs and OBs on the differentiation of HSPCs in the hBM-on-a-chip by staining for CD34, CD38 and CD45RA (Figure 23). HSPCs were pre-labeled with the

membrane dye PKH67 to identify HSPCs for subsequent fluorescence quantification (Figure 23A). We observed increased expression of CD34 in the presence of MSCs and/or OBs (Figure 23B). Staining of CD38 and CD45RA was consistently at or below the intensity measured for the isotype control (Figure 23C, D).

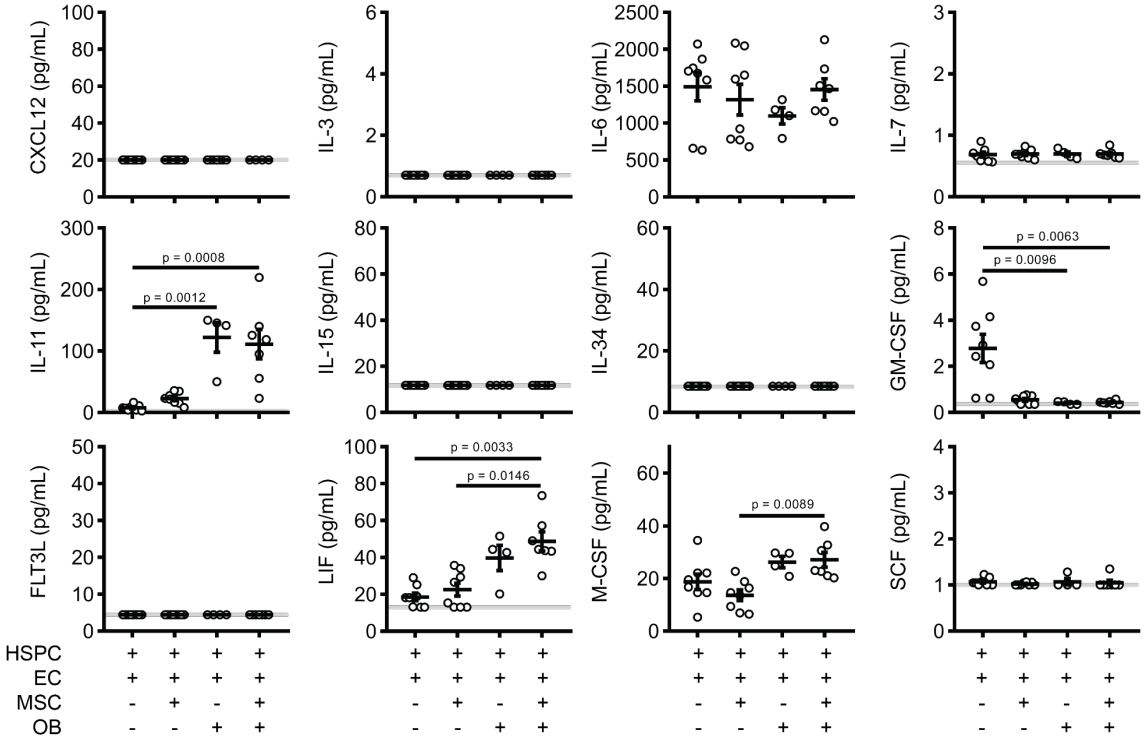

Figure 24. Cytokine secretion in the presence of HSPCs. Hematopoietic cytokine secretion measured in hBM-on-a-chip with HSPCs and ECs only, with or without MSCs and OBs, from device supernatant collected on day 5. Data are shown as mean ± SEM (n = 4 devices EC+OB, n = 7 devices EC+MSC+OB, n = 8 devices EC and EC+MSC). Data analyzed using Kruskal-Wallis w/ Dunn's post-hoc test. Significance between groups ($p<0.05$) is indicated in the figure.

Overall, incorporation of HSPCs into hBM-on-a-chip did not affect the trends in cytokine secretion (Figure 24). Increased concentrations of IL-11, LIF, and M-CSF were measured in OB containing devices. However, we observed increased secretion of IL-6 in all groups, including in EC and EC+MSC devices which had previously secreted less IL-6

than the OB groups. Increased IL-6 production could be a result of activation of the HSPCs, indicating potential incompatibility between the HSPC donors and the HUVEC or MSC donors, which were not HLA-matched.

4.3 Methods

4.3.1 Previously described methods

hBM-on-chip were fabricated using the methods described in CHAPTER 3, see the following sections:

3.3.3 PDMS device fabrication

3.3.5 Surface coating of PDMS

4.3.2 Cell culture

4.3.2.1 BM MSCs

Human BM MSCs (RoosterBio) were initially expanded in hMSC High Performance Media Kit (RoosterBio). After initial expansion, MSCs were verified by flow cytometry to be $CD34^-$, $CD45^-$, $CD73^+$, $CD90^+$, and $CD105^+$. For subsequent passages, MSCs were cultured in αMEM (Sigma Aldrich) supplemented with 10% FBS (Hyclone) and 1% Penicillin-Streptomycin (Hyclone). MSCs were cultured at 37 °C and 5% CO_2. MSCs were used up to passage 6.

4.3.2.2 Human umbilical vein endothelial cells (HUVECs)

Pooled HUVECs (Lonza) were cultured in EGM-2MV (Lonza) on 0.1% bovine gelatin (Sigma-Aldrich) coated TCPS at 37 ºC and 5% CO_2. HUVECs were used up to passage 8.

4.3.2.3 Human bone marrow CD34+ hematopoietic stem and progenitor cells (HSPCs)

Human BM CD34+ cells (Lonza) were expanded for 5 days prior to use in Stemline II (Sigma-Aldrich) supplemented with 100 ng/mL SCF, TPO, and G-CSF (Peprotech) at 37 ºC, 5% CO_2.

4.3.3 Osteogenesis in hBM-on-a-chip

For the formation of the endosteal niche, MSCs were seeded within the central gel channels of devices at a density of $4x10^5$ cells/mL. Cells were cultured within the devices for 21 days in αMEM osteogenic media (10% FBS, 1% penicillin-streptomycin, 10 mM β-glycerophosphate (Sigma-Aldrich), 50 μM ascorbic acid (Sigma-Aldrich), and 100 nM dexamethasone (Sigma-Aldrich)) with daily media exchange.

4.3.4 Alizarin red and von Kossa staining and quantification

Osteogenic devices were washed with PBS, fixed with 4% formaldehyde in PBS for 15 minutes, and then washed with PBS. For Alizarin red staining, devices were washed twice with DI H_2O and then stained for 5 minutes with 2% alizarin red (Sigma-Aldrich) in DI H_2O [pH 4.1-4.3]. Alizarin red stain was removed by several washes with DI H_2O, until liquid was clear. For von Kossa staining, devices were washed twice with DI H_2O and then stained with 1% silver nitrate (Acros Organics) in DI H_2O under a UV lamp for 15 minutes. Devices were washed twice with DI H_2O and then incubated in 5% sodium thiosulfate (Acros Organics) in DI H_2O for 5 minutes. Devices were then washed with DI H_2O until liquid was clear.

Stained devices were imaged using a Lionheart FX (BioTek Instruments). Color brightfield images were analyzed using open-source software ImageJ [130,131]. The red

and green channels were used for von Kossa and Alizarin, respectively, to measure mean intensity and percent area.

4.3.5 Vasculogenesis in hBM-on-a-chip

Vasculogenesis in central gel channel was accomplished using previously reported approaches [168,169]. Briefly, HUVECs ($12x10^6$ cells/mL) and MSCs ($6x10^5$ cells/mL) were suspended in EBM-2MV supplemented with thrombin (4 U/mL) (Sigma-Aldrich). A solution of fibrinogen (8 mg/mL) (Sigma-Aldrich) and collagen I (2 mg/mL) (Corning) in PBS was loaded into a central gel channel reservoir. The HUVEC/MSC cell suspension was added to fibrinogen solution (1:1) and mixed thoroughly. (Final cell suspension: HUVECs ($6x10^6$ cells/mL), MSCs ($3x10^5$ cells/mL), thrombin (2 U/mL), fibrinogen (5 mg/mL)), collagen I (1 mg/mL). Immediately, the MSC/HUVEC cell suspension was withdrawn from the opposite central gel port, drawing the cell suspension through the central gel channel. Devices were then incubated for 15 minutes at 37 ºC, 5% CO_2 to allow the fibrin gel to form. EBM-2MV was added to a reservoir on each side of gel channel and pulled through media channel, into connecting reservoir by using a micropipette to create negative pressure in the connecting 1-mm port. Cells were cultured with daily media exchange for 5 days to allow for vasculogenesis. Media was supplemented with VEGF (50 ng/mL) on all days and angiopoietin-1 (Ang-1) (100 ng/mL) (Peprotech) on days 3, 4, and 5.

4.3.6 Perfusion

To visualize perfusion of microvasculature, 70 kDa dextran-FITC (Sigma-Aldrich) was flowed through the media channel on one side of the device. After 5 days of vasculogenesis, media was aspirated from all hBM-on-a-chip media ports (EC+MSC) and

replaced with 50 µL of 10 µg/mL dextran-FITC in EGM-2MV in two, connected media ports. Devices were immediately imaged using a Lionheart FX (BioTek Instruments) microscope to visualize the flow of dextran through the central channel of the device.

4.3.7 Cytokine and ECM immunofluorescence staining and microscopy

Staining procedure for devices was adapted from Chen *et al* 2017 [170]. Devices were washed with PBS, fixed with 4% formaldehyde (ThermoFisher), and permeabilized with 0.1% Triton X-100. Prior to staining, cells were blocked with 5% BSA, 3% goat serum in PBS. Primary antibodies were diluted (typically 1:100) in blocking buffer and devices were stained overnight at 4 ºC. Devices were then washed with 0.1% BSA in PBS and stained with secondary antibodies (typically 1:200) diluted in wash buffer for 3 hours at RT. Devices were washed with wash buffer and then stained with phalloidin AF647 (1:40). Devices were imaged using a spinning disk confocal microscope (PerkinElmer).

4.3.8 Vascular network analysis

Devices stained with Alexa Fluor 647 anti-human CD31 (BioLegend) and Alexa Fluor 594 Phalloidin (ThermoFisher) were imaged using a Lionheart FX (BioTek Instruments). Images were processed using open-source software ImageJ and contrast corrected images were analyzed using AngioTool [185] to measure percent area and total network length.

4.3.9 Multiplex cytokine detection

Media was collected from devices at designated time by collecting media from one side of device, waiting for 5 minutes to allow for gravity driven flow through the device and then collection of all media from reservoirs. Device media was immediately stored on

ice and then flash frozen in liquid N_2 for storage prior to analysis. Samples were thawed on ice prior to detection and analysis using LEGENDplex human hematopoietic stem cell panel (BioLegend), according to manufacturer's protocol.

4.3.10 Culture of CD34+ BM HSPCs in hBM-on-a-chip

BM CD34+ HSPCs were labelled with PKH67 green fluorescent cell stain (Sigma-Aldrich) and loaded at a final concentration of $3x10^5$ (20:1 HUVEC:HSPC ratio, $6x10^5$ HSPCs/mL in thrombin cell suspension prior to mixing with fibrinogen). This concentration results in ~500 HSPCs within the central channel. Devices were imaged on days 1, 3, and 5 after loading using a Lionheart FX (BioTek Instruments). Images were analyzed using Gen5 (BioTek Instruments) to count the number of HSPCs and progenitors at each time point.

4.3.11 HSPC surface marker staining, imaging, and quantification

After 5 days of culture, devices were washed with PBS and fixed with 4% formaldehyde (ThermoFisher). Prior to staining, cells were blocked with 5% BSA, 3% goat serum in PBS. Primary antibodies were diluted (see Appendix C) in blocking buffer, devices were stained overnight at 4 ºC, and then washed with 0.1% BSA in PBS. Samples were imaged using a spinning disk confocal microscope (PerkinElmer) and expression of surface markers were quantified using Volocity software (PerkinElmer).

4.3.12 Statistical Analysis

Sample sizes and statistical methods are indicated in the figure captions and individual data points are shown. GraphPad Prism was used for statistical analysis. Normality of samples were tested using Shapiro-Wilk normality test. If all samples in an

experiment passed normality test, one-way ANOVA with Tukey's multiple comparison test was used. If a sample did not pass normality test, Kruskal-Wallis with Dunn's multiple comparison test was used.

4.4 Discussion

We have shown that by using the microfluidic devices designed in CHAPTER 3 we are able to recreate basic features of the endosteal and perivascular niches of human BM. This is a unique example of a defined, *in vitro* culture platform that combines both microenvironments in a single system. While there are numerous previously reported platforms for recreating the BM microenvironment, many of these only incorporate single cell types in co-cultures and more complex models require lengthy development as ectopic implants in animal models [104,150]. As evidence mounts that suggests that the endosteal and perivascular niches play unique roles in the regulation of normal and diseased states of hematopoiesis in, a complex, multi-niche culture platform is needed to recapitulate the complexity of BM tissue. The hBM-on-a-chip presented here is one of few examples of such an approach [103].

We have demonstrated that an endosteal niche can be formed within the hBM-on-a-chip through a 21-day differentiation of MSCs and that, due to the design of the device optimized in CHAPTER 3, subsequently we can load ECs, MSCs, and HSPCs on top of this endosteal layer in order to form microvasculature. Cytokine expression is dependent on the inclusion of stromal cells and is elevated when OBs are present. We have also showed that BM HSPCs culture in hBM-on-a-chip have increased levels of expansion in the absence of OBs, however CD34 expression (and stemness) is maintained when OBs

are present in the culture. Functionally, the inclusion of the endosteal layer results in a different microenvironment for hematopoietic cells.

Further characterization of the hBM-on-a-chip and HSPC culture would expand our understanding of the microenvironment being created. The expression of many cytokines, ECM proteins, and signaling molecules that are relevant to specific hematopoietic functions that could be studied in hBM-on-a-chip. Additionally, with the many hematopoietic progenitors that could be arising within the culture, the hBM-on-a-chip should be further defined to understand the hematopoietic and BM microenvironment being created.

There are also several improvements that could be made to hBM-on-a-chip to facilitate its use and to better and more reliably replicate the BM microenvironment. Currently, the time required to create the endosteal niche is lengthy and shortening this step would greatly improve the potential utility of the approach. There are several commercially available differentiation media compositions available that could, in theory, shorten the culture time while maintaining the phenotypic results. One significant challenge with the device in its current design is the consistency of formation of perfusable vasculature. Due to the prolonged culture, prior to loading of the fibrin-collagen co-gel, the hydrogel does not reliably adhere to the PDMS surface (likely because proteins have already adsorbed to the surface) which caused slight delamination that allowed for fluid flow around the hydrogel and not through the newly formed vasculature. Achieving consistent adhesion of the hydrogel to the device structure, through chemical modification or by other means is necessary for translation of this platform into a preclinical setting where increased consistency is necessary. Finally, the device is, while complex, a relatively simple model

of the BM microenvironment, inclusion of additional stromal and mature hematopoietic cell types could improve upon the relevance to native tissue.

CHAPTER 5. AIM 2A: MOBILIZATION OF HSPCS

5.1 Introduction

Although HSPCs are predominately located and maintained within the BM niche by the CXCL12-CXCR4 signaling axis, in normal physiological conditions HSPCs can also be found in peripheral blood in small numbers. It is thought that a constant low frequency flux of HSPCs into the periphery and back into BM is required for normal developmental processes and hematopoietic maintenance [186]. It is unlikely that HSPCs occupy a single, static niche, they are likely migrating within the BM as well as leaving and reentering the BM at a low rate [186,187]. Clinical interventions have been developed to significantly increase the number of HSPCs in peripheral blood so that they can be collected by apheresis for subsequent autologous or, less frequently, allogeneic stem cell transplantation. This is a common therapeutic approach for patients with multiple myeloma or other hematologic malignancies, where HSPCs are mobilized, collected, and then reinjected to reconstitute the hematopoietic system after chemotherapeutic or radiologic ablation of the malignancy (and subsequently, the remaining hematopoietic cells) [188]. G-CSF has long been used in conjunction chemotherapy (typically cyclophosphamide) to mobilize BM HSPCs, however it is not effective in all patients. Previous chemotherapy or radiotherapy regimens, age, and disease burden have all been considered as clinical variables that may cause poor mobilization [189-191]. Over the last 20 years, AMD3100 (Mozobil, Plerixafor) has been developed and is now the second FDA approved mobilizing drug and is used, although at a significant increase in cost, as a second line treatment for patients who have failed G-CSF plus chemotherapy mobilization [192].

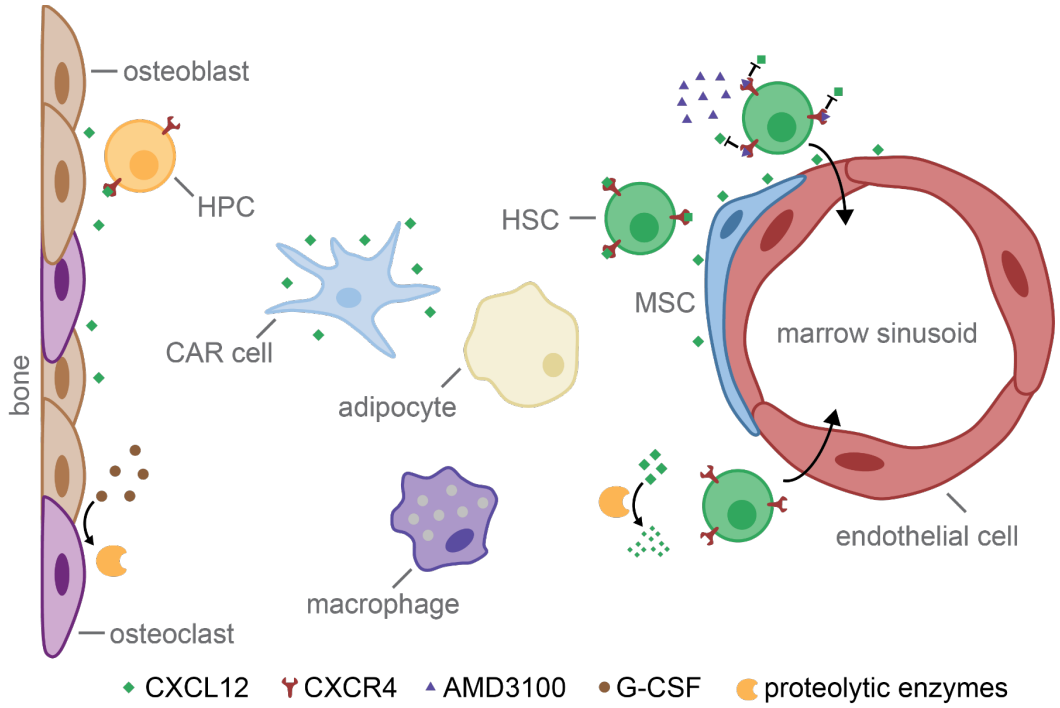

Figure 25. Mobilization of HSPCs from BM microenvironment. Mobilization of HSPCs from BM microenvironment relies on disruption of the CXCL12-CXCR4 signaling axis. AMD3100 (or plerixafor) is a CXCR4 antagonist and directly blocks the binding of CXCL12 by surface expressed CXCR4 on HSPCs, resulting in egress of HSPCs from the BM niche. The mechanism of G-CSF mobilization is less clear. It has been reported that G-CSF treatment results in elevated expression of proteolytic enzymes by osteoblasts, osteoclasts and BM macrophages that, in turn, degrade CXCL12 and chemokine receptors. Alternatively, it has been proposed that G-CSF mobilization is a result of proliferation of BM HSPCs and not specifically migration out of BM.

The specific mechanism of G-CSF mobilization is unknown. G-CSF is expressed endogenously and acts on several hematopoietic and stromal cells in BM resulting in a spectrum of physiologic outcomes, including expansion of hematopoietic progenitors and the differentiation of granulocytes. Specific to mobilization, G-CSF is believed to stimulate macrophages, osteoblasts, and osteoclasts to induce upregulation of proteolytic enzymes (MMP9, cathepsins, etc.) that subsequently degrade CXCL12 and potentially surface bound VLA-4 and CXCR4 on HSPCs [193-198]. By decreasing both the free CXCL12 and HSPCs ability to bind the chemokine, G-CSF may disrupt the signaling axis that keeps

HSPCs in the BM, thus increasing the percentage of HSPCs in peripheral blood. Because G-CSF signals through resident cells and does not directly interrupt the chemokine signaling, onset of mobilization by G-CSF is relatively slow, taking greater than 24 hours to reach maximum mobilization [187]. The effects of G-CSF mobilization are additive when additional doses are given, which has led to the current clinical protocol of 4-6 days of G-CSF treatment prior to the initial collection of HSPCs from peripheral blood [187,188,199]. Aside from direct disruption of the CXCL12-CXCR4 signaling axis, there is a competing explanation for G-CSF mobilization. G-CSF induces proliferation of hematopoietic cells and it has been observed to increase the number of HSPCs in the BM after administration. As a result, the increase in HSPCs in peripheral blood could simply be a byproduct of increased total numbers of HSPCs in all compartments.

In contrast, the mechanism of mobilization by AMD3100 is known and specific. AMD3100 is an antagonist of CXCR4 and directly competes with CXCL12 for binding. CXCR4+ hematopoietic cells are then no longer able to respond to the CXCL12 gradient that maintains higher populations in the BM, and this causes the number of HSPCs in peripheral blood increases. Consequently, the kinetics of mobilization are much faster than G-CSF, with increased numbers of HSPCs observed in peripheral blood as early as 30 minutes post injection [200]. Not only is AMD3100 a faster mobilizer, but when used in conjunction with G-CSF, AMD3100 mobilizes more CD34+ cells and has more predictable kinetics than G-CSF alone [199,201-203]. There is some debate on whether AMD3100 is truly mobilizing HSPCs from the BM. It is possible that administration of AMD3100 results in binding of CXCR4 receptors on hematopoietic cells already in peripheral blood and prevents the migration of these cells back to BM and heightened concentrations of

CXCL12. As a result, the number of HSPCs in peripheral blood increases as BM HSPCs leave the BM niche at a normal rate but can no longer migrate back to the tissue.

In addition to G-CSF and AMD3100, a number of potential mobilizing agents, including Groβ, IL-8, and sphingosine-1-phosphate (S1P) have been tested in preclinical models, although none are currently approved for clinical mobilization [204,205]. Groβ and IL-8 are believed to have the same mechanism of action, where MMP-9 expression is increased in BM resident neutrophils, resulting in an indirect disruption of the CXCL12-CXCR4 signaling axis [190,206,207]. Under normal physiologic conditions, S1P acts as a chemoattractant for BM HSPCs, causing egress from BM in response to injury [205,208].

Here, we assess the ability of the hBM-on-a-chip to study the mobilization of HSPCs and its potential to be a screening tool for novel mobilization agents. Currently preclinical research is restricted to animal models [209] and the hBM-on-a-chip could potentially be used to screen novel therapeutics on a large population of human samples *in vitro* or in a patient specific BM model to assess an individual's mobilization potential.

5.2 Results

5.2.1 Effect of G-CSF and AMD3100 on cytokine expression in hBM-on-a-chip

To investigate the effect of mobilizing agents on the BM microenvironment in hBM-on-a-chip, devices containing OBs, MSCs, and ECs were treated with G-CSF and AMD3100 for 24 hours after 5 days of vasculogenesis. The change in cytokine secretion, from 0 hours (pre-treatment) to 24 hours was measured for a panel of hematopoietic cytokines (Figure 26). IL-6, IL7, IL-11, LIF, and M-CSF were detected in device supernatant, while CXCL12, IL-3, IL-15, IL-34, GM-CSF, FLT3L, and SCF were below

the detection limit of the assay. Of the cytokines that were detected, expression was relatively consistent between 0 and 24 hours, with a moderate increase in IL-6 and M-CSF measured. No significant difference was found between an untreated control and devices treated with 10 ng/mL or 100 ng/mL of G-CSF or AMD3100, suggesting that in the absence of CD34+ HSPCs, G-CSF and AMD3100 do not alter the hematopoietic BM niche.

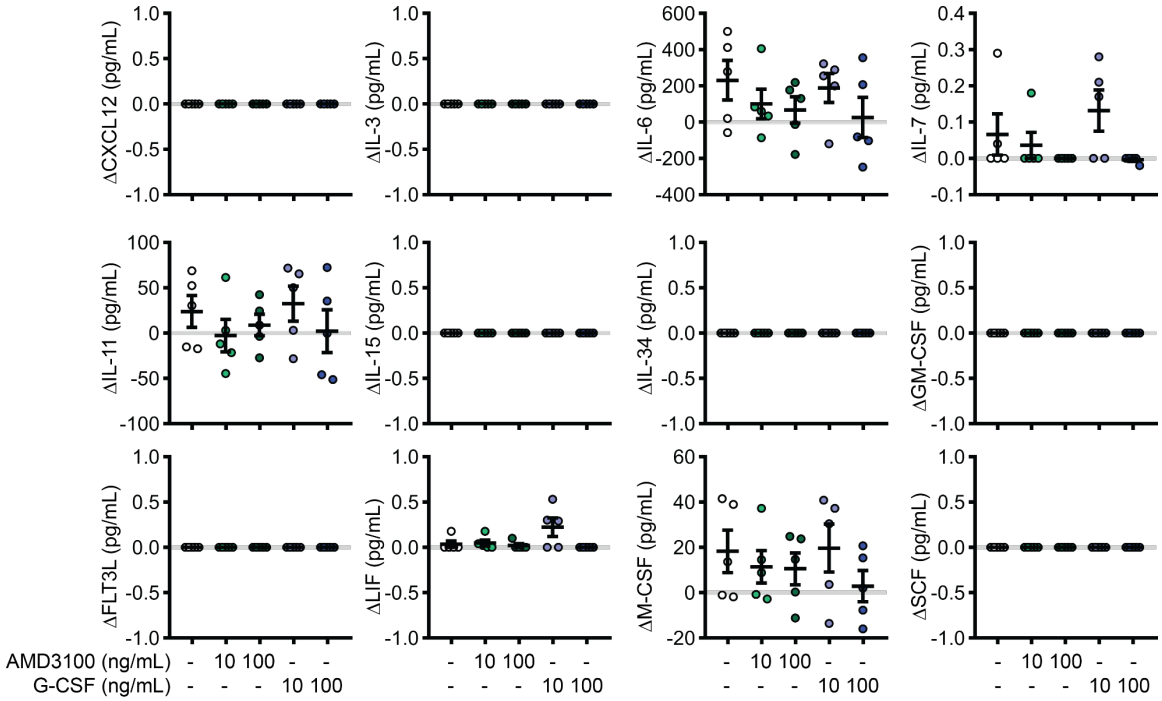

Figure 26. Effect of mobilizing agents on cytokine secretion without HSPCs. Change in hematopoietic cytokine measured in hBM-on-a-chip (without HSPCs) supernatant before (0 hours) and 24 hours after devices were untreated (white) or treated with 10 ng/mL G-CSF (light blue), 100 ng/mL G-CSF (100 ng/mL), 10 ng/mL AMD3100 (light green), or 100 ng/mL AMD3100 (dark green). Data are shown as mean ± SEM (n = 5 devices). Data analyzed using Kruskal-Wallis with Dunn's multiple comparisons test. No significance between groups ($p < 0.1$).

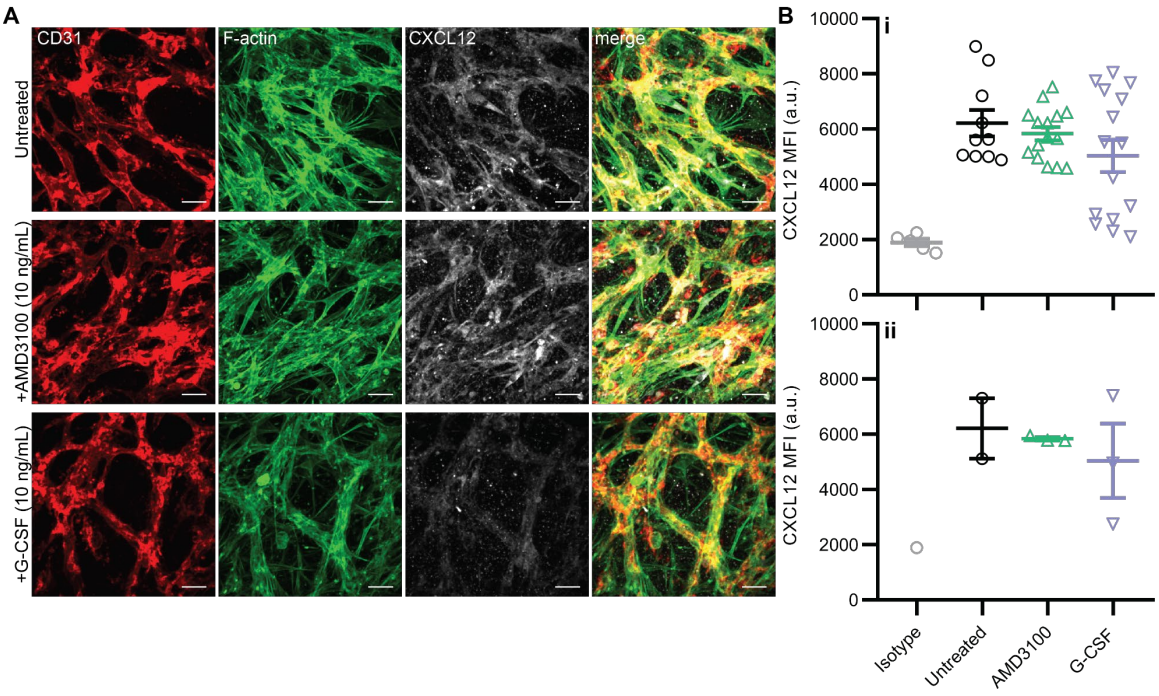

Figure 27. CXCL12 expression after 24-hour treatment with AMD3100 or G-CSF. (A) Immunofluorescence staining of CD31 (red), F-actin (green), and CXCL12 (grey) 24 hours after hBM-on-a-chip (EC+MSC+OB) were untreated or treated with G-CSF (10 ng/mL) or AMD3100 (10 ng/mL). Scale bar: 50 µm. (B) Quantification of CXCL12 fluorescence staining (i) by individual ROI and (ii) by device. Data are shown as mean ± SEM (n = 5 ROIs from 1 device isotype, n = 10 ROIs from 2 devices untreated, n = 15 ROIs from 3 devices AMD3100 and G-CSF). Data analyzed using Kruskal-Wallis w/ Dunn's multiple comparisons test. No significance between experimental groups.

Mobilization of HSPCs relies on the disruption of the CXCL12-CXCR4 signaling axis. Because CXCL12 was not detectable using a bead based multiplex assay, standard ELISA, or a modified ELISA an alternative measurement method was needed to determine whether G-CSF or AMD3100 was modulating the CXCL12 expression. Immunohistochemistry was chosen to measure the relative expression (see Appendix B for more detail). hBM-on-a-chip (EC+MSC+OB) were stained for CXCL12, CD31 (EC marker), and F-actin (all cells) (Figure 27A). CXCL12 was expressed by ECs and perivascular stromal cells. While AMD3100 (10 ng/mL) did not affect CXCL12 expression, we observed a G-CSF (10 ng/mL) decreased in measured CXCL12 in a subset

of samples, however the difference in the sample population was not statistically significant (Figure 27B).

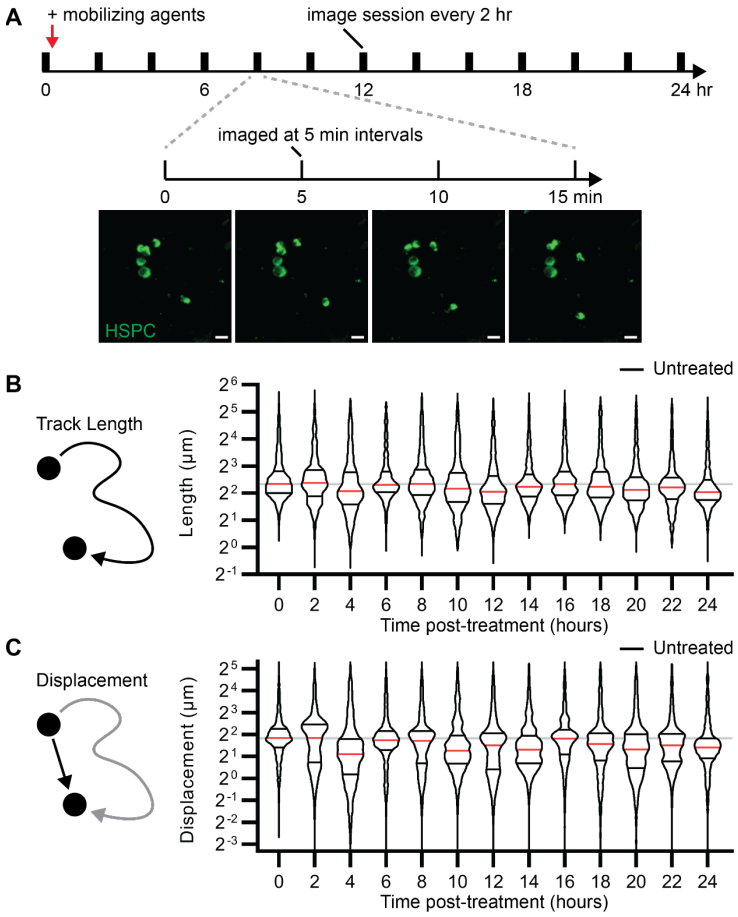

Figure 28. Measuring mobilization in hBM-on-a-chip. (**A**) To observe the "mobilization" of HSPCs, we imaged devices 13 times over a 24-hour period. After the first imaging session, media was collected from the devices and it was exchanged for untreated media or media supplemented with mobilizing agents. During each imaging session, devices were imaged 4 times in 5-minute intervals. Cells were tracked during each imaging session to measure the track length and displacement at each time point. Scale bar: 20 µm. (**B**) Track length and (**C**) displacement over 24 hours in untreated devices. (**B**) and (**C**): data (n = 853-1236 tracked cells per time point pooled from 7 devices) are shown with median (red), quartiles (black), and 0-hour median (gray line).

5.2.2 Mobilization of CD34+ BM by G-CSF and AMD3100

In order to measure the mobilization of HSPCs in hBM-on-a-chip, we designed an experimental assay where devices were imaged every 2 hours over a 24-hour period after treatment with mobilizing agents (Figure 28A). During each imaging session, devices were imaged 4 times in 5-minute intervals and these images were used to track cell movement and measure the length and displacement at discrete points in time during the 24-hour period. Untreated samples showed relatively steady movement of HSPCs when measured by either the length (Figure 28B) or displacement (Figure 28C) over 24 hours.

Treatment of hBM-on-a-chip (EC+MSC+OB+HSPC) with 10 ng/mL or 100 ng/mL G-CSF resulted in a moderate increase in the relative length and displacement of HSPCs at the lower concentration (Figure 29). The absolute, measured values of cell movement show little, if any, difference between untreated and G-CSF treated samples. However, when length and displacement are normalized and the fold change is calculated relative to the 0-hour baseline, differences between the groups emerge. After treatment with 10 ng/mL G-CSF, HSPCs had an increased track length and displacement between approximately 2-14 hours post-treatment. Untreated and samples mobilized with 100 ng/mL G-CSF did not show any sustained increase in HSPC movement, either measured by length or displacement, but instead had a steady decrease from the peak at the 0-hour baseline measurement. Mobilization using AMD3100 at low doses of 1 ng/mL and 10 ng/mL did not result in any increased movement of HSPCs relative to the untreated control (Figure 30).

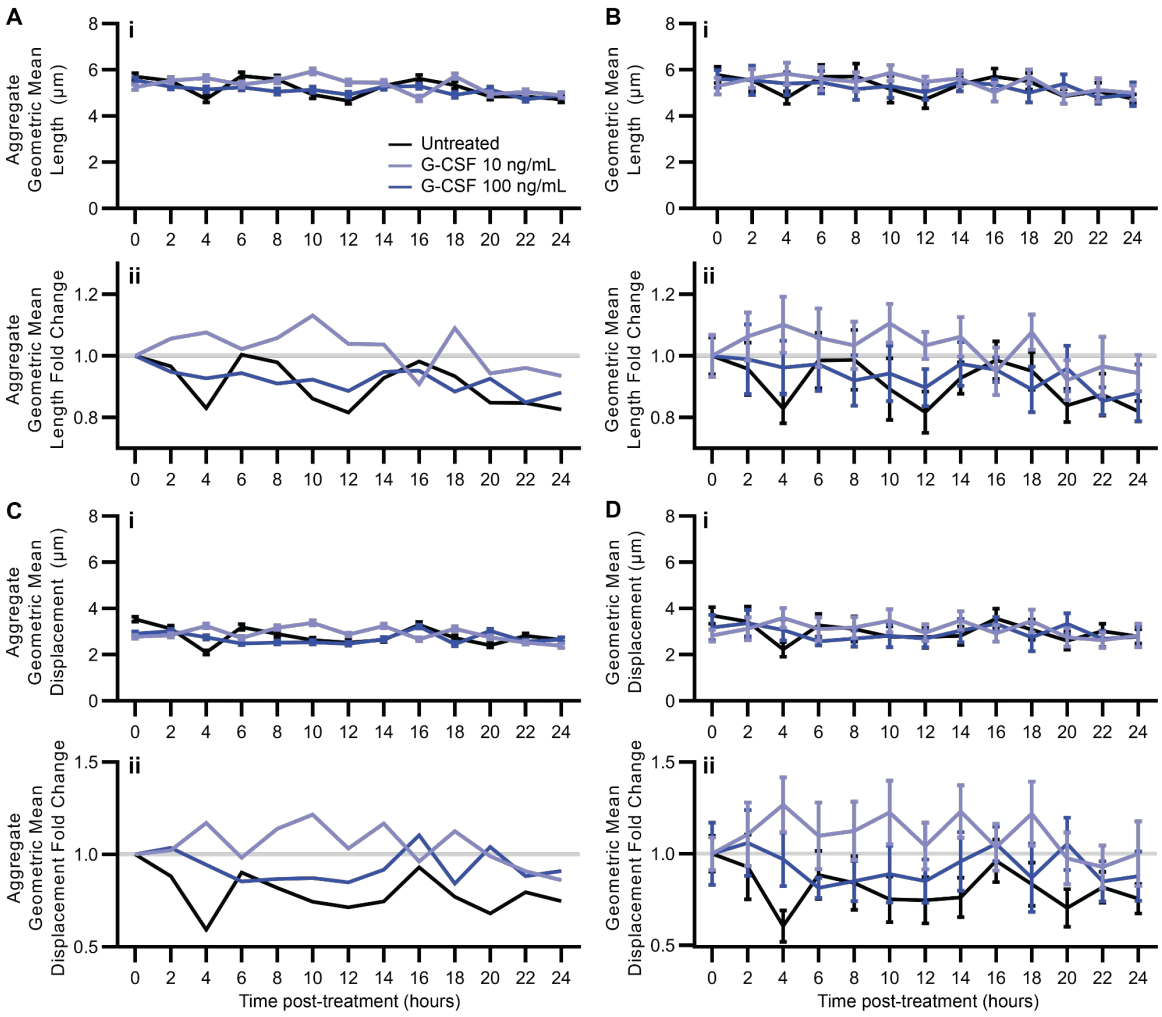

Figure 29. HSPC mobilization by G-CSF in hBM-on-a-chip. hBM-on-a-chip (HSPC+EC+MSC+OB) were untreated (black) or treated with 10 ng/mL G-CSF (light blue) or 100 ng/mL G-CSF (dark blue) and movement of HSPCs was measured over 24-hours. (A) Aggregate geometric mean track length, (B) sample geometric mean length, (C) aggregate geometric mean displacement, and (D) sample geometric mean displacement are represented as (i) absolute values and (ii) fold change for each sample. (A and C) Data are shown as (i, ii) geometric mean (i) ± 95%CI (n = 1627-2835 cells per time point pooled from 7-8 devices). (B and D) Data are shown as mean of geometric means ± SEM (n = 7 devices untreated, n = 8 devices 10 and 100 ng/mL G-CSF). Untreated data are the same as data shown in Figure 28B, C.

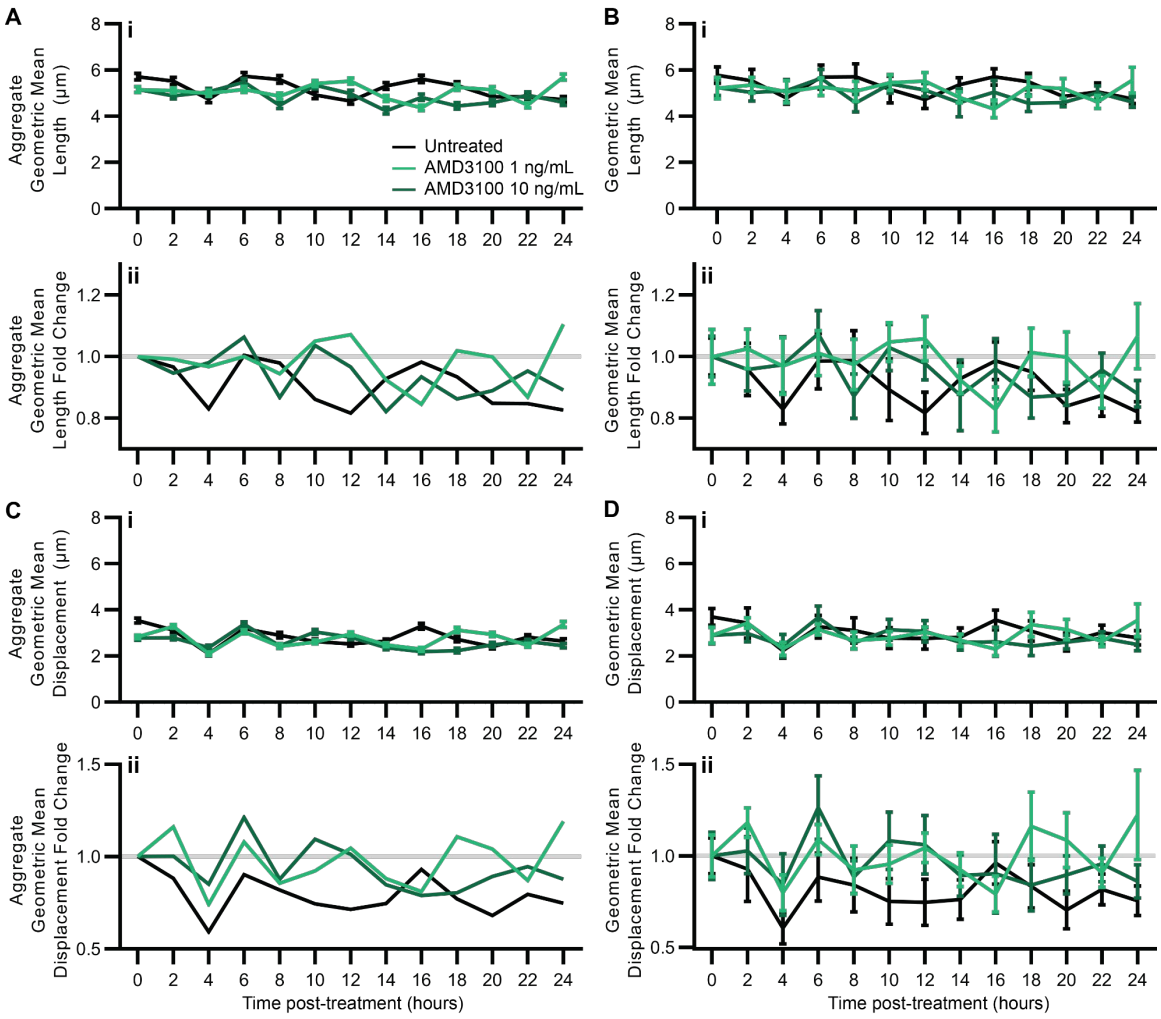

Figure 30. HSPC mobilization by AMD3100 in hBM-on-a-chip. hBM-on-a-chip (HSPC+EC+MSC+OB) were untreated (black) or treated with 1 ng/mL AMD3100 (light green) or 10 ng/mL AMD3100 (dark green) and movement of HSPCs was measured over 24-hours. (A) Aggregate geometric mean track length, (B) sample geometric mean length, (C) aggregate geometric mean displacement, and (D) sample geometric mean displacement are represented as (i) absolute values and (ii) fold change for each sample. (A and C) Data are shown as (i, ii) geometric mean (i) ± 95%CI (n = 1591-2246 cells per time point pooled from 7 devices). (B and D) Data are shown as mean of geometric means ± SEM (n = 7 devices). Untreated data are the same as data shown in Figure 28B, C.

5.2.3 Role of endosteal niche in mobilization

To determine whether the endosteal niche affected mobilization by G-CSF or lack of mobilization by AMD3100, we measured mobilization in hBM-on-a-chip with OBs (a vascularized endosteal niche model) and without OBs (a perivascular niche model). Similar to the previous, dosing experiment (Figure 29), with an endosteal niche present (+OB) devices treated with 10 ng/mL G-CSF had increased HSPC track length from approximately 2-14 hours post-treatment when compared to the untreated +OB control (Figure 31). Without an endosteal niche, there was no trend in increased track length or displacement when compared to the untreated -OB control. Again, there was no evidence of increasing length or displacement of HSPCs when treated with AMD3100 in the presence or absence of the endosteal niche (Figure 32).

5.2.4 High dose mobilization with AMD3100

To investigate whether the lack of mobilization in response to AMD3100 at doses of 1 ng/mL and 10 ng/mL, we tested a higher range of concentrations for mobilization potential (Figure 33). At 100 ng/mL, AMD3100 substantially increased HSPC track length from 2-4 hours post-treatment in the presence of the endosteal niche (+OB). However, the untreated +OB control also showed increased movement of HSPCs during this time frame, so it is inconclusive if any change in HSPC mobility is directly an effect of the treatment.

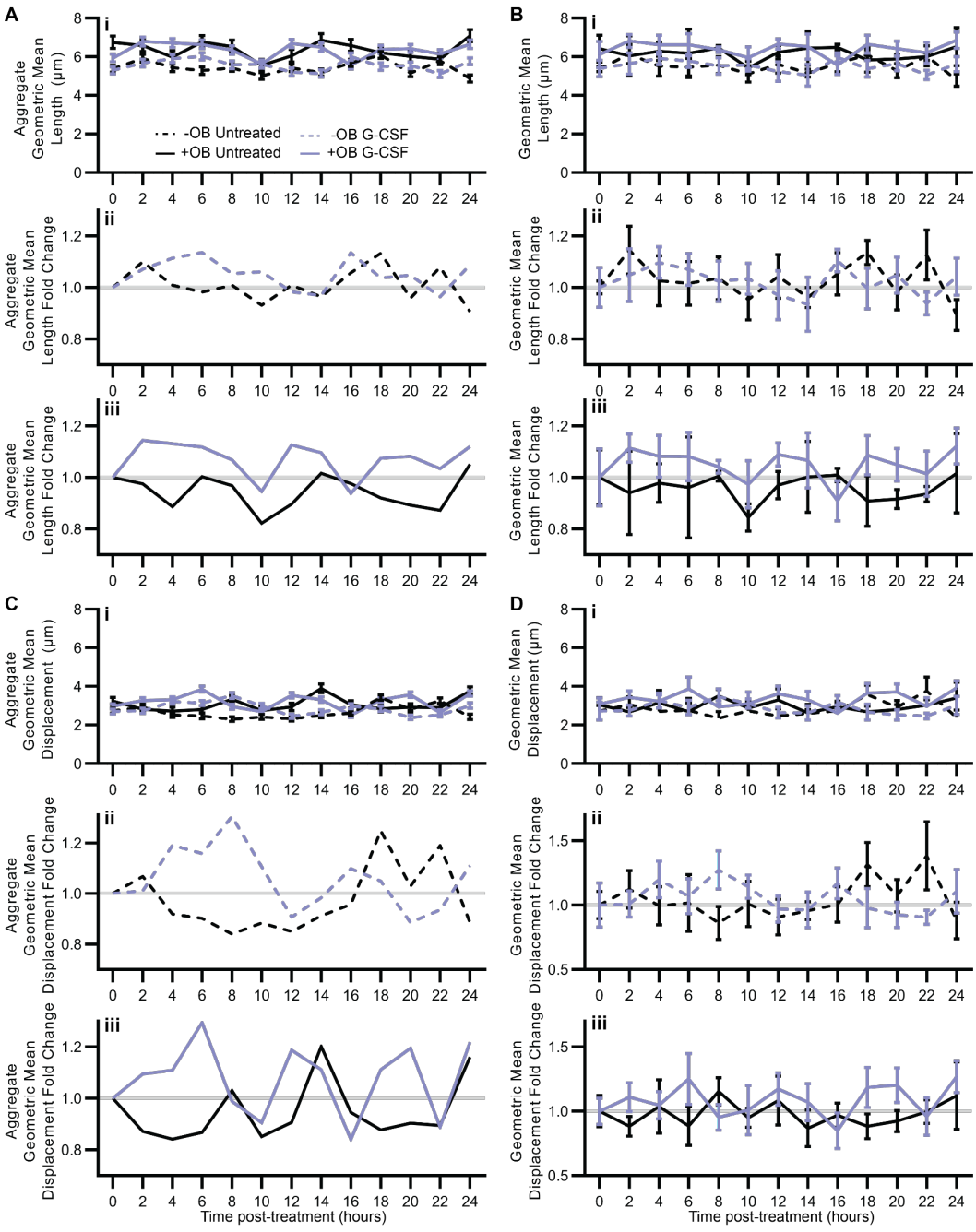

Figure 31. Effect of endosteal niche on G-CSF mobilization. hBM-on-a-chip with OBs (solid lines) and without OBs (dotted lines) were treated with 10 ng/mL G-CSF (light blue) or were untreated (black) and movement of HSPCs was measured over 24-hours. (A) Aggregate geometric mean track length, (B) sample geometric mean length, (C) aggregate geometric mean displacement, and (D) sample geometric mean displacement are represented as (i) absolute values and fold change for samples (ii) without OBs and (iii) with OBs. (A and C) Data are shown as () geometric mean (i) ± 95%CI (n = 746-1815 cells pooled from 3-6 devices). (B and D) Data are shown as mean of geometric means ± SEM (n = 3 devices +OB untreated, n = 5 devices –OB untreated, n = 6 devices –OB and +OB +GCSF).

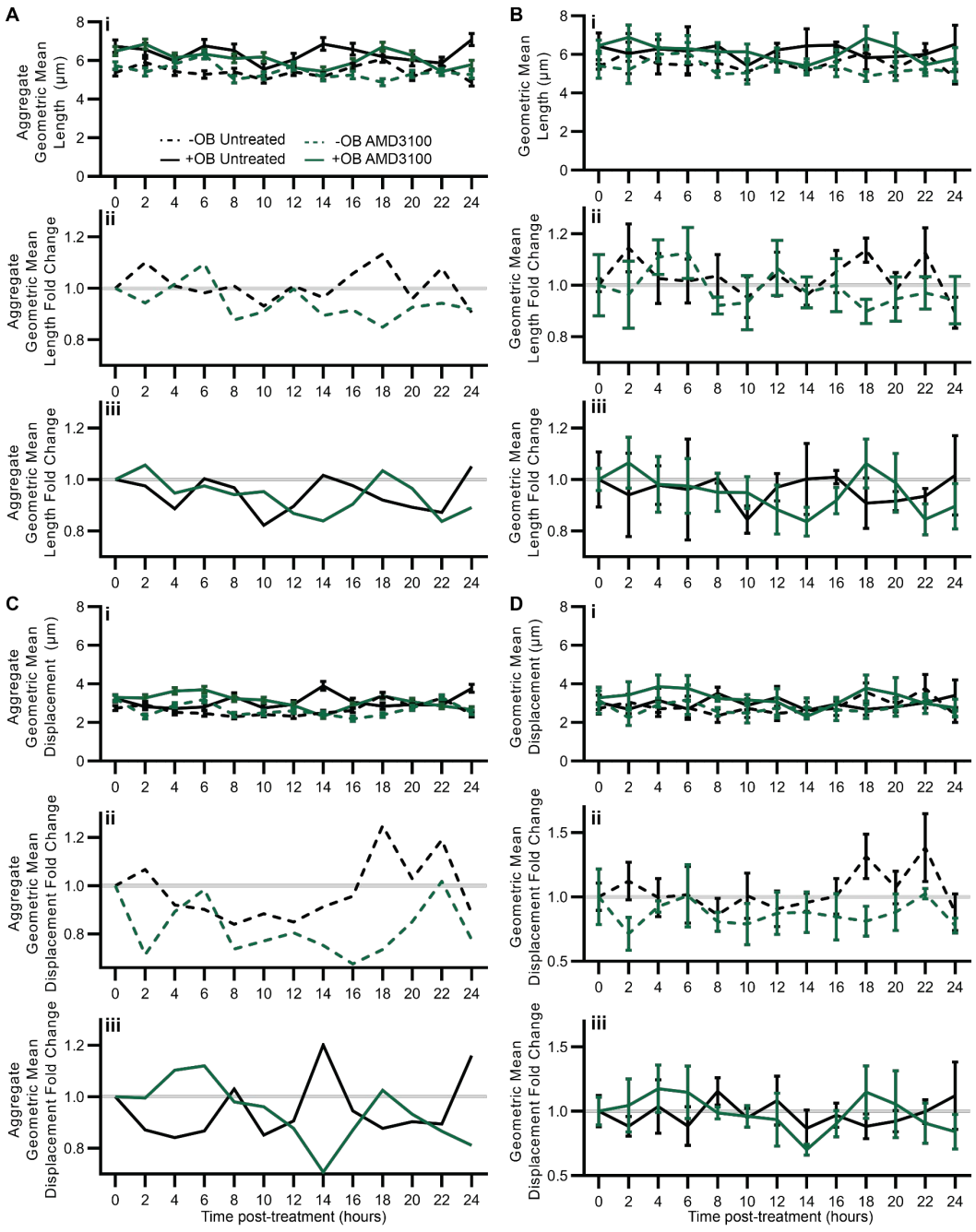

Figure 32. Effect of endosteal niche on AMD3100 mobilization. hBM-on-a-chip with OBs (solid lines) and without OBs (dotted lines) were treated with 10 ng/mL AMD3100 (green) or were untreated (black) and movement of HSPCs was measured over 24-hours. A) Aggregate geometric mean track length, (B) sample geometric mean length, (C) aggregate geometric mean displacement, and (D) sample geometric mean displacement are represented as (i) absolute values and fold change for samples (ii) without OBs and (iii) with OBs. (A and C) Data are shown as () geometric mean (i) ± 95%CI (n = 746-1498 cells pooled from 3-5 devices). (B and D) Data are shown as mean of geometric means ± SEM (n = 3 devices +OB untreated, n = 5 devices -OB untreated, n = 5 devices –OB and +OB +AMD3100).

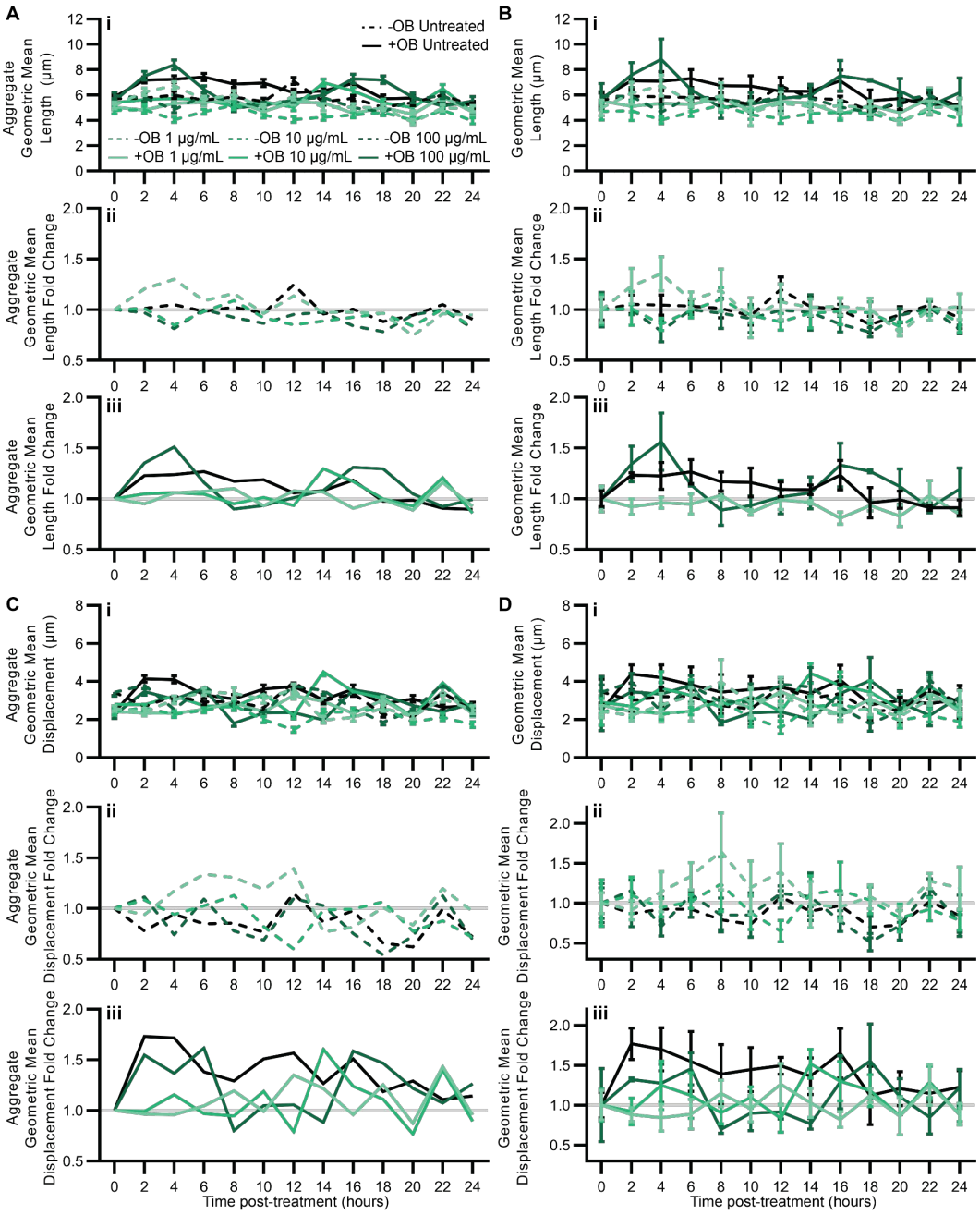

Figure 33. High dose AMD3100 mobilization of HSPCs. hBM-on-a-chip with OBs (solid lines) and without OBs (dotted lines) were treated with 1 µg/mL (light green), 10 µg/mL (green), 100 µg/mL AMD3100 (dark green) or were untreated (black) and movement of HSPCs was measured over 24-hours. (A) Aggregate geometric mean track length, (B) sample geometric mean length, (C) aggregate geometric mean displacement, and (D) sample geometric mean displacement are represented as (i) absolute values and fold change for samples (ii) without OBs and (iii) with OBs. (A and C) Data are shown as () geometric mean (i) ± 95%CI (n = 265-787 tracked cells per time point pooled from 3-4 devices). (B, D) Data are shown as mean of geometric means ± SEM (n = 3 devices –OB 100 µg/mL, +OB 100 µg/mL, n = 4 devices all other groups).

5.2.5 Mobilization with G-CSF and bortezomib

Mobilization of G-CSF is often done after or during chemotherapeutic regimes and prior treatment with chemotherapy. High dose chemotherapy (often with cyclophosphamide) in conjunction with G-CSF is the standard clinical mobilization protocol; however, patients that have had prior chemotherapy regimens can also be at risk for poor mobilization. We treated hBM-on-a-chip (HSPC+EC+MSC±OB) with bortezomib (BTZ), a protease inhibitor used to treated multiple myeloma that has been implicated in improving mobilization via disruption of VLA-4/VCAM-1 interactions between HSPCs and the BM microenvironment [210]. To investigate whether bortezomib induced mobilization of HSPCs or inhibited G-CSF mobilization, we treated hBM-on-a-chip with bortezomib, with and without simultaneous G-CSF treatment, both in devices with (+OB) and without (-OB) the endosteal niche (Figure 34). Bortezomib alone did not induce mobilization of HSPCs in devices with or without the endosteal niche as measured by track length (Figure 34A,B) and displacement (Figure 34C,D). Surprisingly, when samples were mobilized with bortezomib and G-CSF (at the same dose as in previous experiments (Figure 29, Figure 31), we also did not see any evidence of increase in length or displacement of HSPC movement. This suggests that bortezomib inhibited G-CSF mobilization, which has not been observed clinically with bortezomib as it has with other chemotherapeutic agents.

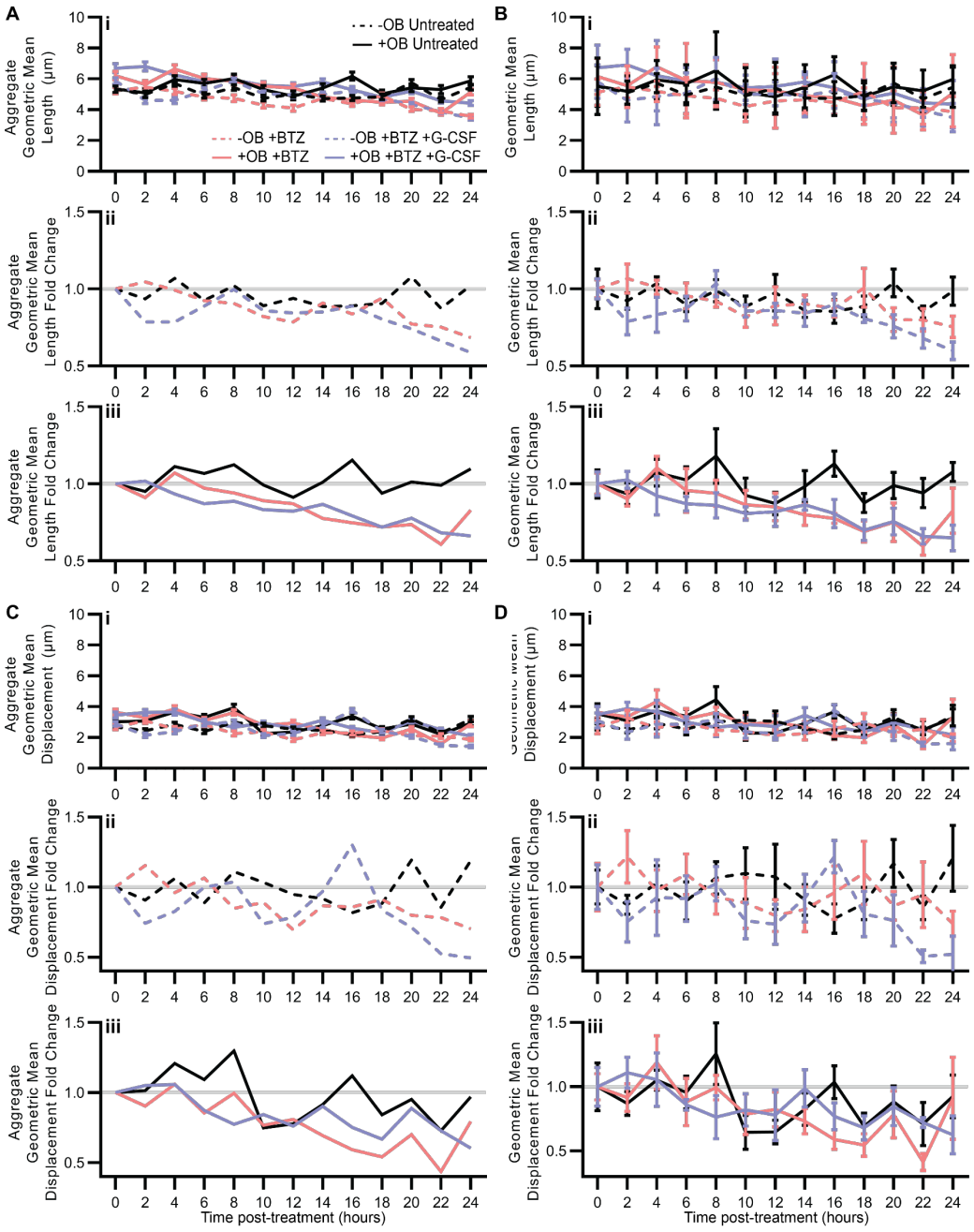

Figure 34. Mobilization with G-CSF with simultaneous bortezomib treatment. hBM-on-a-chip with OBs (solid lines) and without OBs (dotted lines) were treated with 100 nM bortezomib (BTZ) (red), 100 nM BTZ and 10 ng/mL G-CSF (blue) or were untreated (black) and movement of HSPCs was measured over 24-hours. (A) Aggregate geometric mean track length, (B) sample geometric mean length, (C) aggregate geometric mean displacement, and (D) sample geometric mean displacement are represented as (i) absolute values and fold change for samples (ii) without OBs and (iii) with OBs. (A and C) Data are shown as () geometric mean (i) ± 95%CI (n = 634-1004 tracked cells per time point pooled from 5-6 devices). (B, D) Data are shown as mean of geometric means ± SEM (n = 6 devices –OB and +OB untreated, n = 5 devices all other groups).

5.3 Methods

5.3.1 Previously described methods

hBM-on-chip were fabricated and cultured using the methods described in CHAPTER 3 and CHAPTER 4, see the following sections:

3.3.3.3 Version 2.0 device fabrication

3.3.5 Surface coating of PDMS

4.3.2 Cell culture

4.3.3 Osteogenesis in hBM-on-a-chip

4.3.5 Vasculogenesis in hBM-on-a-chip

4.3.10 Culture of CD34+ BM HSPCs in hBM-on-a-chip

5.3.2 Measuring CXCL12 by IHC

Staining procedure for devices was adapted from Chen *et al* 2017 [170]. Devices were washed with PBS, fixed with 4% formaldehyde (ThermoFisher), and permeabilized with 0.1% Triton X-100. Prior to staining, cells were blocked with 5% BSA, 3% goat serum in PBS. Primary antibody was diluted (1:100) in blocking buffer and devices were stained overnight at 4 ºC. Devices were then washed with 0.1% BSA in PBS (wash buffer) and stained with secondary antibody (1:200) diluted in wash buffer for 3 hours at RT. Devices were washed with wash buffer and then stained with Phalloidin AF647 (1:40).

5.3.3 G-CSF, AMD3100 Bortezomib treatment

After 5 days vasculogenesis, hBM-on-a-chip devices were treated with G-CSF (Peprotech), AMD3100 (Sigma Aldrich) and/or bortezomib (Sigma-Aldrich). G-CSF, AMD3100, bortezomib were diluted to indicated concentrations in EGM-2MV (Lonza)

[211]. Media was aspirated from media reservoirs of hBM-on-a-chip and replaced with 50 μL per reservoir (200 μL total per device) by adding 100 μL to one side of the device and allowing the media to flow through to the connecting reservoir.

5.3.4 Multiplex cytokine detection

Device media was collected at 0 hours (immediately prior to treatment with G-CSF or AMD3100) and 24 hours after treatment. Media was collected from devices at designated time by collecting media from one side of device, waiting for 5 minutes to allow for gravity driven flow through the device and then collection of all media from reservoirs. Device media was immediately stored on ice and then flash frozen in liquid N_2 for storage prior to analysis. Samples were thawed on ice prior to detection and analysis using LEGENDplex human hematopoietic stem cell panel (BioLegend), according to manufacturer's protocol.

5.3.5 Measuring mobilization of HSPCs

After 5 days of culture, hBM-on-a-chips were imaged periodically to measure the "mobilization" of CD34+ HSPCs. Baseline measurements were made at 0 hours, after which supernatants were collected and was replaced with media supplemented with mobilizing agents at indicated concentrations. Samples were imaged at intervals of 2 hours for 24 hours for a total of 13 image sessions. During each image session, devices were imaged at intervals of 5 minutes for 15 minutes, for a total of 4 time points. Samples were imaged using a Cytation 3 (BioTek Instruments) and automated imaging of multiple plates was achieved using a BioSpa 3 (BioTek Instruments). Image sequences were imported into Volocity software (PerkinElmer), cells were tracked within each image session, and the length and displacement of individual cells were measured at each time point.

To represent the mobilization data, we show both the aggregate population geometric mean and the mean of sample geometric means. The distribution of cell track length and displacement is lognormal (Figure 28B,C), therefore the geometric mean is a more appropriate representative statistic of the population than the arithmetic mean. Geometric mean length and displacement were measured for both the population of all cells pooled from replicate devices:

$$\bar{x}_{geometric} = \left(\prod_{i=1}^{n} x_i\right)^{\frac{1}{n}} = \sqrt[n]{x_1 x_2 \dots x_n} \tag{3}$$

And the geometric mean was calculated for each individual sample, *j,* to quantify the variability between devices:

$$\bar{x}_{geometric,j} = \left(\prod_{i=1}^{n} x_{i,j}\right)^{\frac{1}{n}} = \sqrt[n]{x_{1,j} x_{2,j} \dots x_{n,j}} \tag{4}$$

5.4 Discussion

In this chapter we have investigated the effect of G-CSF and AMD3100 on the surrogate BM microenvironment in the hBM-on-a-chip and we have developed a potential method for studying the mobilization of HSPCs in the BM mimic devices.

The mobilization of stem cells from BM requires the disruption of the multifaceted biochemical signaling that maintains HSPCs in the BM compartment. Although standard regimens (high dose chemotherapy and G-CSF) and rapid mobilizers (AMD3100) are successful in most patients, there are a subset of patients who still fail to mobilize and there are few clinically approved options beyond those mentioned above [191]. An *in vitro* microenvironment that can mimic the native tissue's response to mobilization would be

useful in preclinical evaluation of novel compounds and, potentially, for patient specific screening of possible regimens.

Due to the complex nature of the mobilization process, most preclinical studies of are performed in animal models, although there are a few examples of *in vitro* methods. Transwell migration assays have been used to study agents that the disrupt HSPC migration toward CXCL12 or other chemokines, and to study agents that are chemokines themselves and work through competitive signaling [212]. There are even fewer examples of 3D culture models that have been used to study the disruption of CXCL12/CXCR4 signaling. One such example is the hydrogel co-culture of HSPCs with MSCs, where treatment with AMD3100 induced the migration of HSPCs out of the hydrogel into the culture media [213]. To our knowledge, no *in vitro* culture systems that incorporate the perivascular niche have been used to study the disruption of the HSPC chemokine signaling.

We first investigated the effects of G-CSF and AMD3100 on cytokine secretion in hBM-on-a-chip. We found no significant difference in the expression of cytokines that were measurable within the device supernatant. Because CXCL12 was not detectable, we attempted to quantify its expression using immunohistochemistry (see Appendix B for more details). As expected, AMD3100, which inhibits CXCR4 specifically, did not affect CXCL12 expression. Although there was no significant difference in CXCL12 expression, we did observe a substantial decrease in expression in a subset of the devices treated with G-CSF. It is unclear if the decrease in CXCL12 expression we observed is characteristic of a population of hBM-on-a-chips, that only a subset of devices will have decreased CXCL12 expression due to an inherent difference in the device composition (cells, material, etc.) that has gone unnoticed. Further study is needed to fully understand this

response.

To measure the mobilization of HSPCs in hBM-on-a-chip, we developed a protocol that allowed for the periodic measurement of cell movement over a 24-hour period. We did so because we did not anticipate HSPCs would be drawn out of the hBM-on-a-chip, because there was no supplemented chemokine or existing gradient within the device that would direct the HSPCs in a specific direction. Rather, we hypothesized that mobilization would disrupt local signaling that was restricting HSPC movement and would therefore lead to an increase in either the magnitude or displacement of migration during a given time period.

Mobilizing with AMD3100, we did not see any change in migration at low doses. Although the result was obscured by high fold change in control, untreated samples, we measured a substantial increase in movement with a high dose of AMD3100 (100 μg/mL) 2-4 hours after treatment, which merits attention for future studies. Mobilizing the HSPCs with G-CSF, we observed a dose specific response that lead to increased total length of migration and displacement over approximately a 14-hour period compared with the 0-hour baseline in both vascularized endosteal niche (+OB) and perivascular (-OB) hBM-on-a-chip devices. The mechanism of G-CSF mobilization is believed to go through any number of BM resident cells (neutrophils, osteoblasts, osteoclasts, macrophages) [193-196] with MSCs being a notable exception. The potential mobilization observed in samples without OBs is curious and, if true, suggests that either MSCs can mediate G-CSF induced disruption of CXCL12 signaling or that G-CSF is directly activating increased movement in HSPCs.

Similarly, the lack of response to G-CSF when co-administered with bortezomib

was unexpected. Bortezomib has been shown to mobilize HSPCs independent of and additively with other treatments in animal models [210]. Due to the relative simplicity of the hBM-on-a-chip, it reasonably could be that a or any number of cell types that are necessary for the *in vivo* response are not present and therefore the model cannot recapitulate the effect of the treatment. Similarly, the state of the HSPCs themselves in hBM-on-a-chip could deviate the observed response in unexpected ways.

While we did observe some effect in response to mobilizing agents, which is encouraging for the utility of hBM-on-a-chip for this application, there are many areas for improvement. First, there is a significant amount of noise, both between time points and between samples, relative to the size of the measured effect that necessitates large sample sizes. While we are reasonably confident in our conclusions, it should be noted that the untreated samples did exhibit periodic fluctuations in track length and displacement, and it should not be discounted that there is a possibility that any effect we observed was random noise. Second, as mentioned above, the hBM-on-a-chip in its current iteration is a relatively simple model of the BM microenvironment and does not contain many key cell types that have been implicated in the mobilization process. Increasing the complexity, while decreasing the inter- and intra-device variability is necessary for using hBM-on-a-chip for studying HSPC mobilization.

CHAPTER 6. AIM 2B: EFFECTS OF RADIATION

6.1 Introduction

Ionizing radiation (IR) can cause damage to BM microenvironment and resident HSPCs occurs in both accidental and clinical situations [214]. In both cases, exposure to IR causes damage to HSPCs and subsequently results in the depletion of mature hematopoietic cells, leading to a range of symptoms associated with hematopoietic syndrome, and in extreme cases, fatality. At low doses of IR, populations of circulating hematopoietic cells decline quickly, within days, but recover weeks after the exposure. At higher doses of IR (the LD_{50} for humans is 4.25 Gy [215]) the acute loss of circulating cells never recovers, and the hematopoietic system fails because HSCs in the BM are no longer able to generate sufficient progenitor cell populations [216]. Understanding the specific impact of IR on HSPCs and the BM niche is important for developing effective countermeasures that can allow for the native or transplanted hematopoietic system to recover or reconstitute a healthy BM.

While the direct effects of IR on the hematopoietic system are well characterized, the corresponding effects of IR on the HSPC niche and stromal cells in the BM compartment are less understood. The specific effects of IR on the BM microenvironment can directly lead to damage to hematopoietic cells (e.g. through the production of reactive oxygen species [215,217,218]), or they can indirectly damage the hematopoietic system (e.g. by the change in expression of proteases or ECM in the BM niche). MSCs, what are sometimes referred to as the other BM stem cell, are surprisingly more resistant to the effects of IR. MSCs have been observed to resistant to ionizing radiation, possibly

providing protection to other radiation damaged cells [219]. Conversely, the activity of both osteoblasts and endothelial cells are altered by exposure to IR. Osteoblasts have been observed to be downregulated [218,220,221], decreasing the deposition of endosteal matrix and possibly, in conjunction with up regulation of osteoclasts, cause loss of bone mass at a larger scale[222]. This could lead to the loss of the endosteal niche for specific progenitor cell populations that may be counteracted by increased osteogenic differentiation of MSCs [223]. Common to radiation damage to all tissue types, the vasculature in BM is damaged and blood flow is disturbed [220]. Damage to endothelial cells likely disrupts the perivascular niche occupied by HSCs and recovery of this microenvironment is essential for the regeneration of the functioning hematopoietic system.

The effects of radiation have, in the past, been studied mostly in animal models, recently organ-on-chip systems have been explored for their potential application in radiobiology [224,225]. Using organ-on-chip systems to examine the biologically response to radiation exposure not only moves preclinical studies away from animal models, but it may better recapitulate the response of human cells in radiation exposure situations. An *ex vivo,* ectopic engineered BM has been used to test the effectiveness of radiation countermeasures. Typical countermeasure treatments, like EPO and G-CSF, increased the production of hematopoietic cells in the engineered BM and were generally consistent with clinical observations [225].

Cs-137 has been the standard source of ionizing radiation in *in vitro* and preclinical *in vivo* studies, including the previously discussed examples of organ-on-chips [225]. Recently, x-ray radiation sources have been introduced to replace Cs-137 irradiators because, since the radiation emission can be turned off, they are much safer instruments

for research use. However, the use of PDMS in device fabrication creates a potential problem for its application in radiation studies when using an x-ray source irradiator because PDMS has been observed to attenuate x-rays, especially during low energy exposures [226].

Here, we use the hBM-on-a-chip to investigate the effects of IR on HSPCs, the BM microenvironment and the role that stromal cells play in protecting HSPCs from radiation damage.

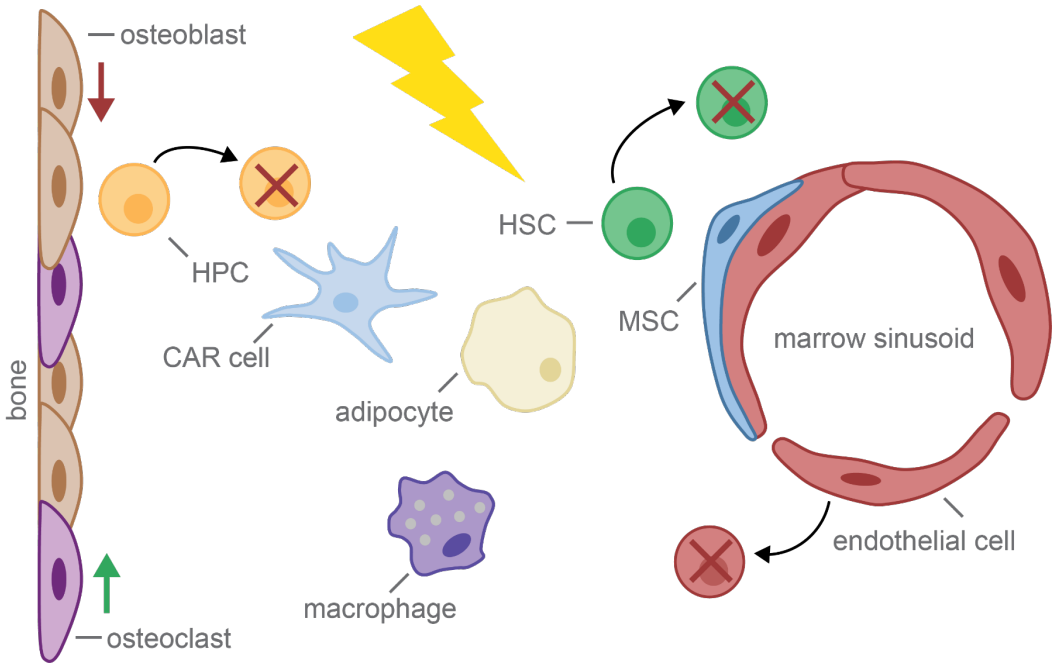

Figure 35. Effects of radiation on BM microenvironment. Ionizing radiation causes cell death because of DNA damage to proliferative cells in the BM compartment, HSCs and their progenitors suffer increasing amounts of cell death as a function of the radiation dose. Osteoblasts have been observed decrease in functionality, leading to loss of bone mass that is exacerbated by potential increased osteoclast activity. Endothelial cells undergo apoptosis and vascularization of irradiated tissue decreases.

6.2 Results

6.2.1 PDMS attenuation of x-ray radiation

To determine the x-ray attenuation of hBM-on-a-chip, dosimeters were exposed to x-ray radiation doses of 2.5 Gy, 5 Gy, and 10 Gy through the well-plate hBM-on-a-chip device and compared to un-shielded, control dosimeters (Figure 30). Dosimeters shielded by the device did not show any reduction in dose compared to the control dosimeters. The measured dose of radiation was less than the theoretical dose for all three groups. The measured dose (both control and PDMS shielded) was 1.73 ± 0.04 Gy, 3.89 ± 0.03 Gy, and 8.03 ± 0.11 Gy (mean ± SEM) for the 2.5 Gy, 5 Gy, and 10 Gy groups, respectively. This corresponds to yields of 69%, 78%, and 80% of the theoretical doses.

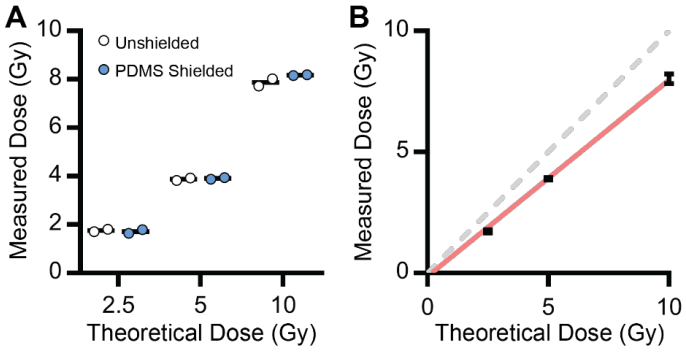

Figure 36. PDMS attenuation of x-ray radiation. (A) Measured radiation dose of NanoDot® dosimeters exposed to 2.5, 5, or 10 Gy x-ray radiation with (blue) or without (white) PDMS shielding. Data is shown as mean (n = 2 dosimeters). (B) Linear regression (Equation 5) of grouped (unshielded and PDMS shielded) dosimeter readings (red) used to interpolate exposure settings for accurate dosing. Data are shown as mean ± SD (n = 4 dosimeters). Perfect correlation (y = x) between theoretical and measured dose is shown by grey dotted line.

Grouping the unshielded control samples and the PDMS shielded samples together, linear regression was performed to determine the difference between the theoretical

radiation dose and the actual radiation dose measured (Equation 5).

$$Dose_{Measured} = 0.8108\, Dose_{Theoretical} - 0.1349\,; R^2 = 0.9987 \quad (5)$$

Exposure settings were subsequently adjusted to account for discrepancy between the irradiator's exposure rate and the measured doses.

6.2.2 Effect of radiation on hBM-on-a-chip microenvironment

To investigate the effect of ionizing radiation on the BM microenvironment in hBM-on-a-chip, after 5 days of vasculogenesis, devices containing OBs, MSCs, and ECs were exposed to 0 Gy, 2.5 Gy, 5 Gy, or 10 Gy x-ray irradiation. Device supernatant was collected at 0 hours (pre-treatment) and 24 hours radiation exposure. To measure cytotoxicity because of radiation, the change in lactate dehydrogenase (LDH) activity of the supernatant after irradiation was measured (Figure 37). Although we did not measure a significant increase in LDH activity, the LDH activity in devices exposed to 5 Gy and 10 Gy x-ray radiation marginally increased after exposure, while the activity in devices exposed to 0 Gy and 2.5 Gy radiation slightly decreased during the same period.

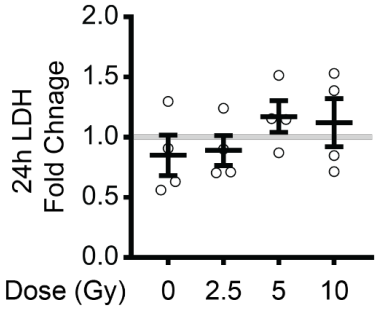

Figure 37. Cytotoxicity due to x-ray radiation without HSPCs. Fold change in LDH released from hBM-on-a-chip (EC+MSC+OB) 24 hours post-x-ray irradiation compared to baseline (0 hours). Data are shown as mean ± SEM (n = 4 devices). Data analyzed using Kruskal-Wallis with Dunn's multiple comparison test. No significance between groups ($p < 0.1$).

The change in cytokine secretion because of x-ray exposure was also measured. IL-6, IL-7, IL-11, M-CSF, and SCF were detected, however CXCL12, IL-3, IL-15, IL-34, GM-CSF, FLT3L, and LIF were not above the detection limit of the assay. While there was no significant difference between the groups, it is worth noting that there was a decrease in secretion of IL-6, IL-7, IL-11, M-CSF, and SCF for all irradiated groups.

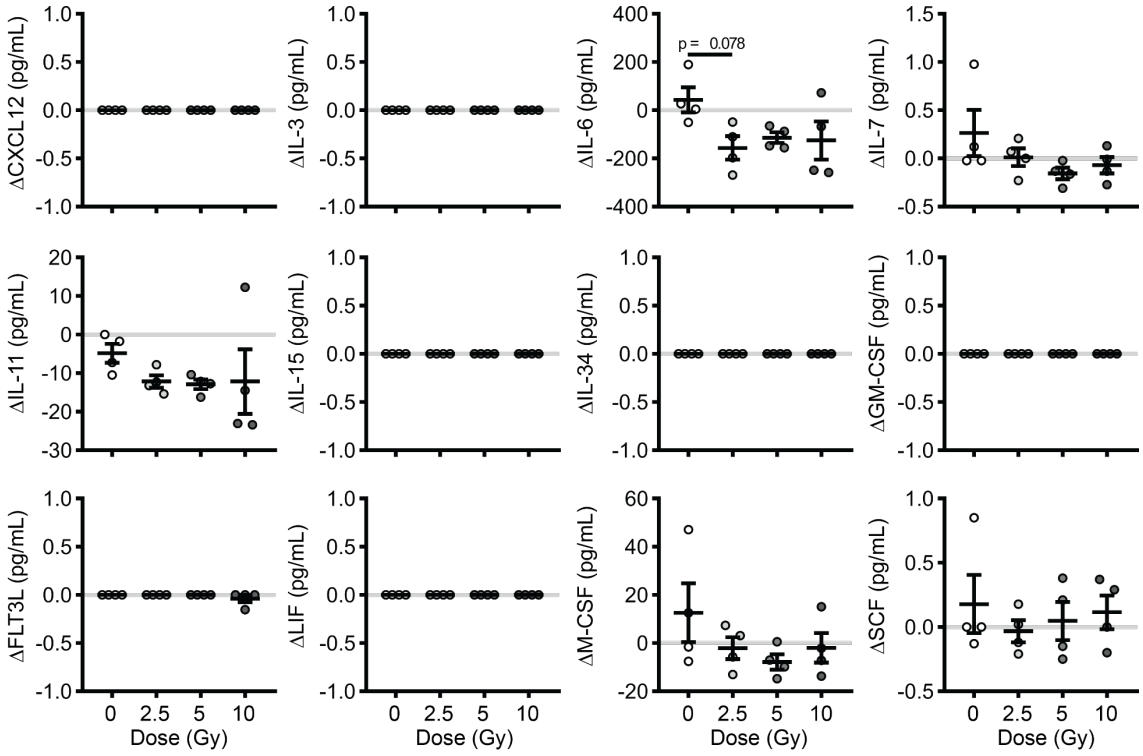

Figure 38. Effect of radiation on cytokine secretion without HSPCs. Change in hematopoietic cytokine measured in hBM-on-a-chip (EC+MSC+OB) supernatant before (0 hours) and 24 hours after devices were exposed to 0 (white), 2.5 (light grey), 5 (grey), or 10 (dark grey) Gy x-ray radiation. Data are shown as mean ± SEM (n = 4 devices). Data analyzed using Kruskal-Wallis with Dunn's multiple comparisons test.

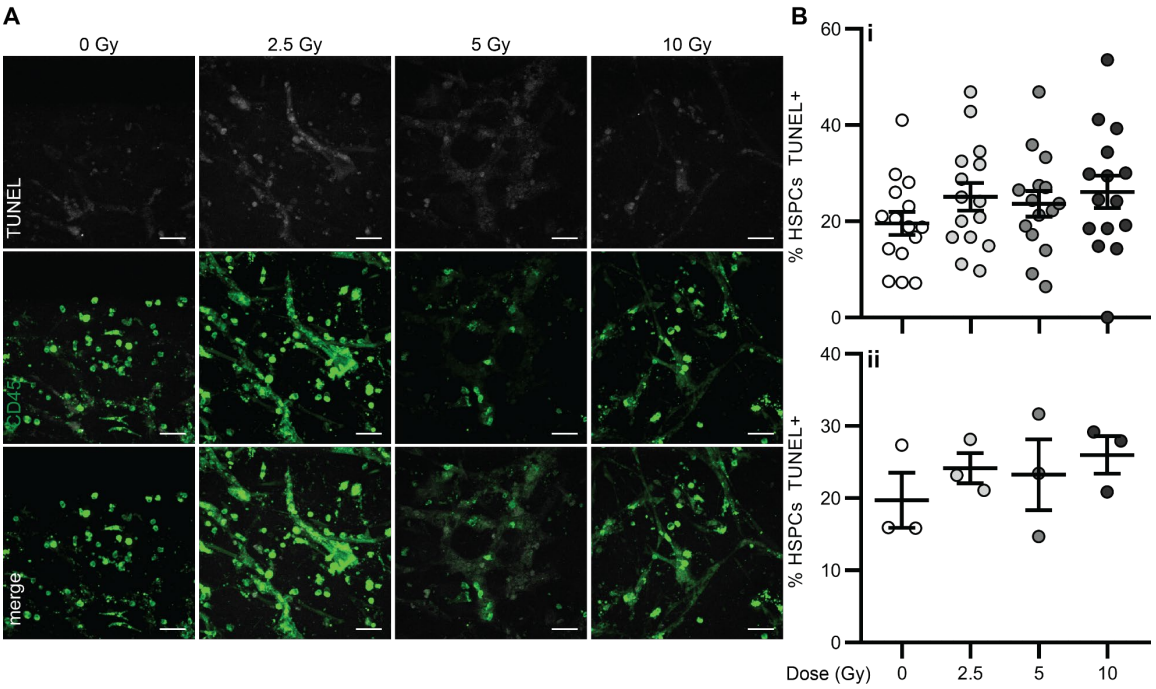

Figure 39. Dose response of HSPCs to x-ray radiation. (A) Representative images of TUNEL (white) and CD45 (green) staining of devices exposed to 0, 2.5, 5, or 10 Gy radiation 24 hours after exposure. Scale bar: 50 μm. (B) Quantification of percentage of TUNEL$^+$ CD45 cells 24 hours after 0 (white), 2.5 (light grey), 5 (grey), 10 dark grey) Gy radiation exposure shown by (i) ROI and (ii) device. Data (n = 15 ROIs (i) from 3 devices (ii)) are shown as mean ± SEM. Data analyzed using Kruskal-Wallis with Dunn's multiple comparisons test. No significance between groups ($p < 0.1$).

6.2.3 Fate of x-ray irradiated HSPCs

hBM-on-a-chip (EC+MSC+OB+HSPC) were irradiated after 5 days of vasculogenesis and the frequency of apoptotic cells 24 hours post exposure was quantified using a TUNEL assay (Figure 39). Because the hBM-on-a-chip is a co-culture, TUNEL staining was not restricted to HSPCs and many non-hematopoietic cells were observed staining positive for TUNEL (Figure 39A). The percentage of TUNEL$^+$ HSPCs was relatively high, 19.7 ± 3.8%, in non-irradiated samples (Figure 39B), suggesting that there is a high rate of on-going apoptosis in the culture hematopoietic cells in hBM-on-a-chip. When exposed to x-ray radiation, there was not a statistically significant increase in

TUNEL$^+$ HSPCs, however there was a trend of increased TUNEL$^+$ HSPCs with increasing dose. HSPCs in hBM-on-a-chip irradiated with 2.5, 5, and 10 Gy radiation were TUNEL$^+$ at frequencies of 24.2 ± 2.1%, 23.3 ± 4.9%, and 26.0 ± 2.6%, respectively.

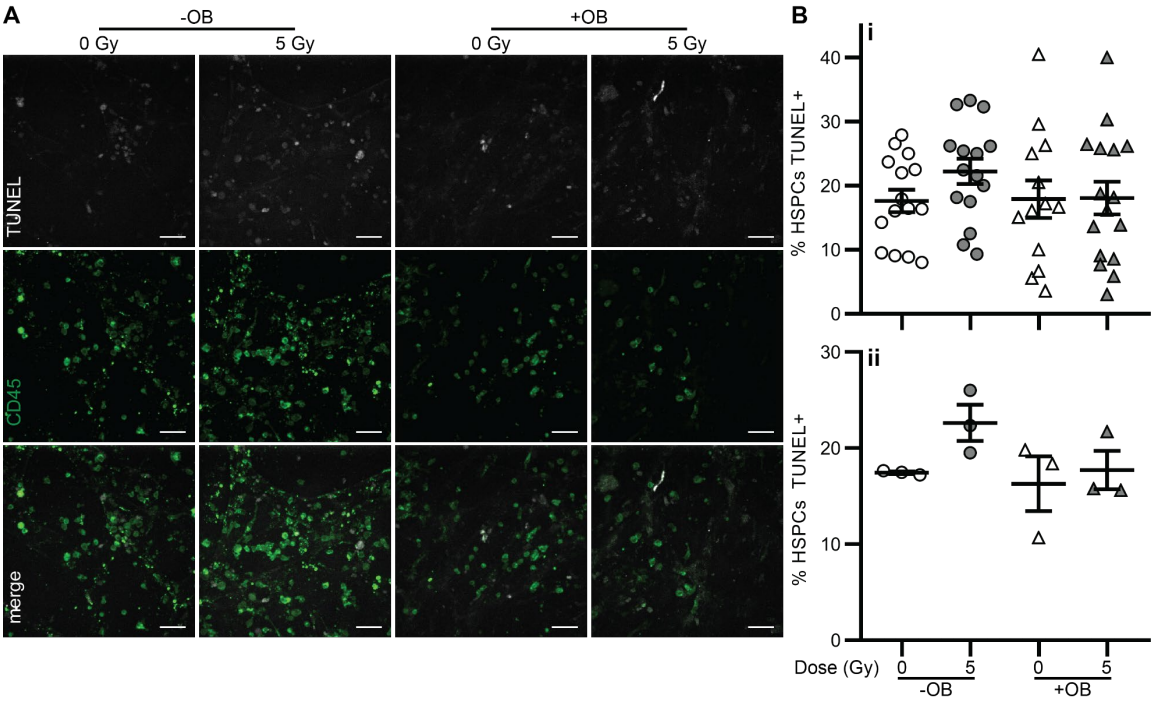

Figure 40. Role of endosteal niche in radiation damage to HSPCs.(A) Representative images of TUNEL (white) and CD45 (green) staining of devices, with or without OBs, exposed to 0 or 5 Gy radiation 24 hours after exposure. Scale bar: 50 μm. (B) Quantification of percentage of TUNEL$^+$ CD45 cells, with (triangles) or without (circles) OBs, 24 hours after 0 (white) or 5 (grey) Gy radiation exposure shown by (i) ROI and (ii) device. Data are shown as mean ± SEM (n = 15 ROIs (i), n = 3 devices (ii)). Data analyzed using Kruskal-Wallis with Dunn's multiple comparisons test. No significance between groups ($p < 0.1$).

6.2.4 Effect of endosteal niche on x-ray irradiated HSPCs

After observing a relatively mild increase in apoptotic HSPCs after exposure to radiation doses upwards of 10 Gy, we sought to determine whether the presence of the endosteal niche was ameliorating the effects of radiation for HSPCs. hBM-on-a-chip with

(EC+MSC+OB+HSPC) and without (EC+MSC+HSPC) the endosteal niche, were exposed to 5 Gy x-ray radiation and again apoptosis was measured 24 hours after exposure via a TUNEL assay (Figure 40). Similarly, high backgrounds of apoptotic HSPCs were observed, 17.5 ± 0.1% of HSPCs in untreated -OB samples and 16.3 ± 2.8% of HSPCs in untreated +OB samples staining positive for TUNEL (Figure 40B). While, again, there was not a statistically significant difference between any of the groups, we saw a similar, moderate increase in $TUNEL^+$ HSPCs in +OB devices exposed to 5 Gy radiation (17.7 ± 2.0%). There was a larger increase in $TUNEL^+$ HSPCs when exposed to 5 Gy radiation without the endosteal niche (-OB) present, with 22.6 ± 1.9% of HSPCs apoptotic.

6.2.5 Post-irradiation treatment with G-CSF

After radiation injury, there are a number of countermeasures that are used to prevent failure of the hematopoietic system, including G-CSF [227]. To test G-CSFs ability to increase hematopoietic survival post-irradiation, we treated perivascular niche (-OB) and vascularized endosteal niche (+OB) hBM-on-a-chip with G-CSF (10 ng/mL) 24 hours after radiation exposure and then measured HSPC apoptosis at 48 hours by a TUNEL assay (Figure 41). Similarly to previous experiment, we measured a high background of $TUNEL^+$ HSPCs and high variability between imaged ROIs (Figure 41i) and device replicates (Figure 41ii). While no differences between groups were statistically significant, there was a modest increase in $TUNEL^+$ HSPCs in the perivascular niche (-OB) devices exposed to 5 Gy radiation (19.1 ± 4.7%) when compared to non-irradiated samples (16.4 ± 2.7%) or irradiated devices treated with G-CSF (17.3 ± 2.3%). Likewise, there was a potential decrease in $TUNEL^+$ HSPCs in irradiated vascularized endosteal niche devices treated with G-CSF (15.4 ± 2.8%) compared to irradiated samples that were untreated (17.9 ± 2.0%).

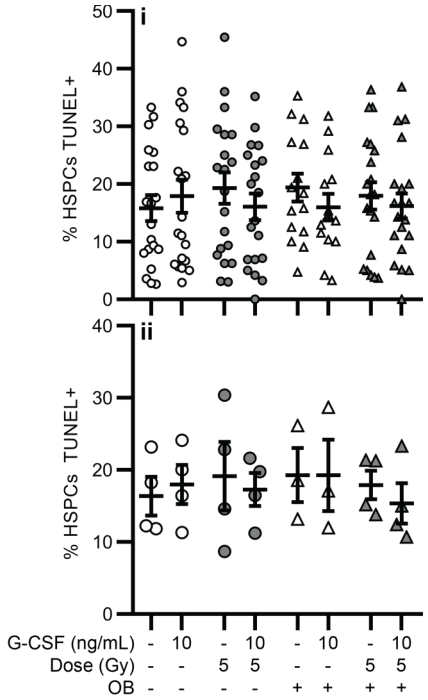

Figure 41. Post-irradiation treatment with G-CSF. Quantification of percentage of TUNEL$^+$ CD45 cells at 48 hours after 0 (white) or 5 (grey) Gy radiation exposure, with (10 ng/mL) or without G-CSF treatment 24 hours post-irradiation, with (triangles) or without (circles) OBs shown by (i) ROI and (ii) device. Data are shown as mean ± SEM (n = 15-20 ROIs (i), n = 3-4 devices (ii)). Data analyzed using Kruskal-Wallis with Dunn's multiple comparisons test. No significance between groups ($p < 0.1$).

6.3 Methods

6.3.1 Previously described methods

hBM-on-chip were fabricated and cultured using the methods described in CHAPTER 3 and CHAPTER 4, see the following sections:

3.3.3.3 Version 2.0 device fabrication

3.3.5 Surface coating of PDMS

4.3.2 Cell culture

4.3.3 Osteogenesis in hBM-on-a-chip

6.3.2 Radiation dose measurement and PDMS attenuation

Dosimeters (nanoDot™, Landauer) were exposed to theoretical radiation doses of 2.5, 5, and 10 Gy using an RS 2000 X-Ray Irradiator (Rad Source) at 2.15 Gy/min. To determine x-ray attenuation by the PDMS in hBM-on-a-chip, dosimeters were placed underneath a well-plate hBM-on-a-chip during exposure. Control samples were exposed without PDMS device shielding. A transit control dosimeter was also measured and the background radiation dose during shipping and use was subtracted from all test dosimeters. Dosimeters were returned to the service provider (Landauer) for dose measurements.

6.3.3 X-ray radiation of hBM-on-a-chip

On day 5, hBM-on-a-chip devices were transported to an animal facility and exposed to ionizing radiation using an RS 2000 X-Ray Irradiator (Rad Source). To control for effects of transportation, untreated samples were also transported to the facility. The duration of the process (transportation to and from the facility and x-ray exposure) was ~1 hour, during which time the samples were not held at 37 °C, 5% CO_2.

6.3.4 Lactate dehydrogenase assay to measure cytotoxicity

Device supernatant was collected (0 hour), replaced prior to radiation exposure and collected 24 hours after exposure. Supernatant was flash frozen immediately upon collection and stored at -20 °C prior to analysis. LDH activity was measured using the Pierce™ LDH Cytotoxicity Assay (ThermoFisher) according to the manufacturer's protocol. For each device, *i,* the 24-hour fold-change in LDH activity was calculated by

dividing the background subtracted A_{490} at 24 hours from the sample matched 0-hour value.

6.3.5 Multiplex cytokine detection

Device media was collected at 0 hours (immediately prior to transport to radiation facility) and 24 hours after exposure. Media was collected from devices at designated time by collecting media from one side of device, waiting for 5 minutes to allow for gravity driven flow through the device and then collection of all media from reservoirs. Device media was immediately stored on ice and then flash frozen in liquid N_2 for storage prior to analysis. Samples were thawed on ice prior to detection and analysis using LEGENDplex human hematopoietic stem cell panel (BioLegend), according to manufacturer's protocol.

6.3.6 TUNEL assay

DNA damage to HSPCs was observed using terminal deoxynucleotidyl transferase-mediated dUTP-biotin nick-end labelling (TUNEL) immunostaining (Click-iT TUNEL Alexa Fluor Assay Kit, ThermoFisher) according to the manufacturer's protocol. Briefly, formaldehyde fixed devices were first permeabilized with Triton-X100 (Avocado). Next, terminal deoxynucleotidyl transferase (TdT) was used to incorporate dUTP into double stranded breaks of DNA. Alexa Fluor 647 azide was then bound to dUTP using click chemistry. As membrane stains of HSPCs do not survive Triton-X100 permeabilization, HSPCs were then stained overnight using anti-human CD45 Alexa Fluor 488 (BioLegend). Samples were imaged using a spinning disk confocal microscope (PerkinElmer) and images were analyzed using Volocity software (PerkinElmer).

6.3.7 G-CSF treatment

Devices were exposed to x-ray radiation at indicated doses 5 days after initiation of

vasculogenesis. 24 hours after radiation exposure, media was removed and replaced with EGM-2MV (Lonza) supplemented with 10 ng/mL G-CSF (Peprotech). Devices were cultured at 37 ºC, 5% CO_2 for an additional 24 hours after G-CSF treatment before being assayed (48 hours after radiation exposure).

6.4 Discussion

Radiation is both an important clinical tool for the treatment of various malignancies and an acute health risk is accidental exposure situations. Within BM, understanding how the endosteal niche and the perivascular niche respond to radiation insult, and how this affects HSPC fate after radiation injury is important for understanding clinical outcomes and developing effective countermeasures that maintain the BM niche for HSPCs. Radiation of the BM microenvironment has largely been studied using animal models, but there are examples that use complex *in vitro* BM models [225].

Here, we investigated the effect of radiation on the BM microenvironment on hBM-on-a-chip and the outcome on HSPCs located in the vascularized endosteal and perivascular niches. Unexpectedly, exposure to relatively high doses of x-ray radiation (up to 10 Gy) did not induce a significant increase in cell death in vascularized endosteal niche hBM-on-a-chip (EC+MSC+OB), as measured by LDH release. There was a corresponding decrease, although not statistically significant, in cytokine expression 24 hours after radiation exposure. This suggested that the expression and, subsequently, the BM niche were potentially altered, albeit without widespread apoptosis of stromal cells. HSPCs cultured in the vascularized endosteal niche (HSPC+EC+MSC+OB) similarly did not exhibit a significant increase in apoptosis 24 hours after exposure as measured by damage

to nuclear DNA (TUNEL). In comparison, we observed an increase, although not statistically significant, in TUNEL$^+$ HSPCs in the perivascular niche (HSPC+EC+MSC) after 5 Gy radiation exposure. MSCs have been reported to be resistant to damage associated with radiation exposure [219] and given the greater number of MSC derived cells in OB containing devices, the density of these radio-resistant (and potentially radio protective) cells could be mitigating damage to HSPCs. Further study measuring the production of reactive oxygen species (ROS) after radiation exposure of the perivascular and vascularized endosteal niches may help explain the difference in HSPC outcome in these microenvironments.

Lack of change in LDH measurement and high background in the TUNEL assay made it difficult to make definitive conclusions regarding the application of hBM-on-a-chip for the study of radiation damage. Other approaches will be required for further study that yields definitive results. Also, the high background of TUNEL$^+$ HSPCs in hBM-on-a-chip may be an indication that the microenvironment created in its current form may not suitable for long-term culture of HSPCs. Altering the media conditions, adding constant fluid flow, or additional BM stromal cells types may improve the viability of HSPCs during prolonged culture.

CHAPTER 7. CONCLUSIONS AND FUTURE DIRECTIONS

7.1 Conclusions

In this dissertation, a novel approach to recapitulating both the endosteal and perivascular microenvironments of human BM was presented. Numerous approaches toward replicating the HSC niche of BM *in vitro* have been developed over several decades. Defined monocultures of HSCs with specific biochemical and physical cues, co-cultures with stromal cells that recreate basic niche interactions, and *in vivo* generated ectopic BM models have been presented as recreations of the HSC niche with vastly different levels of complexity. The hBM-on-a-chip culture system that we have presented here is one of few examples that integrate both the perivascular and endosteal niches entirely *in vitro* [103] and it is unique in its approach. The hBM-on-a-chip is a simple platform that recreates basic physiologic structures but could relatively easily be increased in complexity to accommodate further lines of investigation that require it.

In Aim 1A, the fabrication of hBM-on-a-chip was improved from a relatively labor-intensive process that was flexible and afforded optimization during early studies, to a simple and scalable process at a research laboratory scale. We have demonstrated that the microfluidic approach is easily adapted to a standard well-plate format that enables increased scale, ease of handling, and integration with laboratory instrumentation. We employed the well-plate hBM-on-a-chip in an automated imaging platform (BioSpa, BioTek) that uses mechanized systems to handle plates during imaging procedures over extended periods of time and allow for multiple plates to be automatically imaged in parallel. This overcomes a limitation of scalability of organ-on-a-chip platforms, especially

during early development. Using a well-plate format can also enable the use of additional automated systems, which could include instrumentation for automated liquid handling and cell culture. The loading and culture of these devices, using the techniques presented here, requires significant manual manipulation that requires expertise and, even with said expertise, can lead to significant variation between devices. Automation would not only decrease the labor required for the culture and maintenance of the hBM-on-a-chip, but it would also likely decrease the variation we have observed.

In Aim 1B, we demonstrated that the basic characteristics of the endosteal and perivascular niches could be recreated in hBM-on-a-chip. Using MSCs, we differentiated an endosteal surface within the central channel of the device and were able to subsequently seed ECs and MSCs on top of the endosteal surface and form microvasculature. This approach is flexible – we demonstrated that we can create both a vascularized endosteal niche and a perivascular BM niche – and could likely be used to integrate any number of cell types into the device to achieve the desired microenvironment constituents. We found that HSPCs cultured in the presence of the endosteal niche proliferated less, but retained more expression of CD34, a potency marker, showing that the two microenvironments are functionally different in their interactions with HSPCs.

In Aim 2A, we explored the application of hBM-on-a-chip for studying the mobilization of HSPCs from the BM microenvironment. While inconclusive, G-CSF may reduce the expression of CXCL12 in hBM-on-a-chip, consistent with observations in preclinical animal models [228]. G-CSF increased the length and displacement of HSPC migration, both in the vascularized endosteal niche and the perivascular niche of hBM-on-a-chip, however this mobilization was not observed when the protease inhibitor bortezomib

was also used. This was a surprising result given the evidence that bortezomib alone can induce mobilization [210]. In one sense, this is encouraging that the hBM-on-a-chip can capture the interaction between two therapeutics, however it is also an indication that the hBM-on-a-chip is not fully recapitulating *in vivo* biology. The use of this platform for studying mobilization has potential, although further work is needed to better correlate *in vitro* results with animal and clinical data.

In Aim 2B, we investigated the effects of radiation on hBM-on-a-chip and the resulting effects on HSPCs. We measured limited stromal cell death as a result of high doses of x-ray radiation, but this corresponded with a suspected decrease in cytokine secretion at higher doses that suggest the microenvironment is affected by the radiation exposure. Measurement of damage to HSPCs and resulting apoptosis via the TUNEL assay proved to be difficult and did not yield any statistically significant results. HSPCs cultured in perivascular niche (HSPC+EC+MSC) were potentially more sensitive to radiation exposure when compared to those cultured in the vascularized endosteal niche (HSPC+EC+MSC+OB). If this can be fleshed out further, this has implications for countermeasure approaches to accidental radiation exposure. Radioprotection may not be exclusive to HSPCs, if cancerous cells in BM are similarly protected in the endosteal niche it would have implications in the treatment of BM malignancies.

Increased sample sizes may be required to gain meaningful and conclusive insights from radiation studies if the effect size and standard deviation observed in these studies holds true. If we take the effect of 5 Gy radiation compared to untreated samples measured in “perivascular niche” devices (-OB) as an example (Figure 40), we can perform a power analysis to determine the number of devices necessary to determine the effect size.

Assuming that $\alpha = 0.05$, power = 0.80, mean of control is 17.5%, mean of 5 Gy is 22.5%, and the standard deviation of both populations is approximately 4%, the sample size needed in each group is 10. If this is an overly optimistic assumption of intra-device variability and the standard deviation of the population is actually 5%, sample size would increase to 16 devices per group. However, if variance could be decreased to 3% through improved methods, the sample size required decreases to 6 devices per group. Increasing the sample size is necessary to observe the effect size that these studies have suggested is present, however decreasing the intra-device variability is also necessary for practical execution of these experiments.

The hBM-on-a-chip developed in this dissertation recreates basic structures of human bone marrow and we have shown that it has potential applications in studying the HSPC BM niche in a controlled, human, *in vitro* culture platform.

7.2 Future directions

There are several directions that could be taken to improve upon the device design, fabrication, culture, and its applications in research.

The use of PDMS materials, while flexible and useful for laboratory scale production of devices, have limited utility moving beyond basic research. The issues associated with PDMS absorption of small molecules could potentially be restrictive if the platform was used for further pharmacological studies. Fabricating the device layer from PDMS also results in slight variability in the height of the hBM-on-a-chip within a well-plate, which can be problematic when imaging the devices in an automated fashion. The platform could be improved by removing PDMS from the device construction and using

polycarbonate or similar material that could be manufactured in a more controlled and scalable fashion. Using more controlled fabrication approaches would decrease this variability.

Additionally, commercially available silicon films could (and should) replace the use of in-house made films to produce a more standard and consistent platform. Moving to commercially available PDMS films, while expensive, have the additional benefit of being packaged between two sheets of hard plastic. One sheet can be removed, allowing for the bonding of the PDMS to the device layer and the other can be maintained during culture. This would eliminate the need for coverslips to be bonded to the bottom of the devices to provide structural support during culture, reducing fabrication time and complexity.

The process for culturing hBM-on-a-chip is time intensive. At 26 days from initial seeding of MSCs to having a vascularized hBM-on-a-chip, there is opportunity and necessity to decrease the culture time if the platform is going to be used in a clinical setting. The most apparent step for shortening is the differentiation of MSCs to osteoblasts. The current protocol is a standard differentiation protocol, however there are now differentiation media products that are commercially available that claim to shorten osteoblast differentiation time. The downside with these products is that the materials are proprietary, although the time of culture would be shortened, the mechanism of differentiation is unknown and the culture media itself is not fully defined for the user.

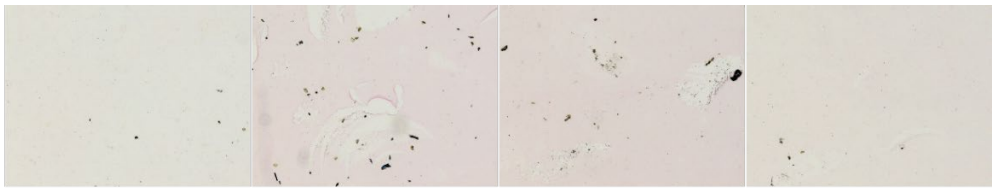

1. BSA (mg/mL)	-	-	-	10
2. PDA (µg/mL)	-	-	100	100
3. Col I (µg/mL)	-	100	100	100

Figure 42. Blocking polydopamine and collagen coating with BSA. PDMS was (1) blocked with BSA (10 µg/mL), (2) coated with polydopamine (PDA) (100 µg/mL), and (3) coated with collagen 1 (100 µg/mL) and stained with picrosirius red to visualize collagen adsorption to the PDMS surface.

One critical limitation of the device in its current design is the inability to generate consistently perfusable vasculature in the presence of OBs due to slight delamination of the fibrin-collagen hydrogel from the PDMS surface. Currently, the entire surface (including walls and top) of the central channel is coated with polydopamine and collagen I prior to MSC loading in the central channel. This coating is likely affecting the ability of the hydrogel to attach sufficiently to the PDMS surface downstream. One approach to mitigate this would be to exclusively coat the bottom surface of PDMS with polydopamine and collagen. This could be achieved through by (1) blocking the PDMS walls and top with BSA or another non-specific protein prior to device assembly, which would limit the adsorption of collagen to these surfaces (Figure 42). Alternatively, (2) the bottom surface of PDMS could be patterned with polydopamine and collagen coating prior to device assembly using a masking technique [229].

There are several potential approaches to improving upon the method of vasculogenesis. Using MSCs or fibroblasts in the outer channels of the device to generate vasculogenic factors is poorly controlled, not defined, and is dependent on biological variability of the cells themselves (lot, passage number, etc.). Methods that use fluid shear

stress to induce vasculogenesis [172,177] allow for the development of microvasculature without added cytokine or stromal support. Adaptation of these methods would lead to a more defined hBM-on-a-chip and, because of the added fluid flow, may allow for increased cellularity and viability of HSPCs during long term culture.

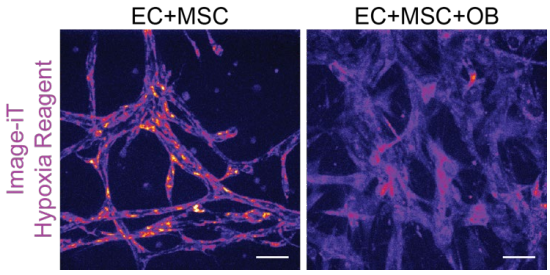

Figure 43. Hypoxia in perivascular and vascularized endosteal niches. Z-projections of hBM-on-a-chip with and without OB stained with Image-iT Green Hypoxia Reagent (ThermoFisher) and cultured for 2 hours at 37 ºC, 5% CO_2, 20% O_2 prior to imaging. Scale bar: 50 µm.

There are myriad additional studies that could be performed to further characterize the microenvironment that is being formed within the hBM-on-a-chip. The experiments in this dissertation were all performed under normal oxygen conditions (~20% O_2), however the oxygen tension of BM is lower and variable through the tissue [50]. Because of the high cellularity of the device, we hypothesized that local hypoxic environments might be present. Using a fluorescent hypoxia reagent, we visualized the hypoxic microenvironment in the perivascular (-OB) and vascularized endosteal (+OB) niches (Figure 43). Preliminary results show a more diffuse hypoxic environment with OBs present and more local, but more intense hypoxia without OBs near vasculature and perivascular stromal cells. It is important to note that because the vasculature is not being constantly perfused with oxygenated media, like how vasculature is constantly supplied with blood, this observation

may be conflict with the hypoxic environment *in vivo*. Culture of hBM-on-a-chip in a range of hypoxic conditions would be interesting and could create unique HSPC niche characteristics.

We characterized the proliferation and maintenance of multipotency (via CD34 expression) of HSPCs, additional investigation into the differentiation of HSPCs would further define the BM microenvironment that is being created. If the goal is to create a representative BM microenvironment from HSPCs, culture times would need to be increased to allow for the differentiation of the milieu of cell types present in native tissue. Due to the slowdown in proliferation we measured within 5 days, different media compositions or fluid flow would likely need to be applied in order to generate the cellular density of BM tissue (if it is possible in this platform).

Increasing the complexity of hBM-on-a-chip through the addition of additional BM cell types would additional nuance and accuracy to this model of BM. There are numerous cell types that are present in BM that were excluded from these studies, including macrophages, osteoclasts, adipocytes, neutrophils, and Schwann cells. Some of these cell types, like adipocytes, would be relatively easy to integrate into the existing methods, however, immune cells may be more difficult to incorporate into cultures where cell types are from multiple donors without HLA-matching.

An interesting approach to creating a more complex BM-on-chip would be to use whole BM as the starting material. Potentially, stromal cells (MSCs, ECs, and OBs) could be isolated from the whole BM, at which point they could be introduced into the culture for differentiation (MSCs) or stored for subsequent seeding after endosteal formation. The advantageous to having single source material are many. Genetically, the cells would be

identical, this would remove any conflicting responses due to competing genotypes in the stromal cell subsets. A BM-on-a-chip from a single material source could have potential to be a truly patient-specific model that would allow for screening and testing on an individual level. Lastly, for studies that are focused on the immune response in the BM microenvironment (e.g. chimeric antigen receptor-T cell efficacy), having cells that are HLA matched is essential for decreasing the amount of non-specific activation and killing.

While increasing the complexity of hBM-on-a-chip is attractive for better replicating the native microenvironment, it would also significantly increase the technical difficulties associated with creating and culturing devices with low relatively low variability. Cell types should be chosen carefully for their inclusion or exclusion from specific models in order to best mimic the least complex microenvironment necessary for modeling the physiologic state of interest. A deliberate and minimalist approach is more likely to lead to successful creation of BM microenvironment models and the collection of meaningful data.

The results we have gathered show that hBM-on-a-chip could be a potential tool for studying mobilization of HSPCs. The lack of G-CSF mobilization in the context of bortezomib treatment was unexpected. Additional studies looking at mobilization with concurrent chemotherapeutic treatment with thalidomide, lenalidomide, dexamethasone, and derivatives of cyclophosphamide would help us better understand the impact of chemotherapeutics on mobilization in hBM-on-a-chip. Given the uncertain data gathered for high dose AMD3100 treatment, further studies are warranted for the mobilization with the drug. There are a few agents that have been tested in preclinical situations, including S1P, Groβ, IL-8, and many more [204]. Screening of these drugs could elucidate which

mechanisms of action the hBM-on-a-chip may be appropriate for testing.

Similarly, there are many potential therapeutics that could be screened for their potential as radiation countermeasures in hBM-on-a-chip if, as previously discussed, the sensitivity of measurements can be improved. Glutathione and bactericidal/permeability-increasing protein [230] are potential therapeutics that could be tested in hBM-on-a-chip. Their relative efficacy in the perivascular and vascularized endosteal niche hBM-on-a-chips could be informative for radiation countermeasure strategies by providing the microenvironment context of their efficacy. The effects of radiation on the hBM-on-a-chip microenvironment could also be further studied. If the perfusion of the devices become more consistent, experiments could be performed that measure the effect of radiation on the permeability of hBM-on-a-chip vasculature and the effect of specific stromal cells on mitigating or aggravating any response. Because restoration of blood flow to irradiated tissue is essential for functional recovery, these studies could be informative for designing small molecule or cell-based therapies that target the non-hematopoietic cells in BM in response to radiation insult.

One apparent application of hBM-on-a-chip would be to use it as a tissue specific model of cancers that inhabit the BM. Multiple myeloma and leukemia, hematopoietic malignancies that occupy BM, are well reported to disrupt BM physiology, disrupting hematopoiesis and the immune system [231-234]. BM stromal cells and the BM microenvironment inevitably play a role in the progression and outcome of therapies that target these cancers. There are a number of examples of *in vitro* BM models that have been used to study the cancer microenvironment in BM [103,168]. The hBM-on-a-chip would be a novel *in vitro* tool for exploring how the endosteal and perivascular niches interact

with cancer cells and it could also serve as a physiologically relevant platform for testing the effectiveness of chemotherapeutics, radiation therapy, or cell-based cancer therapies (e.g. CAR-T cells).

The culture method that we have described here has potential as a preclinical model that substitutes for traditional animal models. While it lacks the complexity of a whole, *in vivo* BM, using human cells in a relatively defined and tunable microenvironment has certain advantages. Additional work that further standardizes hBM-on-a-chip through updated design and fabrication, further characterizes the *in vitro* microenvironment, and adds additional complexity to the model are needed to create a robust, reliable, and higher fidelity model of human BM that can be used to accurately predict and study the human physiologic response.

APPENDIX A. DETAILED SOFT LITHOGRAPHY METHODS

The fabrication of SU-8 master molds was done using the manufacturer's protocol previously published methods. However, slight changes in the protocols were required to account or the specific instrumentation available and to achieve consistent, successful fabrication.

A.1 Mask design

Photomasks were designed using AutoCAD software.

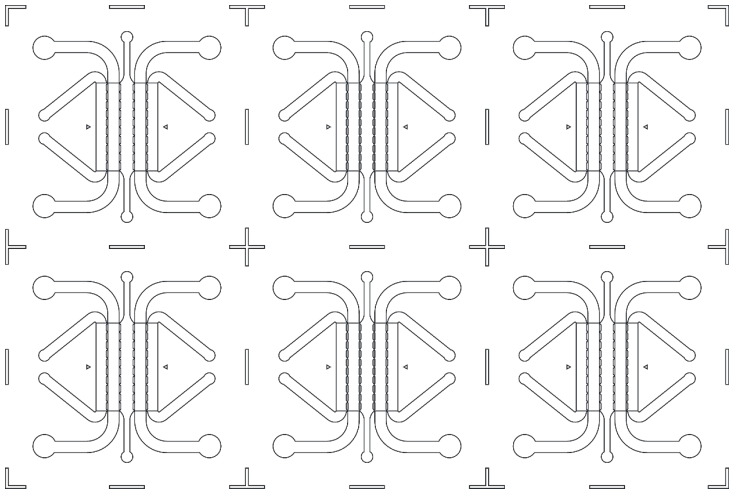

Figure 44. Photomask design of device versions 1.0 and 1.1. Six, 5-channel hBM-on-a-chip devices arranged in a 2x3 array for v1.0 and v1.1 fabrication. Guides are placed between devices for cutting of individual devices.

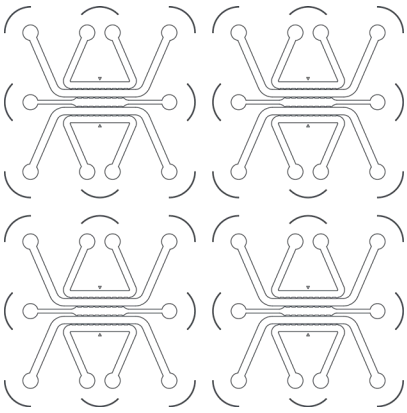

Figure 45. Photomask design of device version 2.0. Four, 5-channel hBM-on-a-chip devices arranged in a 2x2 array for version 2.0 fabrication. Guides are placed that align with edges of 96-well plate to aid in alignment of device layer with 96-well no-bottom plates.

A.2 Fabrication

The coating of silicon wafers with SU-8 2150 generally followed the manufacturer's protocol, however slight modifications were made that improved the adhesion of the SU-8 to the silicon surface and more reproducibly resulted in a successful fabrication process.

A.2.1 Spin coating SU8

Silicon wafers were cleaned with a solvent wash (acetone, methanol, isopropanol), dried with N_2, and subsequently dehydrated on a hot plate at 200 °C for at least 5 minutes. Wafers were transferred to SCS G3P8 spin coater immediately prior to coating. To coat, 5 mL room temperature SU-8 2150 was poured directly from the container (SU-8 2150 is too viscous to be aliquoted or pipetted directly) onto the center of the wafer and the wafer was immediately spun to coat the surface evenly (Table 4).

Table 4. SCS G3P8 protocol for spin coating SU-8 2150.

Step	Ramp (s)	RPM	Dwell (s)
1	5	500	10
2	10	2500*	30
3	5	0	0

Coated wafers were immediately transferred to a 65 °C hotplate for 15 minutes. To avoid rapid change in temperature that can result in surface adhesion problems that are common with thick SU-8 coatings, the SU-8 coated wafers were then ramped up to 95 °C on the same hotplate and then held at 95 °C for 60 minutes. Similarly, after 60 minutes the hotplate was turned off and the wafers were cooled to room temperature on the hotplate surface over ~1 hour.

A.2.2 UV exposure and development

Once the SU-8 coated wafers had cooled to room temperature, the coated parts were transferred to the 100 mm chuck of the Suss Microtec MJB4 mask aligner. The intensity of the UV light source was measured, and an exposure time was calculated that would yield a dose of 300 mJ/cm^2 using Equation 6.

$$Time\ (s) = \frac{Dose\ \left(\frac{mJ}{cm^2}\right)}{Intensity\ \left(\frac{mW}{cm^2}\right)} \tag{6}$$

Coated wafers were exposed through soda-lime or transparency mask and then immediately transferred to 65 °C hotplate and held for 5 minutes. Again, to avoid rapid changes in temperature, exposed wafers were kept on the hotplate and the temperature was adjusted to 95 °C. Exposed wafers were held at 95 °C for 15 minutes after which the

*Spin speed will vary depending on the age of the SU-8. Viscosity will increase over time as solvent evaporates and higher spin speeds will be required to achieve the same thickness.

hotplate was turned off and the wafers cooled to room temperature. Uncrosslinked SU-8 was then removed using SU-8 developer. If after development, small adhesion problems had occurred, wafers were then hard baked by quickly transferring the wafer from 65 °C, to 95 °C, and 200 °C hotplates, holding for 1 minute at each temperature and then in reverse to come back to room temperature.

A.2.3 Profilometry

The height of the fabricated SU-8 features were measured using a Dektak contact profilometer. Wafers with features were transferred to the profilometer platform. A feature in the center of the wafer, typically a cut or alignment guide, was chosen for measurement. The average step height (ASH) between the wafer and the feature was recorded.

APPENDIX B. QUANTIFICATION OF CXCL12 EXPRESSION

CXCL12 was not detectable in the supernatant of hBM-on-a-chip using bead-based multiplex cytokine detection assays (Figure 19, Figure 20, Figure 24, Figure 26, Figure 38), ELISA (not shown), or a modified ELISA assay that expands the detection range of analyte detection (not shown) [235]. Therefore, to measure relative changes in CXCL12 expression, we used immunohistochemistry and quantification of fluorescence signal.

B.1 Methods

B.1.1 Immunohistochemistry staining

Prior to fixation, positive control devices were treated with CXCL12 (Peprotech) by exchanging media with EBM-2MV supplemented with 1 ng/mL CXCL12. Devices were incubated for 30 minutes with CXCL12 supplemented media and then fixed with formaldehyde.

Staining procedure for devices was adapted from Chen *et al* 2017 [170]. Devices were washed with PBS, fixed with 4% formaldehyde (ThermoFisher), and permeabilized with 0.1% Triton X-100. Prior to staining, cells were blocked with 5% BSA, 3% goat serum in PBS. Primary antibody was diluted (1:100) in blocking buffer and devices were stained overnight at 4 ºC. Devices were then washed with 0.1% BSA in PBS (wash buffer) and stained with secondary antibodies (1:200) diluted in wash buffer for 3 hours at RT. Devices were washed with wash buffer and with Phalloidin AF647 (1:40).

B.1.2 Imaging and image analysis

Stained hBM-on-a-chip devices were imaged using a spinning disk confocal

microscope (PerkinElmer). Five ROIs were imaged in each device in an evenly distributed array through the middle of the central channel (Figure 46). At each ROI, a 100 µm z-stack with spacing of 2 µm was acquired in Cy5 (CD31), GFP (CXCL12), and RFP (F-Actin).

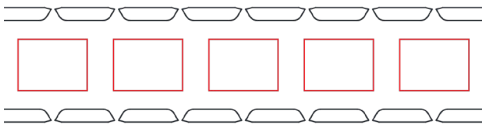

Figure 46. ROIs for CXCL12 imaging. Images were acquired at evenly spaced intervals in consistent locations.

Images were processed and analyzed using open-source ImageJ software [130,131]. Images were background subtracted and had outliers removed prior to z-projections being made using max intensity. CXCL12 expression was measured using the MFI of the GFP channel.

B.2 Results

IHC staining showed CXCL12 expression by endothelial cells and perivascular stromal cells. In order to quantify the expression of CXCL12, we first needed to determine an appropriate method for image processing would eliminate nonspecific signal. Without processing (Figure 47A), the raw images indicated showed little to no signal without a primary antibody, however when an isotype control was used, there were nonspecific punctate signals observed. This same noise can be seen with an anti-CXCL12 antibody, and, although there is clearly a difference in specific staining, there is little differentiation between samples when measuring MFI (Figure 47B).

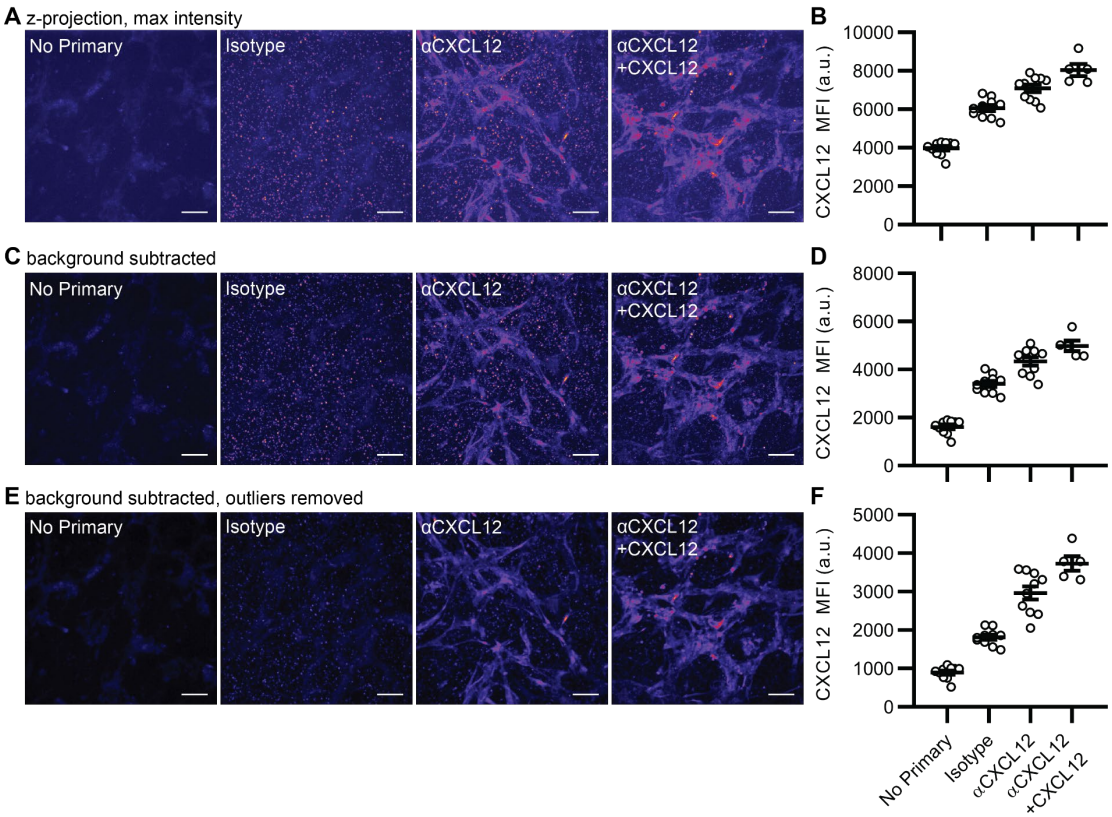

Figure 47. Measuring CXCL12 by IHC. (A) Z-projections created using maximum intensity and (B) quantification of MFI. (C) Background subtracted z-projections and (D) quantification of MFI. (E) Background subtracted, outlier removed z-projections and (F) quantification of MFI. Scale bar: 50 μm. Data (n = 5-10 ROIs from 1-2 devices) are shown as mean ± SEM.

Subtracting background from the images increased the signal-to-noise ratio, however it did not remove the punctate noise from the isotype or anti-CXCL12 samples (Figure 47C, D). Removing outliers from the images successfully removed the punctate noise (Figure 47E) and resulted in greater separation between the MFI of isotype and anti-CXCL12 samples (Figure 47F).

APPENDIX C. DETAILED LIST OF MATERIALS

Table 5. Antibodies and dilutions.

Name	Supplier	Catalog No.	Dilution (Conc.)
Rabbit Anti-CXCL2	Abcam	ab9797	1:100 (5 µg/mL)
Rabbit Anti-Fibronectin	Abcam	Ab2413	1:100 (10 µg/mL)
Rabbit Anti-JAG1	Abcam	ab7771	1:100 (10 µg/mL)
Rabbit Anti-Osteopontin	Abcam	ab8448	1:100 (82 µg/mL)
Rabbit Anti-SCF	Abcam	ab64677	1:100 (10 µg/mL)
Rabbit IgG Isotype	Abcam	ab37415	1:1000 (5 µg/mL)
Anti-CD31 AF647	BioLegend	303112	1:100 (1 µg/mL)
Anti-CD34 BV421	BioLegend	343609	1:100 (1 µg/mL)
Anti-CD38 BV510	BioLegend	303539	1:100 (1.5 µg/mL)
Anti-CD45 AF488	BioLegend	304019	1:100 (2 µg/mL)
Anti-CD45RA AF647	BioLegend	304153	1:50 (1 µg/mL)
Mouse IgG Isotype AF647	BioLegend	400330	1:500 (1 µg/mL)
Mouse IgG Isotype BV 510	BioLegend	400171	1:67 (1.5 µg/mL)
Mouse IgG Isotype BV421	BioLegend	400259	1:50 (1 µg/mL)
Goat Anti-Rabbit AF488	Life Technologies	A11008	1:200 (10 µg/mL)

Table 6. Primary cells.

Name	Supplier	Catalog Number	Lot(s)
BM CD34+ Cells	Lonza	2M-101	0000690910 0000573128
HUVEC	Lonza	C2519A	0000470896
MSCs	RoosterBio	MSC-001	00037

Table 7. Detailed list of materials.

Category	Name	Supplier	Catalog Number(s)
Chemical	β-Glycerophosphate	Sigma-Aldrich	G9422
Chemical	(3-mercaptopropyl) trimethoxy silane	Sigma-Aldrich	175617
Chemical	Alizarin Red S	Sigma-Aldrich	A553325G
Chemical	AMD3100	Sigma-Aldrich	A5602
Chemical	Bortezomib	Sigma-Aldrich	5043140001
Chemical	Bovine gelatin	Sigma-Aldrich	G9391
Chemical	Bovine serum albumin	Sigma-Aldrich	A2153
Chemical	Dexamethasone	Sigma-Aldrich	D2915
Chemical	Dopamine hydrochloride	Sigma-Aldrich	H8502
Chemical	Glycosil Hyaluronic Acid	ESI Bio	GS222
Chemical	Goat serum	ThermoFisher	10000C
Chemical	Image-iT Green Hypoxia Reagent	ThermoFisher	I14833
Chemical	L-Ascorbic Acid	Sigma-Aldrich	255564
Chemical	PEGDA	Alfa Aesar	AA4649703
Chemical	PKH67	Sigma-Aldrich	MIDI67
Chemical	Rat Tail Collagen I	Corning	354249
Chemical	Silver Nitrate	Acros Organics	197680250
Chemical	Sodium Thiosulfate	Acros Organics	202870010
Chemical	Trichloro (1*H*,1*H*,2*H*,2*H*-perfluorooctyl) silane	Sigma-Aldrich	448931
Chemical	Triton X-100	Avocado	A16046
Cytokine	Human Ang-1	PeproTech	130-06
Cytokine	Human CXCL12	Abcam	ab9798
Cytokine	Human G-CSF	PeproTech	300-23
Cytokine	Human SCF	PeproTech	300-07
Cytokine	Human TPO	PeproTech	300-18
Cytokine	Human VEGF	PeproTech	100-20
Kit	Click-iT TUNEL Alexa Fluor 647 Imaging Assay	ThermoFisher	C10247
Kit	CXCL12 ELISA	PeproTech	900-M92
Kit	IL-6 ELISA	PeproTech	900-TM16
Kit	LDH Cytotoxicity Assay Kit	ThermoFisher	C20301
Kit	LEGENDplex Human HSC Panel	BioLegend	740611
Kit	SCF ELISA	PeproTech	900-TM34
Material	96-Well No-Bottom Plates	Greiner Bio-One	655000-06
Material	96-Well Plate Lids	Greiner Bio-One	656170
Material	Silicon Wafer	University Wafer	452
Material	Smooth-Cast 310	Smooth On	N/A
Material	SU-8 2150	MicroChem	NC0216470
Material	SU-8 Developer	MicroChem	NC9901158
Material	Sylgard 184 Silicone Elastomer Kit	Dow Corning	2065622
Media	αMEM	Sigma-Aldrich	M0644
Media	EBM-2MV	Lonza	CC-3202
Media	FBS	HyClone	SH3007103
Media	Penicillin-Streptomycin	HyClone	SV30010
Misc.	Biopsy Punches	Integra Miltex	33-31AA-P/25, 33-31-P/25, 33-34-P/25
Misc.	nanoDot	Landauer	03053-OTO

REFERENCES

[1] Nelson, M. R. & Roy, K. Bone-marrow mimicking biomaterial niches for studying hematopoietic stem and progenitor cells. *J Mater Chem B* **4**, 3490-3503, doi:10.1039/c5tb02644j (2016).

[2] Wang, L. D. & Wagers, A. J. Dynamic niches in the origination and differentiation of haematopoietic stem cells. *Nat Rev Mol Cell Biol* **12**, 643-655, doi:10.1038/nrm3184 (2011).

[3] Schofield, R. The relationship between the spleen colony-forming cell and the haemopoietic stem cell. *Blood Cells* **4**, 7-25 (1978).

[4] Taichman, R. S. & Emerson, S. G. Human osteoblasts support hematopoiesis through the production of granulocyte colony-stimulating factor. *J Exp Med* **179**, 1677-1682, doi:10.1084/jem.179.5.1677 (1994).

[5] Calvi, L. M. *et al.* Osteoblastic cells regulate the haematopoietic stem cell niche. *Nature* **425**, 841-846, doi:10.1038/nature02040 (2003).

[6] Zhang, J. *et al.* Identification of the haematopoietic stem cell niche and control of the niche size. *Nature* **425**, 836-841, doi:10.1038/nature02041 (2003).

[7] Ding, L. & Morrison, S. J. Haematopoietic stem cells and early lymphoid progenitors occupy distinct bone marrow niches. *Nature* **495**, 231-235, doi:10.1038/nature11885 (2013).

[8] Ding, L., Saunders, T. L., Enikolopov, G. & Morrison, S. J. Endothelial and perivascular cells maintain haematopoietic stem cells. *Nature* **481**, 457-462, doi:10.1038/nature10783 (2012).

[9] Dexter, T. M. & Testa, N. G. Differentiation and proliferation of hemopoietic cells in culture. *Methods Cell Biol* **14**, 387-405 (1976).

[10] Wang, T. Y. & Wu, J. H. A continuous perfusion bioreactor for long-term bone marrow culture. *Ann N Y Acad Sci* **665**, 274-284, doi:10.1111/j.1749-6632.1992.tb42591.x (1992).

[11] Takagi, M. Cell processing engineering for ex-vivo expansion of hematopoietic cells. *J Biosci Bioeng* **99**, 189-196, doi:10.1263/jbb.99.189 (2005).

[12] Panoskaltsis, N., Mantalaris, A. & Wu, J. H. Engineering a mimicry of bone marrow tissue ex vivo. *J Biosci Bioeng* **100**, 28-35, doi:10.1263/jbb.100.28 (2005).

[13] Dahlberg, A., Delaney, C. & Bernstein, I. D. Ex vivo expansion of human hematopoietic stem and progenitor cells. *Blood* **117**, 6083-6090,

doi:10.1182/blood-2011-01-283606 (2011).

[14] Di Maggio, N. *et al.* Toward modeling the bone marrow niche using scaffold-based 3D culture systems. *Biomaterials* **32**, 321-329, doi:10.1016/j.biomaterials.2010.09.041 (2011).

[15] Knothe Tate, M. L. Top down and bottom up engineering of bone. *J Biomech* **44**, 304-312, doi:10.1016/j.jbiomech.2010.10.019 (2011).

[16] Jiang, J. & Papoutsakis, E. T. Stem-cell niche based comparative analysis of chemical and nano-mechanical material properties impacting ex vivo expansion and differentiation of hematopoietic and mesenchymal stem cells. *Adv Healthc Mater* **2**, 25-42, doi:10.1002/adhm.201200169 (2013).

[17] Choi, J. S., Mahadik, B. P. & Harley, B. A. Engineering the hematopoietic stem cell niche: Frontiers in biomaterial science. *Biotechnol J* **10**, 1529-1545, doi:10.1002/biot.201400758 (2015).

[18] Sugimura, R. Bioengineering Hematopoietic Stem Cell Niche toward Regenerative Medicine. *Adv Drug Deliv Rev* **99**, 212-220, doi:10.1016/j.addr.2015.10.010 (2016).

[19] Thomas, E. D., Lochte, H. L., Jr., Lu, W. C. & Ferrebee, J. W. Intravenous infusion of bone marrow in patients receiving radiation and chemotherapy. *N Engl J Med* **257**, 491-496, doi:10.1056/NEJM195709122571102 (1957).

[20] Kapp, F. G. *et al.* Protection from UV light is an evolutionarily conserved feature of the haematopoietic niche. *Nature* **558**, 445-448, doi:10.1038/s41586-018-0213-0 (2018).

[21] Migliaccio, A. R., Masselli, E., Varricchio, L. & Whitsett, C. Ex-vivo expansion of red blood cells: how real for transfusion in humans? *Blood Rev* **26**, 81-95, doi:10.1016/j.blre.2011.11.002 (2012).

[22] Thon, J. N. *et al.* Platelet bioreactor-on-a-chip. *Blood* **124**, 1857-1867, doi:10.1182/blood-2014-05-574913 (2014).

[23] Kiel, M. J. *et al.* SLAM family receptors distinguish hematopoietic stem and progenitor cells and reveal endothelial niches for stem cells. *Cell* **121**, 1109-1121, doi:10.1016/j.cell.2005.05.026 (2005).

[24] Lo Celso, C. *et al.* Live-animal tracking of individual haematopoietic stem/progenitor cells in their niche. *Nature* **457**, 92-96, doi:10.1038/nature07434 (2009).

[25] Reismann, D. *et al.* Longitudinal intravital imaging of the femoral bone marrow reveals plasticity within marrow vasculature. *Nat Commun* **8**, 2153, doi:10.1038/s41467-017-01538-9 (2017).

[26] Seita, J. & Weissman, I. L. Hematopoietic stem cell: self-renewal versus differentiation. *Wiley Interdiscip Rev Syst Biol Med* **2**, 640-653, doi:10.1002/wsbm.86 (2010).

[27] Van Laere, A. S. *et al.* A regulatory mutation in IGF2 causes a major QTL effect on muscle growth in the pig. *Nature* **425**, 832-836, doi:10.1038/nature02064 (2003).

[28] Adams, G. B. *et al.* Stem cell engraftment at the endosteal niche is specified by the calcium-sensing receptor. *Nature* **439**, 599-603, doi:10.1038/nature04247 (2006).

[29] Kiel, M. J. & Morrison, S. J. Uncertainty in the niches that maintain haematopoietic stem cells. *Nat Rev Immunol* **8**, 290-301, doi:10.1038/nri2279 (2008).

[30] Putnam, A. J. The Instructive Role of the Vasculature in Stem Cell Niches. *Biomater Sci* **2**, 1562-1573, doi:10.1039/C4BM00200H (2014).

[31] Morrison, S. J. & Scadden, D. T. The bone marrow niche for haematopoietic stem cells. *Nature* **505**, 327-334, doi:10.1038/nature12984 (2014).

[32] Ellis, S. L. & Nilsson, S. K. The location and cellular composition of the hemopoietic stem cell niche. *Cytotherapy* **14**, 135-143, doi:10.3109/14653249.2011.630729 (2012).

[33] Omatsu, Y. *et al.* The essential functions of adipo-osteogenic progenitors as the hematopoietic stem and progenitor cell niche. *Immunity* **33**, 387-399, doi:10.1016/j.immuni.2010.08.017 (2010).

[34] Sugiyama, T., Kohara, H., Noda, M. & Nagasawa, T. Maintenance of the hematopoietic stem cell pool by CXCL12-CXCR4 chemokine signaling in bone marrow stromal cell niches. *Immunity* **25**, 977-988, doi:10.1016/j.immuni.2006.10.016 (2006).

[35] Mendez-Ferrer, S. *et al.* Mesenchymal and haematopoietic stem cells form a unique bone marrow niche. *Nature* **466**, 829-834, doi:10.1038/nature09262 (2010).

[36] Yamazaki, S. *et al.* Nonmyelinating Schwann cells maintain hematopoietic stem cell hibernation in the bone marrow niche. *Cell* **147**, 1146-1158, doi:10.1016/j.cell.2011.09.053 (2011).

[37] Katayama, Y. *et al.* Signals from the sympathetic nervous system regulate hematopoietic stem cell egress from bone marrow. *Cell* **124**, 407-421, doi:10.1016/j.cell.2005.10.041 (2006).

[38] Klein, G. The extracellular matrix of the hematopoietic microenvironment. *Experientia* **51**, 914-926, doi:10.1007/BF01921741 (1995).

[39] Nilsson, S. K. *et al.* Immunofluorescence characterization of key extracellular

matrix proteins in murine bone marrow in situ. *J Histochem Cytochem* **46**, 371-377, doi:10.1177/002215549804600311 (1998).

[40] Siler, U. *et al.* Characterization and functional analysis of laminin isoforms in human bone marrow. *Blood* **96**, 4194-4203 (2000).

[41] Gu, Y. *et al.* Characterization of bone marrow laminins and identification of alpha5-containing laminins as adhesive proteins for multipotent hematopoietic FDCP-Mix cells. *Blood* **93**, 2533-2542 (1999).

[42] Fraser, J. R., Laurent, T. C. & Laurent, U. B. Hyaluronan: its nature, distribution, functions and turnover. *J Intern Med* **242**, 27-33, doi:10.1046/j.1365-2796.1997.00170.x (1997).

[43] Nilsson, S. K. *et al.* Hyaluronan is synthesized by primitive hemopoietic cells, participates in their lodgment at the endosteum following transplantation, and is involved in the regulation of their proliferation and differentiation in vitro. *Blood* **101**, 856-862, doi:10.1182/blood-2002-05-1344 (2003).

[44] Nilsson, S. K. *et al.* Osteopontin, a key component of the hematopoietic stem cell niche and regulator of primitive hematopoietic progenitor cells. *Blood* **106**, 1232-1239, doi:10.1182/blood-2004-11-4422 (2005).

[45] Stier, S. *et al.* Osteopontin is a hematopoietic stem cell niche component that negatively regulates stem cell pool size. *J Exp Med* **201**, 1781-1791, doi:10.1084/jem.20041992 (2005).

[46] Grassinger, J. *et al.* Thrombin-cleaved osteopontin regulates hemopoietic stem and progenitor cell functions through interactions with α9β1 and α4β1 integrins. *Blood* **114**, 49-59, doi:10.1182/blood-2009-01-197988.The (2009).

[47] Hines, M., Nielsen, L. & Cooper-White, J. The hematopoietic stem cell niche: what are we trying to replicate? *Journal of Chemical Technology & Biotechnology* **83**, 421-443, doi:10.1002/jctb.1856 (2008).

[48] Wilson, A. & Trumpp, A. Bone-marrow haematopoietic-stem-cell niches. *Nat Rev Immunol* **6**, 93-106, doi:10.1038/nri1779 (2006).

[49] Eliasson, P. & Jonsson, J. I. The hematopoietic stem cell niche: low in oxygen but a nice place to be. *J Cell Physiol* **222**, 17-22, doi:10.1002/jcp.21908 (2010).

[50] Spencer, J. A. *et al.* Direct measurement of local oxygen concentration in the bone marrow of live animals. *Nature* **508**, 269-273, doi:10.1038/nature13034 (2014).

[51] Engler, A. J., Sen, S., Sweeney, H. L. & Discher, D. E. Matrix elasticity directs stem cell lineage specification. *Cell* **126**, 677-689, doi:10.1016/j.cell.2006.06.044 (2006).

[52] Jansen, L. E., Birch, N. P., Schiffman, J. D., Crosby, A. J. & Peyton, S. R. Mechanics of intact bone marrow. *J Mech Behav Biomed Mater* **50**, 299-307, doi:10.1016/j.jmbbm.2015.06.023 (2015).

[53] Buxboim, A., Rajagopal, K., Brown, A. E. & Discher, D. E. How deeply cells feel: methods for thin gels. *J Phys Condens Matter* **22**, 194116, doi:10.1088/0953-8984/22/19/194116 (2010).

[54] Ohashi, T., Ishii, Y., Ishikawa, Y., Matsumoto, T. & Sato, M. Experimental and numerical analyses of local mechanical properties measured by atomic force microscopy for sheared endothelial cells. *Biomed Mater Eng* **12**, 319-327 (2002).

[55] Engler, A. J., Richert, L., Wong, J. Y., Picart, C. & Discher, D. E. Surface probe measurements of the elasticity of sectioned tissue, thin gels and polyelectrolyte multilayer films: Correlations between substrate stiffness and cell adhesion. *Surf Sci* **570**, 142-154, doi:10.1016/j.susc.2004.06.179 (2004).

[56] Shin, J. W. *et al.* Contractile forces sustain and polarize hematopoiesis from stem and progenitor cells. *Cell Stem Cell* **14**, 81-93, doi:10.1016/j.stem.2013.10.009 (2014).

[57] Higuchi, A., Ling, Q. D., Chang, Y., Hsu, S. T. & Umezawa, A. Physical cues of biomaterials guide stem cell differentiation fate. *Chem Rev* **113**, 3297-3328, doi:10.1021/cr300426x (2013).

[58] Prewitz, M., Seib, F. P., Pompe, T. & Werner, C. Polymeric biomaterials for stem cell bioengineering. *Macromol Rapid Commun* **33**, 1420-1431, doi:10.1002/marc.201200382 (2012).

[59] Edalat, F., Bae, H., Manoucheri, S., Cha, J. M. & Khademhosseini, A. Engineering approaches toward deconstructing and controlling the stem cell environment. *Ann Biomed Eng* **40**, 1301-1315, doi:10.1007/s10439-011-0452-9 (2012).

[60] Fisher, O. Z., Khademhosseini, A., Langer, R. & Peppas, N. A. Bioinspired materials for controlling stem cell fate. *Acc Chem Res* **43**, 419-428, doi:10.1021/ar900226q (2010).

[61] Lutolf, M. P., Gilbert, P. M. & Blau, H. M. Designing materials to direct stem-cell fate. *Nature* **462**, 433-441, doi:10.1038/nature08602 (2009).

[62] Dawson, E., Mapili, G., Erickson, K., Taqvi, S. & Roy, K. Biomaterials for stem cell differentiation. *Adv Drug Deliv Rev* **60**, 215-228, doi:10.1016/j.addr.2007.08.037 (2008).

[63] Saha, K., Pollock, J. F., Schaffer, D. V. & Healy, K. E. Designing synthetic materials to control stem cell phenotype. *Curr Opin Chem Biol* **11**, 381-387, doi:10.1016/j.cbpa.2007.05.030 (2007).

[64] Holst, J. *et al.* Substrate elasticity provides mechanical signals for the expansion of hemopoietic stem and progenitor cells. *Nat Biotechnol* **28**, 1123-1128, doi:10.1038/nbt.1687 (2010).

[65] Adamo, L. *et al.* Biomechanical forces promote embryonic haematopoiesis. *Nature* **459**, 1131-1135, doi:10.1038/nature08073 (2009).

[66] Choi, J. S. & Harley, B. A. The combined influence of substrate elasticity and ligand density on the viability and biophysical properties of hematopoietic stem and progenitor cells. *Biomaterials* **33**, 4460-4468, doi:10.1016/j.biomaterials.2012.03.010 (2012).

[67] Kumar, S. S. *et al.* The combined influence of substrate elasticity and surface-grafted molecules on the ex vivo expansion of hematopoietic stem and progenitor cells. *Biomaterials* **34**, 7632-7644, doi:10.1016/j.biomaterials.2013.07.002 (2013).

[68] Lee-Thedieck, C., Rauch, N., Fiammengo, R., Klein, G. & Spatz, J. P. Impact of substrate elasticity on human hematopoietic stem and progenitor cell adhesion and motility. *J Cell Sci* **125**, 3765-3775, doi:10.1242/jcs.095596 (2012).

[69] Chitteti, B. R., Kacena, M. A., Voytik-Harbin, S. L. & Srour, E. F. Modulation of hematopoietic progenitor cell fate in vitro by varying collagen oligomer matrix stiffness in the presence or absence of osteoblasts. *J Immunol Methods* **425**, 108-113, doi:10.1016/j.jim.2015.07.001 (2015).

[70] Kurth, I., Franke, K., Pompe, T., Bornhauser, M. & Werner, C. Hematopoietic stem and progenitor cells in adhesive microcavities. *Integr Biol (Camb)* **1**, 427-434, doi:10.1039/b903711j (2009).

[71] Muller, E., Grinenko, T., Pompe, T., Waskow, C. & Werner, C. Space constraints govern fate of hematopoietic stem and progenitor cells in vitro. *Biomaterials* **53**, 709-715, doi:10.1016/j.biomaterials.2015.02.095 (2015).

[72] Chua, K. N. *et al.* Surface-aminated electrospun nanofibers enhance adhesion and expansion of human umbilical cord blood hematopoietic stem/progenitor cells. *Biomaterials* **27**, 6043-6051, doi:10.1016/j.biomaterials.2006.06.017 (2006).

[73] Chua, K. N. *et al.* Functional nanofiber scaffolds with different spacers modulate adhesion and expansion of cryopreserved umbilical cord blood hematopoietic stem/progenitor cells. *Exp Hematol* **35**, 771-781, doi:10.1016/j.exphem.2007.02.002 (2007).

[74] Jiang, X., Christopherson, G. T. & Mao, H. Q. The effect of nanofibre surface amine density and conjugate structure on the adhesion and proliferation of human haematopoietic progenitor cells. *Interface Focus* **1**, 725-733, doi:10.1098/rsfs.2011.0033 (2011).

[75] Franke, K., Pompe, T., Bornhauser, M. & Werner, C. Engineered matrix coatings

to modulate the adhesion of CD133+ human hematopoietic progenitor cells. *Biomaterials* **28**, 836-843, doi:10.1016/j.biomaterials.2006.09.031 (2007).

[76] Celebi, B., Mantovani, D. & Pineault, N. Effects of extracellular matrix proteins on the growth of haematopoietic progenitor cells. *Biomed Mater* **6**, 055011, doi:10.1088/1748-6041/6/5/055011 (2011).

[77] Feng, Q., Chai, C., Jiang, X. S., Leong, K. W. & Mao, H. Q. Expansion of engrafting human hematopoietic stem/progenitor cells in three-dimensional scaffolds with surface-immobilized fibronectin. *J Biomed Mater Res A* **78**, 781-791, doi:10.1002/jbm.a.30829 (2006).

[78] Dao, M. A., Hashino, K., Kato, I. & Nolta, J. A. Adhesion to fibronectin maintains regenerative capacity during ex vivo culture and transduction of human hematopoietic stem and progenitor cells. *Blood* **92**, 4612-4621 (1998).

[79] Bhatia, R., Williams, A. D. & Munthe, H. A. Contact with fibronectin enhances preservation of normal but not chronic myelogenous leukemia primitive hematopoietic progenitors. *Exp Hematol* **30**, 324-332 (2002).

[80] Jiang, X. S. *et al.* Surface-immobilization of adhesion peptides on substrate for ex vivo expansion of cryopreserved umbilical cord blood CD34+ cells. *Biomaterials* **27**, 2723-2732, doi:10.1016/j.biomaterials.2005.12.001 (2006).

[81] Cuchiara, M. L., Horter, K. L., Banda, O. A. & West, J. L. Covalent immobilization of stem cell factor and stromal derived factor 1alpha for in vitro culture of hematopoietic progenitor cells. *Acta Biomater* **9**, 9258-9269, doi:10.1016/j.actbio.2013.08.012 (2013).

[82] Lazar-Karsten, P. *et al.* The influence of extracellular matrix proteins and mesenchymal stem cells on erythropoietic cell maturation. *Vox Sang* **101**, 65-76, doi:10.1111/j.1423-0410.2010.01453.x (2011).

[83] Yamada, H. *et al.* Adhesion to fibronectin induces megakaryocytic differentiation of JAS-REN cells. *Anticancer Res* **28**, 261-266 (2008).

[84] Han, P., Guo, X. H. & Story, C. J. Enhanced expansion and maturation of megakaryocytic progenitors by fibronectin. *Cytotherapy* **4**, 277-283, doi:10.1080/146532402320219790 (2002).

[85] Kawaguchi, T. *et al.* Fibronectin promotes proplatelet formation in the human megakaryocytic cell line UT-7/TPO. *Cell Biol Int* **36**, 39-45, doi:10.1042/CBI20110383 (2012).

[86] Balduini, A. *et al.* Adhesive receptors, extracellular proteins and myosin IIA orchestrate proplatelet formation by human megakaryocytes. *J Thromb Haemost* **6**, 1900-1907, doi:10.1111/j.1538-7836.2008.03132.x (2008).

[87] Malara, A. *et al.* Extracellular matrix structure and nano-mechanics determine megakaryocyte function. *Blood* **118**, 4449-4453, doi:10.1182/blood-2011-04-345876 (2011).

[88] Rosenzweig, M., Pykett, M., Marks, D. F. & Johnson, R. P. Enhanced maintenance and retroviral transduction of primitive hematopoietic progenitor cells using a novel three-dimensional culture system. *Gene Ther* **4**, 928-936, doi:10.1038/sj.gt.3300480 (1997).

[89] Bagley, J., Rosenzweig, M., Marks, D. F. & Pykett, M. J. Extended culture of multipotent hematopoietic progenitors without cytokine augmentation in a novel three-dimensional device. *Exp Hematol* **27**, 496-504, doi:Doi 10.1016/S0301-472x(98)00053-8 (1999).

[90] Banu, N., Rosenzweig, M., Kim, H., Bagley, J. & Pykett, M. Cytokine-augmented culture of haematopoietic progenitor cells in a novel three-dimensional cell growth matrix. *Cytokine* **13**, 349-358, doi:10.1006/cyto.2001.0836 (2001).

[91] Ehring, B. *et al.* Expansion of HPCs from cord blood in a novel 3D matrix. *Cytotherapy* **5**, 490-499, doi:10.1080/14653240310003585 (2003).

[92] Naughton, B. A. & Naughton, G. K. Hematopoiesis on nylon mesh templates. Comparative long-term bone marrow culture and the influence of stromal support cells. *Ann N Y Acad Sci* **554**, 125-140, doi:10.1111/j.1749-6632.1989.tb22415.x (1989).

[93] Meissner, P., Schroder, B., Herfurth, C. & Biselli, M. Development of a fixed bed bioreactor for the expansion of human hematopoietic progenitor cells. *Cytotechnology* **30**, 227-234, doi:10.1023/A:1008085932764 (1999).

[94] Ferreira, M. S. *et al.* Cord blood-hematopoietic stem cell expansion in 3D fibrin scaffolds with stromal support. *Biomaterials* **33**, 6987-6997, doi:10.1016/j.biomaterials.2012.06.029 (2012).

[95] Mortera-Blanco, T., Mantalaris, A., Bismarck, A., Aqel, N. & Panoskaltsis, N. Long-term cytokine-free expansion of cord blood mononuclear cells in three-dimensional scaffolds. *Biomaterials* **32**, 9263-9270, doi:10.1016/j.biomaterials.2011.08.051 (2011).

[96] Nichols, J. E. *et al.* In vitro analog of human bone marrow from 3D scaffolds with biomimetic inverted colloidal crystal geometry. *Biomaterials* **30**, 1071-1079, doi:10.1016/j.biomaterials.2008.10.041 (2009).

[97] Sullenbarger, B., Bahng, J. H., Gruner, R., Kotov, N. & Lasky, L. C. Prolonged continuous in vitro human platelet production using three-dimensional scaffolds. *Exp Hematol* **37**, 101-110, doi:10.1016/j.exphem.2008.09.009 (2009).

[98] Lee, J. *et al.* Implantable microenvironments to attract hematopoietic stem/cancer

cells. *Proc Natl Acad Sci U S A* **109**, 19638-19643, doi:10.1073/pnas.1208384109 (2012).

[99] Li, Y., Ma, T., Kniss, D. A., Yang, S. T. & Lasky, L. C. Human cord cell hematopoiesis in three-dimensional nonwoven fibrous matrices: in vitro simulation of the marrow microenvironment. *J Hematother Stem Cell Res* **10**, 355-368, doi:10.1089/152581601750288966 (2001).

[100] Sasaki, T., Takagi, M., Soma, T. & Yoshida, T. Analysis of hematopoietic microenvironment containing spatial development of stromal cells in nonwoven fabrics. *J Biosci Bioeng* **96**, 76-78 (2003).

[101] Braccini, A. *et al.* Three-dimensional perfusion culture of human bone marrow cells and generation of osteoinductive grafts. *Stem Cells* **23**, 1066-1072, doi:10.1634/stemcells.2005-0002 (2005).

[102] Tan, J. *et al.* Maintenance and expansion of hematopoietic stem/progenitor cells in biomimetic osteoblast niche. *Cytotechnology* **62**, 439-448, doi:10.1007/s10616-010-9297-6 (2010).

[103] Marturano-Kruik, A. *et al.* Human bone perivascular niche-on-a-chip for studying metastatic colonization. *Proc Natl Acad Sci U S A* **115**, 1256-1261, doi:10.1073/pnas.1714282115 (2018).

[104] Holzapfel, B. M. *et al.* Tissue engineered humanized bone supports human hematopoiesis in vivo. *Biomaterials* **61**, 103-114, doi:10.1016/j.biomaterials.2015.04.057 (2015).

[105] Ma, K. *et al.* Electrospun nanofiber scaffolds for rapid and rich capture of bone marrow-derived hematopoietic stem cells. *Biomaterials* **29**, 2096-2103, doi:10.1016/j.biomaterials.2008.01.024 (2008).

[106] Tomimori, Y., Takagi, M. & Yoshida, T. The construction of an in vitro three-dimensional hematopoietic microenvironment for mouse bone marrow cells employing porous carriers. *Cytotechnology* **34**, 121-130, doi:10.1023/A:1008157303025 (2000).

[107] Sasaki, T., Takagi, M., Soma, T. & Yoshida, T. 3D culture of murine hematopoietic cells with spatial development of stromal cells in nonwoven fabrics. *Cytotherapy* **4**, 285-291, doi:10.1080/146532402320219808 (2002).

[108] Okamoto, T. *et al.* Effect of heparin addition on expansion of cord blood hematopoietic progenitor cells in three-dimensional coculture with stromal cells in nonwoven fabrics. *J Artif Organs* **7**, 194-202, doi:10.1007/s10047-004-0272-x (2004).

[109] Batnyam, O. *et al.* Biohybrid hematopoietic niche for expansion of hematopoietic stem/progenitor cells by using geometrically controlled fibrous layers. *Rsc Adv* **5**,

80357-80364, doi:10.1039/c5ra13332g (2015).

[110] Kang, Y. G. *et al.* A three-dimensional hierarchical scaffold fabricated by a combined rapid prototyping technique and electrospinning process to expand hematopoietic stem/progenitor cells. *Biotechnol Lett* **38**, 175-181, doi:10.1007/s10529-015-1952-8 (2016).

[111] Fauzi, I., Panoskaltsis, N. & Mantalaris, A. Early exposure of murine embryonic stem cells to hematopoietic cytokines differentially directs definitive erythropoiesis and cardiomyogenesis in alginate hydrogel three-dimensional cultures. *Stem Cells Dev* **23**, 2720-2729, doi:10.1089/scd.2014.0105 (2014).

[112] Mahadik, B. P., Pedron Haba, S., Skertich, L. J. & Harley, B. A. The use of covalently immobilized stem cell factor to selectively affect hematopoietic stem cell activity within a gelatin hydrogel. *Biomaterials* **67**, 297-307, doi:10.1016/j.biomaterials.2015.07.042 (2015).

[113] Demange, E. *et al.* Survival of cord blood haematopoietic stem cells in a hyaluronan hydrogel for ex vivo biomimicry. *J Tissue Eng Regen Med* **7**, 901-910, doi:10.1002/term.1482 (2013).

[114] Rinker, T. E., Hammoudi, T. M., Kemp, M. L., Lu, H. & Temenoff, J. S. Interactions between mesenchymal stem cells, adipocytes, and osteoblasts in a 3D tri-culture model of hyperglycemic conditions in the bone marrow microenvironment. *Integr Biol (Camb)* **6**, 324-337, doi:10.1039/c3ib40194d (2014).

[115] Mahadik, B. P., Wheeler, T. D., Skertich, L. J., Kenis, P. J. & Harley, B. A. Microfluidic generation of gradient hydrogels to modulate hematopoietic stem cell culture environment. *Adv Healthc Mater* **3**, 449-458, doi:10.1002/adhm.201300263 (2014).

[116] Pittenger, M. F. *et al.* Multilineage potential of adult human mesenchymal stem cells. *Science* **284**, 143-147 (1999).

[117] Greenbaum, A. *et al.* CXCL12 in early mesenchymal progenitors is required for haematopoietic stem-cell maintenance. *Nature* **495**, 227-230, doi:10.1038/nature11926 (2013).

[118] Kim, D. H. *et al.* Gene expression profile of cytokine and growth factor during differentiation of bone marrow-derived mesenchymal stem cell. *Cytokine* **31**, 119-126, doi:10.1016/j.cyto.2005.04.004 (2005).

[119] Ehninger, A. & Trumpp, A. The bone marrow stem cell niche grows up: mesenchymal stem cells and macrophages move in. *J Exp Med* **208**, 421-428, doi:10.1084/jem.20110132 (2011).

[120] Avigdor, A. *et al.* CD44 and hyaluronic acid cooperate with SDF-1 in the

trafficking of human CD34+ stem/progenitor cells to bone marrow. *Blood* **103**, 2981-2989, doi:10.1182/blood-2003-10-3611 (2004).

[121] Leisten, I. *et al.* 3D co-culture of hematopoietic stem and progenitor cells and mesenchymal stem cells in collagen scaffolds as a model of the hematopoietic niche. *Biomaterials* **33**, 1736-1747, doi:10.1016/j.biomaterials.2011.11.034 (2012).

[122] Linsley, C., Wu, B. & Tawil, B. The effect of fibrinogen, collagen type I, and fibronectin on mesenchymal stem cell growth and differentiation into osteoblasts. *Tissue Eng Part A* **19**, 1416-1423, doi:10.1089/ten.TEA.2012.0523 (2013).

[123] Rico, P., Mnatsakanyan, H., Dalby, M. J. & Salmerón-Sánchez, M. Material-Driven Fibronectin Assembly Promotes Maintenance of Mesenchymal Stem Cell Phenotypes. *Adv Funct Mater* **26**, 6563-6573, doi:10.1002/adfm.201602333 (2016).

[124] Chung, C. & Burdick, J. A. Influence of three-dimensional hyaluronic acid microenvironments on mesenchymal stem cell chondrogenesis. *Tissue Eng Part A* **15**, 243-254, doi:10.1089/ten.tea.2008.0067 (2009).

[125] Kim, J. *et al.* Bone regeneration using hyaluronic acid-based hydrogel with bone morphogenic protein-2 and human mesenchymal stem cells. *Biomaterials* **28**, 1830-1837, doi:10.1016/j.biomaterials.2006.11.050 (2007).

[126] Zhu, H. *et al.* The role of the hyaluronan receptor CD44 in mesenchymal stem cell migration in the extracellular matrix. *Stem Cells* **24**, 928-935, doi:10.1634/stemcells.2005-0186 (2006).

[127] Lei, Y., Gojgini, S., Lam, J. & Segura, T. The spreading, migration and proliferation of mouse mesenchymal stem cells cultured inside hyaluronic acid hydrogels. *Biomaterials* **32**, 39-47, doi:10.1016/j.biomaterials.2010.08.103 (2011).

[128] Abdeen, A. A., Weiss, J. B., Lee, J. & Kilian, K. A. Matrix composition and mechanics direct proangiogenic signaling from mesenchymal stem cells. *Tissue Eng Part A* **20**, 2737-2745, doi:10.1089/ten.TEA.2013.0661 (2014).

[129] Nuttelman, C. R., Tripodi, M. C. & Anseth, K. S. Synthetic hydrogel niches that promote hMSC viability. *Matrix biology : journal of the International Society for Matrix Biology* **24**, 208-218, doi:10.1016/j.matbio.2005.03.004 (2005).

[130] Schneider, C. A., Rasband, W. S. & Eliceiri, K. W. NIH Image to ImageJ: 25 years of image analysis. *Nat Methods* **9**, 671-675, doi:10.1038/nmeth.2089 (2012).

[131] Schindelin, J. *et al.* Fiji: an open-source platform for biological-image analysis. *Nat Methods* **9**, 676-682, doi:10.1038/nmeth.2019 (2012).

[132] Ruan, J. L. *et al.* An improved cryosection method for polyethylene glycol

hydrogels used in tissue engineering. *Tissue Eng Part C Methods* **19**, 794-801, doi:10.1089/ten.TEC.2012.0460 (2013).

[133] Broudy, V. C. Stem cell factor and hematopoiesis. *Blood* **90**, 1345-1364 (1997).

[134] Kurihara, N., Bertolini, D., Suda, T., Akiyama, Y. & Roodman, G. D. IL-6 stimulates osteoclast-like multinucleated cell formation in long term human marrow cultures by inducing IL-1 release. *J Immunol* **144**, 4226-4230 (1990).

[135] Muraguchi, A. *et al.* The essential role of B cell stimulatory factor 2 (BSF-2/IL-6) for the terminal differentiation of B cells. *J Exp Med* **167**, 332-344, doi:10.1084/jem.167.2.332 (1988).

[136] Jansen, L., McCarthy, T., Lee, M. & Peyton, S. A synthetic, three-dimensional bone marrow hydrogel. *bioRxiv*, 275842, doi:10.1101/275842 (2018).

[137] Mantalaris, A., Keng, P., Bourne, P., Chang, A. Y. & Wu, J. H. Engineering a human bone marrow model: a case study on ex vivo erythropoiesis. *Biotechnol Prog* **14**, 126-133, doi:10.1021/bp970136+ (1998).

[138] Allenby, M. C., Panoskaltsis, N., Tahlawi, A., Dos Santos, S. B. & Mantalaris, A. Dynamic human erythropoiesis in a three-dimensional perfusion bone marrow biomimicry. *Biomaterials* **188**, 24-37, doi:10.1016/j.biomaterials.2018.08.020 (2019).

[139] Poznansky, M. C. *et al.* Efficient generation of human T cells from a tissue-engineered thymic organoid. *Nat Biotechnol* **18**, 729-734, doi:10.1038/77288 (2000).

[140] Taqvi, S., Dixit, L. & Roy, K. Biomaterial-based notch signaling for the differentiation of hematopoietic stem cells into T cells. *J Biomed Mater Res A* **79**, 689-697, doi:10.1002/jbm.a.30916 (2006).

[141] Fernandez, I., Ooi, T. P. & Roy, K. Generation of functional, antigen-specific CD8+ human T cells from cord blood stem cells using exogenous Notch and tetramer-TCR signaling. *Stem Cells* **32**, 93-104, doi:10.1002/stem.1512 (2014).

[142] Sabaghi, F. *et al.* Evaluation of human cord blood CD34+ hematopoietic stem cell differentiation to megakaryocyte on aminated PES nanofiber scaffold compare to 2-D culture system. *Artif Cells Nanomed Biotechnol* **44**, 1062-1068, doi:10.3109/21691401.2015.1011800 (2016).

[143] Pietrzyk-Nivau, A. *et al.* Three-Dimensional Environment Sustains Hematopoietic Stem Cell Differentiation into Platelet-Producing Megakaryocytes. *PLoS One* **10**, e0136652, doi:10.1371/journal.pone.0136652 (2015).

[144] Pallotta, I., Lovett, M., Kaplan, D. L. & Balduini, A. Three-dimensional system for the in vitro study of megakaryocytes and functional platelet production using silk-

based vascular tubes. *Tissue Eng Part C Methods* **17**, 1223-1232, doi:10.1089/ten.tec.2011.0134 (2011).

[145] Di Buduo, C. A. *et al.* Programmable 3D silk bone marrow niche for platelet generation ex vivo and modeling of megakaryopoiesis pathologies. *Blood* **125**, 2254-2264, doi:10.1182/blood-2014-08-595561 (2015).

[146] Carrion, B. *et al.* Recreating the perivascular niche ex vivo using a microfluidic approach. *Biotechnol Bioeng* **107**, 1020-1028, doi:10.1002/bit.22891 (2010).

[147] Kim, S., Lee, H., Chung, M. & Jeon, N. L. Engineering of functional, perfusable 3D microvascular networks on a chip. *Lab Chip* **13**, 1489-1500, doi:10.1039/c3lc41320a (2013).

[148] Krupnick, A. S., Shaaban, A., Radu, A. & Flake, A. W. Bone marrow tissue engineering. *Tissue Eng* **8**, 145-155, doi:10.1089/107632702753503135 (2002).

[149] Bladergroen, B. A. *et al.* In vivo recruitment of hematopoietic cells using stromal cell-derived factor 1 alpha-loaded heparinized three-dimensional collagen scaffolds. *Tissue Eng Part A* **15**, 1591-1599, doi:10.1089/ten.tea.2008.0348 (2009).

[150] Torisawa, Y. S. *et al.* Bone marrow-on-a-chip replicates hematopoietic niche physiology in vitro. *Nat Methods* **11**, 663-669, doi:10.1038/nmeth.2938 (2014).

[151] Nikiforow, S. & Ritz, J. Dramatic Expansion of HSCs: New Possibilities for HSC Transplants? *Cell Stem Cell* **18**, 10-12, doi:10.1016/j.stem.2015.12.011 (2016).

[152] Kurth, I., Franke, K., Pompe, T., Bornhauser, M. & Werner, C. Extracellular matrix functionalized microcavities to control hematopoietic stem and progenitor cell fate. *Macromol Biosci* **11**, 739-747, doi:10.1002/mabi.201000432 (2011).

[153] Lutolf, M. P., Doyonnas, R., Havenstrite, K., Koleckar, K. & Blau, H. M. Perturbation of single hematopoietic stem cell fates in artificial niches. *Integr Biol (Camb)* **1**, 59-69, doi:10.1039/b815718a (2009).

[154] Kobel, S. & Lutolf, M. P. Biomaterials meet microfluidics: building the next generation of artificial niches. *Curr Opin Biotechnol* **22**, 690-697, doi:10.1016/j.copbio.2011.07.001 (2011).

[155] Lee-Thedieck, C. & Spatz, J. P. Artificial niches: biomimetic materials for hematopoietic stem cell culture. *Macromol Rapid Commun* **33**, 1432-1438, doi:10.1002/marc.201200219 (2012).

[156] Whitesides, G. M. The origins and the future of microfluidics. *Nature* **442**, 368-373, doi:10.1038/nature05058 (2006).

[157] Whitesides, G. M., Ostuni, E., Takayama, S., Jiang, X. & Ingber, D. E. Soft lithography in biology and biochemistry. *Annu Rev Biomed Eng* **3**, 335-373,

doi:10.1146/annurev.bioeng.3.1.335 (2001).

[158] Khademhosseini, A., Langer, R., Borenstein, J. & Vacanti, J. P. Microscale technologies for tissue engineering and biology. *Proc Natl Acad Sci U S A* **103**, 2480-2487, doi:10.1073/pnas.0507681102 (2006).

[159] Huh, D., Hamilton, G. A. & Ingber, D. E. From 3D cell culture to organs-on-chips. *Trends Cell Biol* **21**, 745-754, doi:10.1016/j.tcb.2011.09.005 (2011).

[160] Zhang, B. Y., Korolj, A., Lai, B. F. L. & Radisic, M. Advances in organ-on-a-chip engineering. *Nat Rev Mater* **3**, 257-278, doi:10.1038/s41578-018-0034-7 (2018).

[161] Huh, D. *et al.* Reconstituting organ-level lung functions on a chip. *Science* **328**, 1662-1668, doi:10.1126/science.1188302 (2010).

[162] Kim, H. J., Huh, D., Hamilton, G. & Ingber, D. E. Human gut-on-a-chip inhabited by microbial flora that experiences intestinal peristalsis-like motions and flow. *Lab Chip* **12**, 2165-2174, doi:10.1039/c2lc40074j (2012).

[163] Jang, K. J. *et al.* Human kidney proximal tubule-on-a-chip for drug transport and nephrotoxicity assessment. *Integr Biol (Camb)* **5**, 1119-1129, doi:10.1039/c3ib40049b (2013).

[164] Seo, J. *et al.* Human blinking 'eye-on-a-chip'. *Invest Ophth Vis Sci* **57**, 3872-3872 (2016).

[165] Edington, C. D. *et al.* Interconnected Microphysiological Systems for Quantitative Biology and Pharmacology Studies. *Sci Rep* **8**, 4530, doi:10.1038/s41598-018-22749-0 (2018).

[166] Toepke, M. W. & Beebe, D. J. PDMS absorption of small molecules and consequences in microfluidic applications. *Lab Chip* **6**, 1484-1486, doi:10.1039/b612140c (2006).

[167] Huang, C. P. *et al.* Engineering microscale cellular niches for three-dimensional multicellular co-cultures. *Lab Chip* **9**, 1740-1748, doi:10.1039/b818401a (2009).

[168] Jeon, J. S. *et al.* Human 3D vascularized organotypic microfluidic assays to study breast cancer cell extravasation. *Proc Natl Acad Sci U S A* **112**, 214-219, doi:10.1073/pnas.1417115112 (2015).

[169] Jeon, J. S. *et al.* Generation of 3D functional microvascular networks with human mesenchymal stem cells in microfluidic systems. *Integr Biol (Camb)* **6**, 555-563, doi:10.1039/c3ib40267c (2014).

[170] Chen, M. B. *et al.* On-chip human microvasculature assay for visualization and quantification of tumor cell extravasation dynamics. *Nat Protoc* **12**, 865-880, doi:10.1038/nprot.2017.018 (2017).

[171] Oh, S. *et al.* "Open-top" microfluidic device for in vitro three-dimensional capillary beds. *Lab Chip* **17**, 3405-3414, doi:10.1039/c7lc00646b (2017).

[172] Phan, D. T. T. *et al.* A vascularized and perfused organ-on-a-chip platform for large-scale drug screening applications. *Lab Chip* **17**, 511-520, doi:10.1039/c6lc01422d (2017).

[173] Desai, S. P., Freeman, D. M. & Voldman, J. Plastic masters-rigid templates for soft lithography. *Lab Chip* **9**, 1631-1637, doi:10.1039/b822081f (2009).

[174] Wu, W., Wu, J., Kim, J. H. & Lee, N. Y. Instantaneous room temperature bonding of a wide range of non-silicon substrates with poly(dimethylsiloxane) (PDMS) elastomer mediated by a mercaptosilane. *Lab Chip* **15**, 2819-2825, doi:10.1039/c5lc00285k (2015).

[175] Halldorsson, S., Lucumi, E., Gomez-Sjoberg, R. & Fleming, R. M. T. Advantages and challenges of microfluidic cell culture in polydimethylsiloxane devices. *Biosens Bioelectron* **63**, 218-231, doi:10.1016/j.bios.2014.07.029 (2015).

[176] Levario, T. J., Zhan, M., Lim, B., Shvartsman, S. Y. & Lu, H. Microfluidic trap array for massively parallel imaging of Drosophila embryos. *Nat Protoc* **8**, 721-736, doi:10.1038/nprot.2013.034 (2013).

[177] Wang, X. *et al.* Engineering anastomosis between living capillary networks and endothelial cell-lined microfluidic channels. *Lab Chip* **16**, 282-290, doi:10.1039/c5lc01050k (2016).

[178] Chuah, Y. J. *et al.* Simple surface engineering of polydimethylsiloxane with polydopamine for stabilized mesenchymal stem cell adhesion and multipotency. *Sci Rep* **5**, 18162, doi:10.1038/srep18162 (2015).

[179] Jaiswal, N., Haynesworth, S. E., Caplan, A. I. & Bruder, S. P. Osteogenic differentiation of purified, culture-expanded human mesenchymal stem cells in vitro. *J Cell Biochem* **64**, 295-312 (1997).

[180] Long, M. W. Osteogenesis and bone-marrow-derived cells. *Blood Cells Mol Dis* **27**, 677-690, doi:10.1006/bcmd.2001.0431 (2001).

[181] Chamberlain, G., Fox, J., Ashton, B. & Middleton, J. Concise review: mesenchymal stem cells: their phenotype, differentiation capacity, immunological features, and potential for homing. *Stem Cells* **25**, 2739-2749, doi:10.1634/stemcells.2007-0197 (2007).

[182] Tenstad, E., Tourovskaia, A., Folch, A., Myklebost, O. & Rian, E. Extensive adipogenic and osteogenic differentiation of patterned human mesenchymal stem cells in a microfluidic device. *Lab Chip* **10**, 1401-1409, doi:10.1039/b926738g (2010).

[183] Haase, K. & Kamm, R. D. Advances in on-chip vascularization. *Regen Med* **12**, 285-302, doi:10.2217/rme-2016-0152 (2017).

[184] Kim, S., Kim, W., Lim, S. & Jeon, J. S. Vasculature-On-A-Chip for In Vitro Disease Models. *Bioengineering (Basel)* **4**, doi:10.3390/bioengineering4010008 (2017).

[185] Zudaire, E., Gambardella, L., Kurcz, C. & Vermeren, S. A computational tool for quantitative analysis of vascular networks. *PLoS One* **6**, e27385, doi:10.1371/journal.pone.0027385 (2011).

[186] Lapidot, T. & Petit, I. Current understanding of stem cell mobilization: the roles of chemokines, proteolytic enzymes, adhesion molecules, cytokines, and stromal cells. *Exp Hematol* **30**, 973-981 (2002).

[187] Cottler-Fox, M. H. *et al.* Stem cell mobilization. *Hematology Am Soc Hematol Educ Program*, 419-437 (2003).

[188] Pesek, G. & Cottler-Fox, M. Hematopoietic stem cell mobilization: a clinical protocol. *Methods Mol Biol* **904**, 69-77, doi:10.1007/978-1-61779-943-3_5 (2012).

[189] Kumar, S. *et al.* Impact of lenalidomide therapy on stem cell mobilization and engraftment post-peripheral blood stem cell transplantation in patients with newly diagnosed myeloma. *Leukemia* **21**, 2035-2042, doi:10.1038/sj.leu.2404801 (2007).

[190] Vose, J. M. *et al.* Advances in mobilization for the optimization of autologous stem cell transplantation. *Leukemia & lymphoma* **50**, 1412-1421, doi:10.1080/10428190903096701 (2009).

[191] Sahin, U. & Demirer, T. Current strategies for the management of autologous peripheral blood stem cell mobilization failures in patients with multiple myeloma. *J Clin Apher* **33**, 357-370, doi:10.1002/jca.21591 (2018).

[192] Chaudhary, L. *et al.* Peripheral blood stem cell mobilization in multiple myeloma patients treat in the novel therapy-era with plerixafor and G-CSF has superior efficacy but significantly higher costs compared to mobilization with low-dose cyclophosphamide and G-CSF. *J Clin Apher* **28**, 359-367, doi:10.1002/jca.21280 (2013).

[193] Bonig, H. & Papayannopoulou, T. Mobilization of hematopoietic stem/progenitor cells: general principles and molecular mechanisms. *Methods Mol Biol* **904**, 1-14, doi:10.1007/978-1-61779-943-3_1 (2012).

[194] Petit, I. *et al.* G-CSF induces stem cell mobilization by decreasing bone marrow SDF-1 and up-regulating CXCR4. *Nat Immunol* **3**, 687-694, doi:10.1038/ni813 (2002).

[195] Levesque, J. P., Hendy, J., Takamatsu, Y., Simmons, P. J. & Bendall, L. J.

Disruption of the CXCR4/CXCL12 chemotactic interaction during hematopoietic stem cell mobilization induced by GCSF or cyclophosphamide. *J Clin Invest* **111**, 187-196, doi:10.1172/JCI15994 (2003).

[196] Greenbaum, A. M. & Link, D. C. Mechanisms of G-CSF-mediated hematopoietic stem and progenitor mobilization. *Leukemia* **25**, 211-217, doi:10.1038/leu.2010.248 (2011).

[197] Bonig, H. & Papayannopoulou, T. Hematopoietic stem cell mobilization: updated conceptual renditions. *Leukemia* **27**, 24-31, doi:10.1038/leu.2012.254 (2013).

[198] Klein, G., Schmal, O. & Aicher, W. K. Matrix metalloproteinases in stem cell mobilization. *Matrix biology : journal of the International Society for Matrix Biology* **44-46**, 175-183, doi:10.1016/j.matbio.2015.01.011 (2015).

[199] Cashen, A. F., Lazarus, H. M. & Devine, S. M. Mobilizing stem cells from normal donors: is it possible to improve upon G-CSF? *Bone marrow transplantation* **39**, 577-588, doi:10.1038/sj.bmt.1705616 (2007).

[200] Liles, W. C. *et al.* Mobilization of hematopoietic progenitor cells in healthy volunteers by AMD3100, a CXCR4 antagonist. *Blood* **102**, 2728-2730, doi:10.1182/blood-2003-02-0663 (2003).

[201] DiPersio, J. F. *et al.* Plerixafor and G-CSF versus placebo and G-CSF to mobilize hematopoietic stem cells for autologous stem cell transplantation in patients with multiple myeloma. *Blood* **113**, 5720-5726, doi:10.1182/blood-2008-08-174946 (2009).

[202] Fowler, C. J. *et al.* Rescue from failed growth factor and/or chemotherapy HSC mobilization with G-CSF and plerixafor (AMD3100): an institutional experience. *Bone marrow transplantation* **43**, 909-917, doi:10.1038/bmt.2008.409 (2009).

[203] Mohty, M. & Ho, A. D. In and out of the niche: perspectives in mobilization of hematopoietic stem cells. *Exp Hematol* **39**, 723-729, doi:10.1016/j.exphem.2011.05.004 (2011).

[204] Hoggatt, J. & Pelus, L. M. Hematopoietic stem cell mobilization with agents other than G-CSF. *Methods Mol Biol* **904**, 49-67, doi:10.1007/978-1-61779-943-3_4 (2012).

[205] Hopman, R. K. & DiPersio, J. F. Advances in stem cell mobilization. *Blood Rev* **28**, 31-40, doi:10.1016/j.blre.2014.01.001 (2014).

[206] Lemoli, R. M. & D'Addio, A. Hematopoietic stem cell mobilization. *Haematologica* **93**, 321-324, doi:10.3324/haematol.12616 (2008).

[207] Hoggatt, J. *et al.* Rapid Mobilization Reveals a Highly Engraftable Hematopoietic Stem Cell. *Cell* **172**, 191-204 e110, doi:10.1016/j.cell.2017.11.003 (2018).

[208] Ratajczak, M. Z. *et al.* Novel insight into stem cell mobilization-plasma sphingosine-1-phosphate is a major chemoattractant that directs the egress of hematopoietic stem progenitor cells from the bone marrow and its level in peripheral blood increases during mobilization due to activation of complement cascade/membrane attack complex. *Leukemia* **24**, 976-985, doi:10.1038/leu.2010.53 (2010).

[209] Pitchford, S. C. & Rankin, S. M. Combinatorial stem cell mobilization in animal models. *Methods Mol Biol* **904**, 139-154, doi:10.1007/978-1-61779-943-3_12 (2012).

[210] Ghobadi, A. *et al.* Bortezomib is a rapid mobilizer of hematopoietic stem cells in mice via modulation of the VCAM-1/VLA-4 axis. *Blood* **124**, 2752-2754, doi:10.1182/blood-2014-08-595967 (2014).

[211] Li, J. K. *et al.* Inhibition of CXCR4 activity with AMD3100 decreases invasion of human colorectal cancer cells in vitro. *World J Gastroenterol* **14**, 2308-2313, doi:10.3748/wjg.14.2308 (2008).

[212] Ogle, M. E. *et al.* Sphingosine-1-Phosphate Receptor-3 Supports Hematopoietic Stem and Progenitor Cell Residence Within the Bone Marrow Niche. *Stem Cells* **35**, 1040-1052, doi:10.1002/stem.2556 (2017).

[213] Sharma, M. B., Limaye, L. S. & Kale, V. P. Mimicking the functional hematopoietic stem cell niche in vitro: recapitulation of marrow physiology by hydrogel-based three-dimensional cultures of mesenchymal stromal cells. *Haematologica* **97**, 651-660, doi:10.3324/haematol.2011.050500 (2012).

[214] Paix, A. *et al.* Total body irradiation in allogeneic bone marrow transplantation conditioning regimens: A review. *Critical reviews in oncology/hematology* **123**, 138-148, doi:10.1016/j.critrevonc.2018.01.011 (2018).

[215] Barcellos-Hoff, M. H., Park, C. & Wright, E. G. Radiation and the microenvironment - tumorigenesis and therapy. *Nat Rev Cancer* **5**, 867-875, doi:10.1038/nrc1735 (2005).

[216] Fliedner, T. M., Graessle, D., Paulsen, C. & Reimers, K. Structure and function of bone marrow hemopoiesis: mechanisms of response to ionizing radiation exposure. *Cancer Biother Radiopharm* **17**, 405-426, doi:10.1089/108497802760363204 (2002).

[217] Wang, Y. *et al.* Total body irradiation causes residual bone marrow injury by induction of persistent oxidative stress in murine hematopoietic stem cells. *Free Radic Biol Med* **48**, 348-356, doi:10.1016/j.freeradbiomed.2009.11.005 (2010).

[218] Cao, X. *et al.* Irradiation induces bone injury by damaging bone marrow microenvironment for stem cells. *Proc Natl Acad Sci U S A* **108**, 1609-1614, doi:10.1073/pnas.1015350108 (2011).

[219] Sugrue, T., Lowndes, N. F. & Ceredig, R. Mesenchymal stromal cells: radio-resistant members of the bone marrow. *Immunol Cell Biol* **91**, 5-11, doi:10.1038/icb.2012.61 (2013).

[220] Greenberger, J. S. & Epperly, M. Bone marrow-derived stem cells and radiation response. *Seminars in radiation oncology* **19**, 133-139, doi:10.1016/j.semradonc.2008.11.006 (2009).

[221] Dominici, M. *et al.* Restoration and reversible expansion of the osteoblastic hematopoietic stem cell niche after marrow radioablation. *Blood* **114**, 2333-2343, doi:10.1182/blood-2008-10-183459 (2009).

[222] Green, D. E. & Rubin, C. T. Consequences of irradiation on bone and marrow phenotypes, and its relation to disruption of hematopoietic precursors. *Bone* **63**, 87-94, doi:10.1016/j.bone.2014.02.018 (2014).

[223] Poncin, G. *et al.* Characterization of spontaneous bone marrow recovery after sublethal total body irradiation: importance of the osteoblastic/adipocytic balance. *PLoS One* **7**, e30818, doi:10.1371/journal.pone.0030818 (2012).

[224] Jalili-Firoozinezhad, S. *et al.* Modeling radiation injury-induced cell death and countermeasure drug responses in a human Gut-on-a-Chip. *Cell Death Dis* **9**, 223, doi:10.1038/s41419-018-0304-8 (2018).

[225] Torisawa, Y. S. *et al.* Modeling Hematopoiesis and Responses to Radiation Countermeasures in a Bone Marrow-on-a-Chip. *Tissue Eng Part C Methods* **22**, 509-515, doi:10.1089/ten.TEC.2015.0507 (2016).

[226] Guha, S., Perry, S. L., Pawate, A. S. & Kenis, P. J. Fabrication of X-ray compatible microfluidic platforms for protein crystallization. *Sens Actuators B Chem* **174**, 1-9, doi:10.1016/j.snb.2012.08.048 (2012).

[227] Cary, L. H., Ngudiankama, B. F., Salber, R. E., Ledney, G. D. & Whitnall, M. H. Efficacy of radiation countermeasures depends on radiation quality. *Radiat Res* **177**, 663-675 (2012).

[228] Semerad, C. L. *et al.* G-CSF potently inhibits osteoblast activity and CXCL12 mRNA expression in the bone marrow. *Blood* **106**, 3020-3027, doi:10.1182/blood-2004-01-0272 (2005).

[229] Rhee, S. W. *et al.* Patterned cell culture inside microfluidic devices. *Lab Chip* **5**, 102-107, doi:10.1039/b403091e (2005).

[230] Guinan, E. C. *et al.* Bactericidal/permeability-increasing protein (rBPI21) and fluoroquinolone mitigate radiation-induced bone marrow aplasia and death. *Sci Transl Med* **3**, 110ra118, doi:10.1126/scitranslmed.3003126 (2011).

[231] Yaccoby, S. *et al.* Myeloma interacts with the bone marrow microenvironment to

induce osteoclastogenesis and is dependent on osteoclast activity. *British Journal of Haematology* **116**, 278-290, doi:10.1046/j.1365-2141.2002.03257.x (2002).

[232] Corre, J. *et al.* Bone marrow mesenchymal stem cells are abnormal in multiple myeloma. *Leukemia* **21**, 1079-1088, doi:10.1038/sj.leu.2404621 (2007).

[233] Colmone, A. *et al.* Leukemic cells create bone marrow niches that disrupt the behavior of normal hematopoietic progenitor cells. *Science* **322**, 1861-1865, doi:10.1126/science.1164390 (2008).

[234] Bhatia, R., McGlave, P. B., Dewald, G. W., Blazar, B. R. & Verfaillie, C. M. Abnormal function of the bone marrow microenvironment in chronic myelogenous leukemia: role of malignant stromal macrophages. *Blood* **85**, 3636-3645 (1995).

[235] Li, J. *et al.* Dramatic enhancement of the detection limits of bioassays via ultrafast deposition of polydopamine. *Nat Biomed Eng* **1**, 0082, doi:10.1038/s41551-017-0082 (2017).